Wireless Communication Systems using Signal Space Diversity

Nauman F. Kiyani

Wireless Communication Systems using Signal Space Diversity

PROEFSCHRIFT

ter verkrijging van de graad van doctor
aan de Technische Universiteit Delft,
op gezag van de Rector Magnificus Prof. dr. ir. J.T. Fokkema,
voorzitter van het College voor Promoties,
in het openbaar te verdedigen op dinsdag 27 januari 2009 om 12.30 uur
door

Nauman Farooq KIYANI

Master of Science
University of Gävle, Sweden
geboren te Kohat, Pakistan.

Dit proefschrift is goedgekeurd door de promotor:

Prof. dr. ir. I.G.M.M. Niemegeers

Copromotor: Dr. ir. J.H. Weber

Samenstelling promotiecommissie:

Rector Magnificus	voorzitter
Prof. dr. ir. I.G.M.M. Niemegeers	Technische Universiteit Delft, promotor
Dr. ir. J.H. Weber	Technische Universiteit Delft, copromotor
Prof. dr. G.L. Stüber	Georgia Institute of Technology
Prof. dr. ir. C.H. Slump	Technische Universiteit Twente
Prof. dr. ir. J. Biemond	Technische Universiteit Delft
Prof. dr. ir. J.P.M.G. Linnartz	Technische Universiteit Eindhoven
Prof. dr. ir. L.P. Ligthart	Technische Universiteit Delft

ISBN 9780-90-79746-03-3

Author email: n.f.kiyani@gmail.com

To Abujee and Mamajee

Let your deeds themselves praise you, for here I leave them in all their glory, lacking words to extol them. – Cervantes, Don Quixote de la Mancha

Summary

Wireless Communication Systems using Signal Space Diversity

The next generation communication devices are foreseen to not only support a large variety of applications, ranging from speech, audio and video graphics but also be able to maintain connection with many other devices (rather than a single base station) in different changing environments. The aim of the dissertation is to analyze digital modulation and coding techniques for wireless communication systems in realistic transmission scenarios. Furthermore, an important objective of the dissertation is to explore the degrees of freedom that can make the wireless communication systems overall more adaptive, thereby, resulting in systems that either consume less power for a given performance or offer more performance for a given amount of average energy than conventional systems. The techniques/algorithms analyzed in the dissertation are versatile and suitable for both narrowband as well as wideband wireless communication systems for indoor and low-mobility outdoor scenarios.

Signal space diversity, also known as modulation diversity, is used to increase

the overall received signal-to-noise ratio (SNR) and to reduce the probability of error. A thorough performance analysis of modulation diversity systems is presented in the thesis to understand the differences from conventional systems in narrowband and wideband channels and also to achieve the maximum possible performance. General methods are presented to optimize the system parameters and to exploit the degrees of freedom available. Channel coding, cooperative demodulation and decoding, and orthogonal frequency division multiplexing (OFDM) schemes are coupled with modulation diversity to reduce the overall power consumption and improve system performance.

Nauman F. Kiyani

This research was financially supported by the Dutch Technology Foundation (Stichting voor de Technische Wetenschappen (STW)) under the framework of multicarrier adaptive transceiver (McAT) project DTC. 6438.

Contents

Chapter 1

Introduction

In this chapter, fundamentals of the wireless communication channels, the criteria to measure or analyze the performance of a wireless communication system, the contribution and an overview of the structure of the thesis are presented. Throughout, the dissertation it is assumed that the reader is familiar with the basic theory of wireless communication and for the sake of clarity and comprehension, occasionally, certain concepts of relevance are briefly reviewed. Initially, in this chapter an introduction to the current and emerging wireless systems and services and their ever growing need of higher data rates and stringent quality of service requirements is presented in a historical context. The main hinderance, i.e., the land mobile radio channel, and the tools to analyze the performance of a wireless system in a land mobile radio channel are briefly reviewed. Finally, the scope, the contribution, and the organization of the thesis are presented.

1.1 Background

To communicate means *"to convey knowledge of or information about: make known"*.[1] Communication has been an integral part of the human society since the very dawn of mankind. The ability to communicate amongst and far beyond has been an archaic human desire and endeavor. The fulfillment of which has led to the spread of knowledge, civilization and scientific growth of human societies. In the last millennium, we have very rapidly moved from fire and animal based messaging to electrical signals. As we step forward in the new millennium wireless technologies are leading the way in which we communicate.

Wireless systems and services have undergone an extraordinary change in the last few decades. From analog based systems in early and mid-1980s, known as the first generation (1G) systems, to digital modulation based telephony systems in the early 1990s known as the second generation (2G) wireless systems [1] offering better spectral efficiency and voice quality. Third-generation (3G) wireless systems have evolved from the previous generations with an aim to provide universal access and global roaming. More importantly, 3G and beyond systems, are expected to provide support to multidimensional (multi-information media, multi-transmission media and multi-layered network) high speed wireless communication systems [2]. The convergence of telephony with internet in the coming years is expected to raise the data rates required for each hand-held device towards 600Mb/s [1–3]. This convergence is already having a deep impact not only on economies but also on societies and human behavior. Future communication systems for radio local-area networks used for, e.g., video streaming, data streaming, "hot-spots", hand-held gaming devices, interactive TV and wireless ethernet, i.e., the successors of 3G are envisioned to be,

[1] Defined as per Merriam-Webster dictionary

- broadband: support high data rates,
- low-power: energy efficient to ensure long talk and standby times,
- adaptive: to accommodate varying channel and application requirements.

These systems are intended to provide voice, data and multimedia services while satisfying more stringent availability and quality of service (QoS) requirements.

It has become increasingly clear that dominant consideration in the design and employment of such systems would be their ability to perform with a high QoS over any mobile radio channel perturbed by a host of impairments [4–8]. The multipath fading effect of the mobile radio channel has plagued the system designers for over half a century but the evolution of communication systems has further motivated the research to overcome and provide newer solutions to achieve even better QoS.

The above exegesis leads us to two basic themes to be introduced in this chapter, i.e., mobile radio channels and QoS measures. In Section 1.2 the principal characteristics and models for fading channels are briefly reviewed. Section 1.3 overviews the several measures of performance related to evaluation of QoS. The scope and the frame work of the thesis is presented in Section 1.4. Finally, in Sections 1.5 and 1.6, the organization and a summary of the contributions of the dissertation is presented, respectively.

1.2 Mobile Radio Channels

The design of an efficient wireless communication system requires a comprehensive understanding of the radio propagation environment. However, the radio wave propagation through wireless channels is a complicated phenomenon characterized

by various effects such as operating frequency, the mode of propagation, i.e., line-of-sight (LoS) radio links, multipath, diffraction/scatter and shadowing. The characterization and statistical modeling of these effects has been extensively studied in the literature, e.g., [4–9]. The result is a range of relatively simple and statistically accurate models for a particular propagation environment and underlying communication scenario.

In this section, we briefly review the principal characteristics and models for fading channels to be discussed in the rest of the dissertation. For detailed analysis we refer the reader to [4–9] and the references therein.

1.2.1 Main Characteristics

When a received signal experiences fading during transmission the main characteristics of the received signal to be considered are:

- envelope and phase variation,
- slow and fast fading,
- frequency flat and frequency selective fading.

The envelope and phase of the received signal fluctuate over time in a fading environment. For coherent communication systems phase variation can severely degrade the system performance. Generally, in literature the systems are analyzed by assuming perfect phase effect correction at the receiver and, therefore, such systems are referred to as ideal coherent demodulation systems. For non-coherent systems, the phase information is not needed. However, for both coherent and non-coherent systems knowledge of the fading envelope characteristics is required.

Slow and fast fading is characterized by the channel coherence time T_c. T_c is defined as the period of time in which the fading is correlated. The coherence

time is also related to the channel Doppler spread f_d [10],

$$T_c \simeq \frac{1}{f_d}. \tag{1.1}$$

If the symbol duration, T_s, is smaller than T_c, then the fading is said to be slow; otherwise it is considered fast. In fast fading, the fading is uncorrelated from symbol to symbol whereas in slow fading a particular fade level would affect many consecutive symbols leading to burst errors. Therefore, it becomes important to consider the variation of the fading channel from one symbol to another. Correlation models are used to determine the variations. Some of these models are tabulated in Table 1.1 with their respective autocorrelation models and power spectral densities (PSD) with the variance of the fading process normalized to unity.

Table 1.1: *Spectra and Autocorrelation properties of different types of fading process.*

Type of Fading Spectrum	Fading Autocorrelation	Normalized PSD
Rectangular	$\frac{\sin(2\pi f_d T_s)}{2\pi f_d T_s}$	$(2f_d)^{-1}, \quad \lvert f\rvert \leq f_d$
Land Mobile	$J_0(2\pi f_d T_s)$	$\left\{\pi^2(f^2-f_d^2)\right\}^{-1/2}, \quad \lvert f\rvert \leq f_d$
Gaussian	$exp\left[-(\pi f_d T_s)^2\right]$	$exp\left[-\left(\frac{f}{f_D}\right)^2\right](\sqrt{\pi} f_d)^{-1}$

Data from [10]
$J_0(\cdot)$ is the zero-order Bessel function of the first kind.

An important aspect of fading channels is frequency selectivity which is dependent upon the transmitted signal's bandwidth in comparison to the coherence bandwidth of the channel f_{ch} . In addition, f_{ch} is related to the maximum delay spread of the channel $\tau_{\max}$ by

$$f_{ch} \simeq \frac{1}{\tau_{\max}}. \tag{1.2}$$

The fading is said to be *frequency nonselective* or *frequency flat* , if all the spectral components of the transmitted signal are affected in a similar manner. Equivalently, it implies that the transmitted signal's bandwidth is smaller than f_{ch}. Such a system is also referred to as *narrowband* system. Conversely, if the transmitted signal is affected by different amplitude gains and phase shifts, the fading is said to be *frequency selective*. Furthermore, the system is said to be *wideband* as the transmitted signal's bandwidth is larger than the f_{ch}. A measure of the frequency range over which the fading process is correlated is also given by f_{ch}.

1.2.2 Modeling of Flat Channels

The narrowband systems are affected by the fading channels' amplitude and phase. The amplitude, α is a random variable (RV) with a probability density function (PDF), $p(\alpha)$, which is dependent on the nature of the radio propagation environment. The mean square value of α is denoted as $E[\alpha^2] = \Omega$. $E[\cdot]$ denotes the statistical average. The transmitted signal is further perturbed by additive white Gaussian noise (AWGN), characterized by a one-sided PSD N_0 (W/Hz), which is assumed to be statistically independent of fading. The instantaneous signal-to-noise power ratio (SNR) per bit is given by $\gamma = \alpha^2 E_b/N_0$ and the average SNR per bit by $\bar{\gamma} = \Omega E_b/N_0$, where E_b is the energy per bit. The amount of fading (AF) or fading figure as defined by [11] gives a measure of the severity of fading and is given as

$$AF = \frac{\mathrm{var}(\alpha^2)}{E[\alpha^2]^2} = \frac{E[(\alpha^2 - \Omega)^2]}{\Omega^2}, \tag{1.3}$$

where $\mathrm{var}(\cdot)$ denotes the variance.

The constructive or destructive combination of randomly delayed, reflected, scattered and diffracted signals results in a multipath fading effect. This fading

results in short-term signal variations as the fading is relatively fast. The statistical behavior of the fading envelope is described by a family of distributions, e.g., Rayleigh , Nakagami-n (Rice), Nakagami-m, log-normal and composite multipath/shadowing. In the following discussion we confine ourselves to Rayleigh, Nakagami-n and Nakagami-m distributions and present a brief overview.

Rayleigh Model

In the absence of a direct line-of-sight (LOS) path, the channel amplitude, α, has a Rayleigh distribution given as [5]

$$p(\alpha) = \frac{\alpha}{b_0} e^{\left(-\frac{\alpha}{2b_0}\right)}, \tag{1.4}$$

where average envelope power $E[\alpha^2] = \Omega = 2b_0$, implying

$$p(\alpha) = \frac{2\alpha}{\Omega} e^{\left(-\frac{\alpha^2}{\Omega}\right)}, \qquad \alpha \geq 0. \tag{1.5}$$

The instantaneous SNR per bit of the channel, γ, is associated with the squared envelope α^2 and is exponentially distributed at any time with PDF

$$p(\gamma) = \frac{1}{\bar{\gamma}} e^{\left(\frac{\gamma}{\bar{\gamma}}\right)}, \qquad \gamma \geq 0. \tag{1.6}$$

In addition the moment associated with this fading can be shown to be given as

$$E[\gamma^k] = \Gamma(1+k)\bar{\gamma}^k, \tag{1.7}$$

where $\Gamma(\cdot)$ is the gamma function [12]. The experimental data for mobile systems with no LOS paths between the transmitter and receiver are in good agreement with the Rayleigh fading model [5]. Furthermore, Rayleigh fading propagation

models also apply to troposphere [13], ionosphere [14] and ship-to-ship [15] radio links.

Nakagami - n Model

In the presence of one strong direct LOS component, Nakagami-n, also known as Rice distribution [16], is employed to model the radio link. The channel fading amplitude, α, follows the distribution given by [17]

$$p(\alpha) = \frac{2(1+n^2)e^{-n^2}\alpha}{\Omega} e^{\left[-\frac{(1+n^2)\alpha^2}{\Omega}\right]} I_0\left(2n\alpha\sqrt{\frac{1+n^2}{\Omega}}\right), \quad \alpha \geq 0, \tag{1.8}$$

where $I_0(\cdot)$ is the modified Bessel function of the first kind and n is the Nakagami-n factor related to the Rician K factor by $K = n^2$. Furthermore, γ has the following non-central chi-square distribution

$$p(\gamma) = \frac{K+1}{\bar{\gamma}} e^{\left[-\frac{(K+1)\gamma}{\bar{\gamma}}\right]} I_0\left(2\sqrt{\frac{K(K+1)\gamma}{\bar{\gamma}}}\right), \quad \gamma \geq 0. \tag{1.9}$$

The moments associated with this model are given by [17]

$$E[\gamma^k] = \frac{\Gamma(1+k)^{\,k}}{1+K} \, {}_1F_1(-k;1;-K)\bar{\gamma}^k, \tag{1.10}$$

where ${}_1F_1(\cdot;\cdot;\cdot)$ is the Kummer confluent hypergeometric function [12].

Nakagami - m Model

The Nakagami-m distribution fits the empirical data and is known to provide a closer match to land-mobile and indoor multipath propagation [18–20], as well as scintillating ionospheric radio links [14]. The Nakagami-m distribution describes

the magnitude of the received envelope by the distribution

$$p(\alpha) = \frac{2m^m \alpha^{2m-1}}{\Omega^m \Gamma(m)} \exp\left(-\frac{m\alpha^2}{\Omega}\right), \quad \alpha \geq 0 \tag{1.11}$$

where m is the Nakagami-m fading parameter which ranges from $\frac{1}{2}$ to ∞. Figure 1.1 shows the Nakagami-m PDF for different values of m. The instantaneous

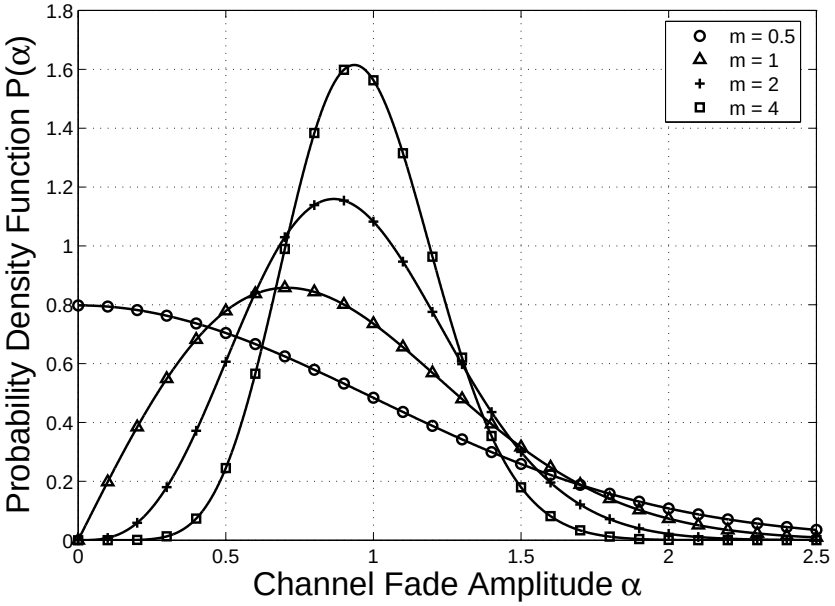

Figure 1.1: *Nakagami PDF for $\Omega = 1$ and various values of the fading parameter m.*

SNR, γ, has a gamma distribution given by

$$P(\gamma) = \left(\frac{m}{\bar{\gamma}}\right)^m \frac{\gamma^{m-1}}{\Gamma(m)} \exp\left(-\frac{m\gamma}{\bar{\gamma}}\right), \quad \gamma \geq 0, \quad m \geq 0.5, \tag{1.12}$$

and the moments can be given as

$$E[\gamma^k] = \frac{\Gamma(m+k)}{\Gamma(m)m^k} \bar{\gamma}^k. \tag{1.13}$$

The Nakagami-m distribution spans via the m-parameter the widest range of all the multipath distributions. It can model fading conditions that are either more or less severe than the Rayleigh fading and when $m = 1$, the Nakagami-m distribution becomes the Rayleigh distribution. The one-sided Gaussian distribution is modeled with $m = 1/2$ and when $m \to \infty$ the distribution converges to a nonfading AWGN channel. Furthermore, the Rice distribution can be closely approximated by using the following relation between the Rice factor K and the Nakagami shape factor m [5]:

$$\begin{aligned} K &= \frac{\sqrt{m^2 - m}}{m - \sqrt{m^2 - m}}, \quad m > 1 \\ m &= \frac{(K+1)^2}{(2K+1)} \end{aligned} \tag{1.14}$$

1.2.3 Modeling of Frequency-selective Channels

The fading caused by a frequency selective channel can be modeled as a linear filter characterized by a complex valued low pass equivalent impulse response [4],

$$h(t) = \sum_{l=1}^{L} \alpha_l e^{-j\theta_l} \delta(t - \tau_l), \tag{1.15}$$

where l is the channel path index, L is the number of resolvable paths, $\delta(\cdot)$ is the Dirac delta function and $\{\alpha\}_{l=1}^{L}$, $\{\theta\}_{l=1}^{L}$ and $\{\tau\}_{l=1}^{L}$ are the random channel amplitudes, phases and delays, respectively. The first channel with delay $\tau_1 = 0$, without a loss of generality [4, 5], is assumed to be the reference channel and $\tau_1 < \tau_2 < \cdots < \tau_L$. Under the slow fading assumption, L is assumed to constant over a symbol interval and the sets $\{\alpha\}_{l=1}^{L}$, $\{\theta\}_{l=1}^{L}$ and $\{\tau\}_{l=1}^{L}$ are mutually independent and constant. If the various paths of a given impulse response are

generated by different scatterers, they tend to exhibit negligible correlations [21] and it is therefore, reasonable in that case to assume that $\{\alpha\}_{l=1}^{L}$ are statistically independent RVs. However, if the fading is correlated the $\{\alpha\}_{l=1}^{L}$ are considered as correlated RVs [22–24].

Similar to the flat fading models, the fading amplitude α_l of the l^{th} resolvable path is assumed to be a RV with a mean square value $E[\alpha^2] = \Omega$ and a PDF described by any family of distributions (Rayleigh, Rice or Nakagami-m) as described before. Also, as in the flat fading channel a wideband signal is perturbed by AWGN with a one-sided power spectral density N_0 (W/Hz). The instantaneous SNR per bit of the l^{th} channel is given by $\gamma_l = \alpha_l^2 E_b/N_0$ and the average SNR per bit of the l^{th} channel is given by $\bar{\gamma}_l = \Omega_l E_b/N_0$. The average fading power is typically assumed to follow an exponentially decaying power delay profile (also referred to as the multipath intensity profile (MIP)) with equispaced delays. The MIP can be given as

$$\bar{\gamma}_l = \bar{\gamma}_1 e^{-\varsigma(l-1)}, \tag{1.16}$$

where $l = 1, 2, \cdots, L$, $\bar{\gamma}_1$ is the average SNR of the first (reference) propagation path and ς is the average fading power decay factor.

Indoor office buildings [21] and congested urban areas [25] are characterized very well by an exponentially decaying power delay profile. It is important to state that in the impulse response the first arriving path typically exhibits a lower amount of fading than subsequent paths, since it may contain the LOS path [26]. Furthermore, since the specular power component typically decreases with respect to delay, the last arriving paths exhibit higher amounts of fading [26, 27].

1.3 System Performance Measures

The three most important criteria to measure or analyze the system performance are

- average signal-to-noise ratio,
- outage probability,
- average bit error probability.

Average signal-to-noise ratio (SNR), $\bar{\gamma}$, is the most commonly used measure to characterize a digital communication system. It is typically very easy to evaluate and serves as an excellent indicator of the overall fidelity of the system. It is commonly measured at the receiver and thus is directly related to the data detection process.

Outage probability (P_{out}) is defined as the probability that the instantaneous SNR, γ, falls below a certain specified threshold, γ_{th}, or equivalently the probability that the instantaneous error probability exceeds a specified value. Thus, P_{out} can be given as

$$P_{\text{out}} = \int_0^{\gamma_{th}} p(\gamma)\mathrm{d}\gamma, \tag{1.17}$$

where $p(\gamma)$ is the PDF of γ. P_{out} is the cumulative distribution function (CDF) of γ evaluated at $\gamma = \gamma_{th}$.

Average bit error probability (BEP) is one of the most revealing performance criterion of a communication system. It is able not only to describe the system performance but also sheds light on the system behavior. However, it is the most difficult of the three to compute as it is a nonlinear function of the instantaneous SNR dependent upon the modulation/detection scheme being employed by the system.

1.4 Framework and Scope of the Thesis

In this section, we present the motivation and the context of the research presented in this dissertation. Initially a short background is presented for the research problems addressed in the dissertation. It is not our intention to present an exhaustive literature survey and, therefore, we present a brief summary of the relevant literature background and give a comparison with our work.

The next generation communication devices are foreseen to not only support a large variety of applications, ranging from speech, audio and video graphics but also be able to maintain connection with many other devices (rather than a single base station) in different changing environments. These devices are to be position aware but also be "*wearable*" rather than portable. Such small devices demand a small battery but a long talk or standby time. The combination of both, a large array of functionalities and a small power supply thus requires the development of low-power, efficient communication algorithms to achieve low energy consumption.

The aim of the dissertation is to analyze digital modulation and coding techniques for wireless communication systems in realistic transmission scenarios. Furthermore, to explore the degrees of freedom that can be exploited to make the wireless communication systems overall more adaptive, thereby, resulting in a system that either consumes less power for a given performance or offers more performance for a given amount of average energy than a conventional system. The techniques/algorithms have to be versatile and suitable for both narrowband as well as wideband wireless communication systems for indoor and low-mobility outdoor scenarios. It is important to state that the choice of a proper modulation and channel coding scheme is in itself, is a trade-off between efficiency, reliability and complexity. Channel coding techniques allow for reduced power

consumption as compared to the uncoded case but result in more latency and complexity. Another important aspect for performance improvement is diversity. Diversity, a very well known concept, has the greatest potential for radio link performance improvement. Under this broader scope the initial task is to short list the potential candidates for modulation, coding and diversity. Signal space diversity (SSD), also known modulation diversity, a relatively new diversity technique is a strong candidate. Any diversity technique tries to provide statistically independent copies of the transmitted sequence at the receiver to increase the overall received SNR and to reduce the detection error. Diversity tries to exploit the low probability of occurrence of deep fades in all the diversity branches and, therefore, is able to lower the overall probability of error and outage. Many techniques have been proposed to achieve the independence of the channels required by diversity. SSD is an attractive option as it does not require any bandwidth or power expansion. Moreover, it takes advantage of the inherent orthogonality in signal space to achieve gain in fading channels. Subsequently, we provide a brief literature overview of signal space diversity and the associated problems that we investigated in our research.

Literature Overview and Problems Addressed: Signal space diversity (SSD), also known as coordinate interleaving or modulation diversity, was proposed in 1996 [28] as coordinate interleaving scheme for performance improvement over fading channels. In 1998 [29], the same scheme was introduced as an improved PSK scheme for fading channels and was generalized in 1998 [30] as a signal space diversity scheme. In 2003 [31], it was presented as modulation diversity scheme for frequency selective channels, however, the emphasis was on equalization techniques. The great interest in SSD is due to the fact that the scheme does not require bandwidth and power expansion. Furthermore, the SSD leads to significant performance im-

provement over conventional wireless communication systems. The basic premise of SSD systems is to use rotated multidimensional signal constellations where the components of the signal constellation points are sent over independent fading channels. The independence of fading channels can be accomplished by the use of interleavers.

Although the research community is showing great interest in SSD there are certain important research questions left unanswered. These research problems can be categorized under these broad terms.

Performance analysis: A thorough performance analysis of modulation diversity systems is required to understand the differences from conventional systems in narrowband and wideband channels and also to achieve the maximum possible performance.

Criteria to optimize system parameters: A general method is required to optimize the system parameters for multilevel signal constellations in narrowband and wideband channels.

Impact of practical impairments: Practical impairments, for instance, phase noise and outdated channel estimates, degrade the wireless communication systems' performance. Therefore, it is required to analyze the wireless communication systems using SSD in the presence of these practical impairments to be considered as a viable solution for wireless applications.

Extension with Channel coding: All the current wireless communication systems use channel coding for improved performance. Therefore, it is needed to analyze SSD systems' performance with forward error correcting codes and to identify the criteria to optimize the systems' parameters.

Iterative demodulation and decoding: Cooperative demodulation and chan-

nel decoding leads to enhanced performance. Wireless communication systems using SSD need to be analyzed with iterative demodulation and decoding schemes and the factors or degrees of freedom need to be identified.

Extension with multicarrier modulation schemes: Multicarrier modulation schemes provide a simple solution to intersymbol interference (ISI) and, therefore, are being widely used in wireless applications. Extension of SSD with multicarrier modulation schemes is needed to provide not only better QoS but also, to provide compatibility with current wireless communication systems.

These research problems are addressed in the dissertation. In the subsequent section we present a summary of all the major results of the dissertation.

Framework: This research was financially supported by the Dutch Technology Foundation (Stichting voor de Technische Wetenschappen (STW)) under the framework of multicarrier adaptive transceiver (McAT) project DTC. 6438. The research was a part of the research activities of the Electronics Research Laboratory and the Wireless and Mobile Communications Group both part of the Faculty of Electrical Engineering Mathematics and Computer Science (EEMCS) of Delft University of Technology, Delft, the Netherlands.

1.5 Summary of the Main Results

Summary of the contributions of the dissertation are given below:

- We analyze the performance of an uncoded system using modulation diversity in a general Nakagami multipath fading channel, with arbitrary fading parameter. Closed form expressions are derived to determine the perfor-

mance in terms of average SNR and average BEP for correlated and uncorrelated multipath fading channels. Furthermore, we also highlighted the effect of different symbol constellation mappings on the system performance.

- We analyze the effect of phase noise on the performance of an uncoded system in a general Nakagami multipath fading channel. We derive closed form expressions for average BEP in terms of average SNR for partially coherent systems employing modulation diversity.

- We analyze the performance of maximum ratio combining (MRC) coupled with modulation diversity in correlated and uncorrelated Nakagami multipath frequency selective fading channels with a single symbol transmission assumption. Different correlation models for channel paths are considered. We derive closed expressions for average BEP in terms of average SNR for systems using modulation diversity and operating in frequency selective channels when no cochannel and inter-symbol interference is considered (under the assumption of single symbol transmission).

- The effect of channel estimation error on the performance of MRC receivers with modulation diversity is also investigated in frequency selective multipath fading channels. A closed form expression for average BEP in terms of average SNR with outdated or imperfect channel estimates is derived. Furthermore, the effect of different signal constellation mappings on the system performance is also highlighted.

- Modulation diversity with practically sized regular random low density parity check (LDPC) and convolution codes is proposed and the performance in terms of average SNR and average BEP is analyzed and compared to an uncoded modulation diversity receiver.

- Iterative demodulation and decoding of coded modulation diversity using LDPC and convolutional codes is proposed. A symbol-to-bit de-mapper for multi-level modulation schemes is extended to incorporate iterative demodulation with SSD. The performance in terms of average SNR and average BEP is analyzed and the factors effecting the performance are identified and analyzed.

- Extrinsic information transfer (EXIT) charts are used to analyze the performance of a system employing iterative demodulation and decoding with modulation diversity. Factors (degrees of freedom) that can effect the convergence behavior of the iterative demodulation and decoding of the proposed system are identified and their effect are analyzed.

- An extension of coded system with modulation diversity, iterative demodulation and decoding (ID), and orthogonal frequency division multiplexing (OFDM) (OFDM SSD-ID) in a frequency selective fading channel is presented. The factors effecting the performance of the system such as, the choice of error correcting codes, the rotation angle, the constellation mapping and the SNR region of operation, are analyzed. Furthermore, EXIT charts are also employed to analyze the convergence behavior and the degrees of freedom available.

1.6 Organization of the Thesis

The dissertation can be broadly divided into two major parts. In the first part, comprising of Chapters 2 and 3, the uncoded system performance in narrowband and wideband channels is analyzed, while in the second part, comprising of Chapters 4, 5 and 6, the coded systems' performance is analyzed in narrowband and

wideband channels. In both parts modulation diversity is considered as the possible technique to mitigate fading and to meet the required QoS requirements. At the start of each chapter an abstract of the chapter is provided to facilitate the reading.

1.6.1 Uncoded Systems

Chapter 2 firstly provides an overview of modulation diversity and a generic uncoded model of a system employing SSD in frequency flat channels. A performance analysis of the system employing SSD is presented in different fading environments. Furthermore, the performance analysis of a system impaired by the presence of phase noise is also investigated.

In Chapter 3, performance analysis of a system employing coordinate interleaving and constellation rotation in frequency selective fading channels for L-branch maximum ratio combining (MRC) is presented. The achievable performance with MRC is analyzed in correlated and uncorrelated Nakagami multipath fading channels for single symbol transmission. The effect of channel estimation errors is also investigated.

1.6.2 Coded Systems

Chapters 4, 5 and 6 consider channel coding coupled with SSD in frequency flat and frequency selective channels.

In Chapter 4, we present a brief overview of low density parity check (LDPC) codes and convolutional codes. Furthermore, a comparison of a coded modulation diversity system, using LDPC and convolution codes, with an uncoded system is presented for multi-level modulation schemes.

In Chapter 5, the highly promising scheme known as bit interleaved coded

modulation (BICM) with iterative decoding and demodulation (BICM-ID) is also considered and modified to incorporate modulation diversity. Furthermore, an SSD BICM-ID system is proposed and closed form expressions are derived to analyze its performance in comparison to conventional BICM-ID systems. Extrinsic information (EXIT) charts are used to analyze the impact of the rotation angle on the performance of the system. Factors (degrees of freedom) that effect the convergence behavior of the iterative demodulation and decoding of the proposed system are identified and their effect is analyzed.

In Chapter 6, the analysis of the system is extended to frequency selective channels. The proposed SSD BICM-ID scheme is coupled with OFDM and an analysis is presented. EXIT chart analysis is carried out and various factors effecting the convergence of iterative demodulation and decoding are highlighted.

Lastly, in Chapter 7, we present the conclusions and the major contributions of the dissertation. Also, we highlight a number of issues which remain unsolved and may constitute a possible list of topics for future research.

Chapter 2

Analysis of SSD Systems in Narrowband Channels

In this chapter an introduction to modulation diversity, also known as signal space diversity (SSD), is presented. It is shown that modulation diversity provides a significant performance gain in Nakagami multipath fading environments as compared to the conventional systems. Closed form expressions for average probability of bit error (P_b) are derived in terms of average SNR for coherent and partially coherent systems employing modulation diversity in Nakagami multipath fading environments with arbitrary fading parameters. Furthermore, the effect of symbol mappings and the choice of the rotation angle on the system performance is also highlighted.

2.1 Introduction

The wireless communication systems are adversely affected by fading. The transmitter has to deliver more power, in some cases much more than an additive white Gaussian noise (AWGN) channel to achieve the same average probability of bit error P_b. To combat fading and to reduce the overall transmit power requires an effective technique, for instance, diversity. Diversity is a classic and a well documented concept [4, 5, 7, 8, 32] that can mitigate the performance degradation caused by fading channels. Diversity is a prime candidate for current and emerging wireless communication systems to provide radio link performance improvement and to meet the stringent quality of service (QoS) requirements.

Any diversity technique tries to provide statistically independent copies of the transmitted sequence at the receiver to increase the overall received signal-to-noise ratio (SNR) and to reduce the detection error. Diversity tries to exploit the low probability of occurrence of deep fades in all the diversity branches and therefore, is able to lower the overall probability of error and outage. Many techniques have been proposed to achieve the independence of the channels required by diversity. Some of the most important can be categorized as:

- Space diversity by using multiple receive antennas (also known as antenna diversity).
- Antenna polarization diversity by using cross-polarized antennas in the receiver. Only two diversity branches are available while in space diversity any number of branches, in principle, can be made available.
- Frequency diversity by using multiple frequency channels whose separation is larger than the coherence bandwidth of the channel. Some examples are frequency hopping or multicarrier systems.

- Time diversity by using different time slots separated by an interval longer than the coherence time of the channel.
- Multipath diversity by resolving different multipath components at different delays.
- Signal space diversity (SSD), (also known as coordinate interleaving or modulation diversity) by sending the components of multidimensional signal constellation point over independent fading channels. It is a recently proposed scheme with great potential.

In this chapter and in general in this dissertation, we would focus on SSD and analyze its performance with other conventional diversity and conventional communication systems. SSD is not a new technique as it was first introduced in 1996 [28] and generalized in [30]. Ever since, the very conception of SSD, the research community has shown great interest in it. However, there are certain important research questions remaining unanswered which prove the viability of employing SSD in wireless communication systems. Some of the these questions include the exact calculation of optimum rotation angles, the effect of different signal constellation mappings and the realistic effect of phase noise on system performance. In this chapter we analyze and present closed form expressions for the maximum achievable performance of SSD systems in various frequency flat fading scenarios. The SSD system seem vulnerable to error in phase noise. We investigate this effect and present close expressions for average P_b in terms of average SNR and phase noise.

The rest of the chapter is organized as follows. Section 2.2 introduces modulation diversity. A generic system model description is presented in Section 2.3, followed by an intuitive reasoning to the gain provided by the modulation diversity system in Section 2.4. Section 2.5 presents the performance analysis

of a conventional QPSK system in Nakagami-m multipath fading channels with arbitrary fading parameter. Section 2.6 presents closed form expressions for average bit error probability in terms of average SNR for SSD systems in various fading scenarios including correlated and uncorrelated fading environments. An upper bound on the P_b is derived and the effect of signal constellation rotation and signal constellation mapping is highlighted. Section 2.7 presents a practical impediment, i.e., phase noise, to the maximum achievable performance promised by the previous sections for a system employing SSD. Closed form expressions for average bit error probability of SSD systems operating in the presence of phase noise are derived. Lastly, in Section 2.8 we conclude the chapter by summarizing the results and the major contributions.

2.2 Signal Space Diversity

Signal space diversity (SSD), also referred to in the literature as modulation diversity [31] or coordinate interleaving [28], can provide performance improvement over fading channels without using extra bandwidth and power expansion [28–31, 33–40]. The basic premise of SSD is that multidimensional signal constellations are used and the components of each signal constellation point are transmitted over independent fading channels. The independence of the fading channels can easily be accomplished by interleaving.

It was argued that maximizing the minimum squared Euclidean distance between the signal points does not necessarily minimize the error probability over fading channels [41]. Therefore, an optimum scheme for an AWGN channel may not be the best possible solution for a fading channel. It was shown in [29, 30] that for a block fading wireless communication link, diversity can be introduced into the system by separately interleaving the in-phase and quadrature compo-

nents of a QPSK scheme and by performing symbol-by-symbol detection. The performance of such a scheme was shown to be dependent upon the constellation rotation angle in a fading channel and is not affected when employed in an AWGN channel.

In the following section we present a generic model for a system employing SSD.

2.3 System Model

In M-ary phase shift keying (MPSK) or M-ary quadrature amplitude modulation (MQAM) constellations the inphase (I) and the quadrature phase (Q)-channels are orthogonal and can be separated at the receiver[1]. It is assumed that the channel state information (CSI) is available via channel estimation techniques at the receiver. For instance, one common method to estimate the channel is by the use of pilot symbol assisted modulation (PSAM) [43], which periodically inserts pilots into the stream of data symbols to extract the channel induced fading.

Figure 2.1 shows a block diagram of a system employing coordinate interleaving and constellation rotation, hereafter referred as an "SSD system". The concept of coordinate interleaving and constellation rotation is generic to all MPSK/MQAM constellations. We confine ourselves to MPSK signal constellations. A conventional MPSK signal constellation is denoted by

$$\mathcal{S}_M = \{s_l = e^{j2\pi(l/M)} : l = 0, 1, \ldots, M-1\}, \tag{2.1}$$

where the energy has been constrained to unity and each symbol corresponds to

[1]For further details on MPSK and MQAM we refer the reader to [42].

$m = \log_2 M$ bits. Anti-clockwise rotation over an angle θ leads to the constellation

$$\mathcal{S}_M^\theta = \{s_l = e^{j(2\pi(l/M)+\theta)} : l = 0, 1, \ldots, M-1\}. \tag{2.2}$$

The symbol mapper can be represented by a one-to-one mapping function $\wp$: $\{0,1\}^m \rightarrow \mathcal{S}_M^\theta, s = \wp(\mathbf{b})$, where, $\mathbf{b} = (b_1, \cdots, b_m), b_j \in \{0,1\}$ represents the binary sequence and s is chosen from the set $\mathcal{S}_M^\theta$ consisting of M complex signal points. In case of N symbol transmission, let the sequence of rotated I and Q - components be denoted as $\mathbf{x} = (x_0, x_1, \ldots, x_{N-1})$ and $\mathbf{y} = (y_0, y_1, \ldots, y_{N-1})$, respectively. Let η and μ represent the I and Q interleavers, resulting in sequences $\tilde{\mathbf{x}} = \eta(\mathbf{x}) = (\tilde{x}_0, \tilde{x}_1, \ldots, \tilde{x}_{N-1})$ and $\tilde{\mathbf{y}} = \mu(\mathbf{y}) = (\tilde{y}_0, \tilde{y}_1, \ldots, \tilde{y}_{N-1})$, respectively. The transmitted waveform for the rotated and interleaved system is given by

$$\begin{aligned} \tilde{s}(t) &= \sum_{i=0}^{N-1} \tilde{x}_i g(t - iT_s)\cos(2\pi f_c t) \\ &+ \sum_{i=0}^{N-1} \tilde{y}_i g(t - iT_s)\sin(2\pi f_c t), \end{aligned} \tag{2.3}$$

where

$$g(t) = \begin{cases} 1, & 0 \le t \le T_s, \\ 0, & \text{otherwise}, \end{cases}$$

T_s is the symbol period and f_c is the carrier frequency.

For QPSK only two symbol mappings are possible, i.e., Gray and Natural, whereas for 8PSK and higher PSK a large array of signal constellation mappings are possible as was shown for 8PSK in [44]. For conciseness, we use an M-element vector $(a_0, \cdots, a_{M-1})$ to represent an MPSK mapper where a_n is the decimal number of the binary representation of the rotated MPSK signal constellation

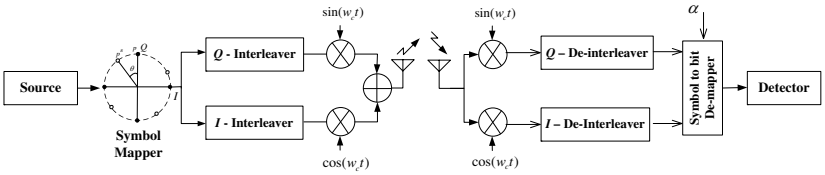

Figure 2.1: *System model (referred to as SSD system).*

Table 2.1: *Symbol representations and bit-maps for unrotated QPSK.*

QPSK symbols	$s_0 = 1$	$s_1 = j$	$s_2 = -1$	$s_3 = -j$
bit-map (Gray)	00	01	11	10
bit-map (Natural)	00	01	10	11

point. For instance, the Gray and Natural mapping for QPSK can be given as $(0, 1, 3, 2)$ and $(0, 1, 2, 3)$, respectively. We, in this chapter confine ourselves to QPSK signal constellation for comparison with results in literature. For the QPSK the symbol representations and the associated bit-maps are also given in Table 2.1.

The communication channel is assumed to be frequency non-selective slowly fading with a multiplicative factor representing the fading effect and an additive term representing the additive white Gaussian noise. The received signal samples in baseband can be given as

$$\tilde{r_i} = |\tilde{\alpha_i}|e^{j\tilde{\phi_i}}\tilde{s_i} + \tilde{n_i}, \quad i = 0, \cdots, N-1, \tag{2.4}$$

where $\tilde{\alpha_n} = |\tilde{\alpha_n}|e^{j\tilde{\phi_n}}$ are statistically independent random variables with a probability density function (PDF) described by any of the family of distributions, e.g., Rayleigh, Nakagami-n (Rice) or Nakagami-m. $\tilde{\phi_n}$ represents the phase shift that is introduced by the fading channel, $\tilde{s_i}$ is the transmitted symbol and $\tilde{n_i}$ are

complex Gaussian random variables with zero mean and a variance of $N_0/2$ in each dimension. As CSI is available at the receiver, the phase shift, therefore, can be removed without any error. Thus after phase removal the received sample takes the form

$$\tilde{r_i} = |\tilde{\alpha_i}|\tilde{s_i} + \tilde{z_i}, \tag{2.5}$$

where $\tilde{z_i} = \tilde{z_i}^I + j\tilde{z_i}^Q$ represents the complex white Gaussian noise. The received sequences $\tilde{\mathbf{r}}^{\mathbf{I}}$ and $\tilde{\mathbf{r}}^{\mathbf{Q}}$ are de-interleaved resulting in $\mathbf{r}^{\mathbf{I}} = \eta^{-1}(\tilde{\mathbf{r}}^{\mathbf{I}})$ and $\mathbf{r}^{\mathbf{Q}} = \rho^{-1}(\tilde{\mathbf{r}}^{\mathbf{Q}})$. The fading sequence $\tilde{\alpha} = (\tilde{\alpha}_0, \tilde{\alpha}_1, \ldots, \tilde{\alpha}_{N-1})$ is also de-interleaved resulting in $\alpha^{\mathbf{I}} = \eta^{-1}(\tilde{\alpha})$ and $\alpha^{\mathbf{Q}} = \rho^{-1}(\tilde{\alpha})$. The receiver then performs a maximum likelihood (ML) detection.

As we have two orthogonal channels, let the squared Euclidean distances between two different signal constellation points in the I and Q-directions be represented by d_I^2 and d_Q^2, respectively. The distances are given as

$$\begin{aligned} d_I^2 &= \left(\cos(\phi_1 + \theta) - \cos(\phi_2 + \theta)\right)^2, \\ d_Q^2 &= \left(\sin(\phi_1 + \theta) - \sin(\phi_2 + \theta)\right)^2, \end{aligned} \tag{2.6}$$

where ϕ_1, ϕ_2 represent the phases of the two signal constellation points under consideration, respectively.

In order to explain the working of a system employing coordinate interleaving and constellation rotation, in the following section an intuitive explanation is provided to explain as to why SSD provides a performance gain.

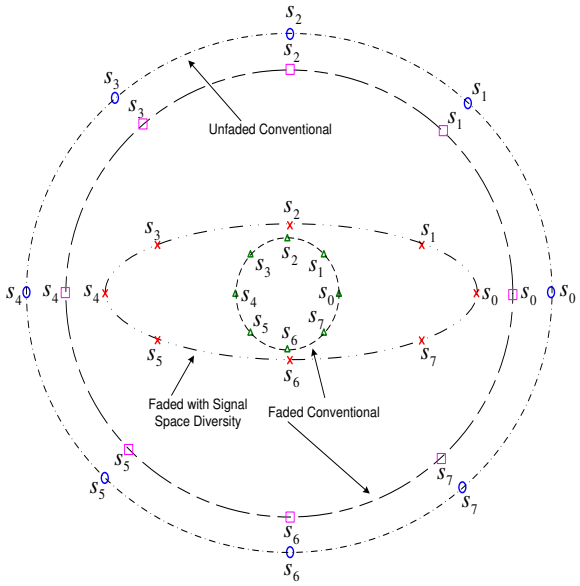

Figure 2.2: *Conventional 8PSK constellation under channel fading.*

2.4 Intuitive Explanation

An intuitive explanation for the benefit of SSD can be given with reference to Figures 2.2 and 2.3. In a conventional system, the I and the Q components experience the same fading, which may be deep (the small circle) or only moderate (larger circle). Of course, in case of a deep-fade, the system is quite error-prone. In a system with signal space diversity, however, the I and the Q components experience different fading (indicated by the ellipse). In spite of the fact that the Q component was exposed to severe fading, the distances between the signal points on the ellipse are considerably larger than the corresponding distances of the signal points on the small circle. The possible added value of rotation becomes evident in the comparison of Figures 2.2 and 2.3, which clearly show that the symbol distance profiles on the ellipse change under rotation. The figures

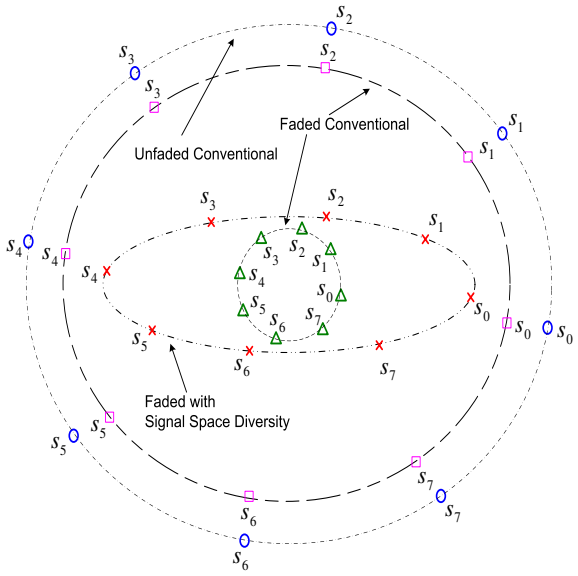

Figure 2.3: *Rotated 8PSK constellation under channel fading.*

show that the Gray signal constellation mapping may not be the best possible solution for a system employing coordinate interleaving as far away neighbors get to play a more dominant role. For instance, note that on the example ellipse symbol s_2 is closer to s_6 than to s_4. Therefore, the optimal rotation angles for MPSK cannot be intuitively judged based on a symmetry argument when I and Q components experience different fades. The figures show that the system with SSD no longer exhibits equi-probable symbol error probabilities as is the case with the conventional 8PSK scheme. Therefore, in systems employing signal space diversity, the performance cannot be evaluated by transmitting continuously a single symbol.

In the following section we derive closed form expressions for the average bit error probability of a system employing SSD in various fading environments. In order to highlight the diversity gain that is achieved by coordinate interleaving

coupled with constellation rotation we firstly consider the conventional QPSK system (i.e., a system without coordinate interleaving and signal constellation rotation), as an example constellation from MPSK and analyze its performance.

2.5 Performance Analysis of Conventional QPSK System

Assuming perfect CSI, the average probability of error for a conventional QPSK system is calculated by averaging the conditional probability of error on the fading statistic as given in [5]

$$P_b = \int_0^\infty Q\left(\sqrt{\bar{\gamma}\alpha^2(d^2_{\min})}\right) p(\alpha)d\alpha, \tag{2.7}$$

where $\bar{\gamma} = E_b/N_0$ is the average SNR per bit and $d^2_{\min}$ represents the minimum squared Euclidean distance between any two different signal constellations points. The $d^2_{\min}$ is a constant having a value of 2. $d^2_{\min}$ can also be represented as a sum given as

$$d^2_{\min} = d^2_{I_{\min}} + d^2_{Q_{\min}}. \tag{2.8}$$

If we consider only the nearest neighbors, (2.6) can be simplified as,

$$\begin{aligned} d^2_{I_{\min}} &= 1 \pm \sin(2\theta), \\ d^2_{Q\min} &= 1 \mp \sin(2\theta). \end{aligned}$$

In (2.7), $\bar{\gamma}$ is the average SNR per bit and $Q(x)$ is the Gaussian $Q-$ function defined as [45]

$$Q(x) = \frac{1}{\pi}\int_0^{\pi/2} e^{\frac{-x^2}{2\sin^2(\psi)}}\,\mathrm{d}\psi, \qquad x \geq 0. \tag{2.9}$$

Let the channel amplitude α be Rayleigh distributed given as

$$p(\alpha) = 2\alpha e^{-\alpha^2}, \qquad \alpha \geq 0, \tag{2.10}$$

with $E[\alpha^2] = 1$. Using (2.8), (2.9) and (2.10) in (2.7) we have

$$\begin{aligned} P_b &= \frac{1}{\pi}\int_0^{\pi/2}\int_0^{\infty} e^{\left(\frac{-\alpha^2\bar{\gamma}(d^2_{I_{\min}}+d^2_{Q_{\min}})}{2\sin^2(\psi)}\right)} 2\alpha e^{-\alpha^2}\mathrm{d}\alpha\mathrm{d}\psi \\ &= \frac{1}{\pi}\int_0^{\pi/2}\left(\frac{\sin^2(\psi)}{\sin^2(\psi)+\frac{\bar{\gamma}}{2}(d^2_{I_{\min}}+d^2_{Q_{\min}})}\right)\mathrm{d}\psi \\ &= \frac{1}{2}\left(1-\sqrt{\frac{\frac{\bar{\gamma}}{2}(d^2_{I_{\min}}+d^2_{Q_{\min}})}{1+\frac{\bar{\gamma}}{2}(d^2_{I_{\min}}+d^2_{Q_{\min}})}}\right) \\ &= \frac{1}{2}\left(1-\sqrt{\frac{\bar{\gamma}}{1+\bar{\gamma}}}\right). \end{aligned} \tag{2.11}$$

Equation (2.11) is widely reported in the literature, e.g., in [4–7]. It is evident from (2.11) that the system in the absence of coordinate interleaving is invariant to constellation rotation. This invariance to constellation rotation is due to the fact that the I and the Q-channels experience the same fade. Although there were two orthogonal channels available but as they experience the same fade no diversity gain is achieved. In the subsequent analysis we will consider a scenario where the I and the Q-channels experience different fades.

The entire analysis for a conventional QPSK for Rayleigh fading channels can be extended to Nakagami-m fading channels. The PDF of Nakagami-m is given as in Chapter 1

$$p(\alpha) = \begin{cases} \frac{2m^m\alpha^{2m-1}}{\Gamma[m]}e^{-m\alpha^2}, & m \geq 0.5, \quad \alpha \geq 0 \\ 0, & \text{otherwise}, \end{cases} \tag{2.12}$$

with $E[\alpha^2] = 1$,and m is the shape parameter that models the versatile channel conditions [17]. It can be shown that P_b for conventional QPSK system in Nakagami-m fading channels is given as

$$P_b = \frac{1}{\pi} \int_0^{\pi/2} \left(\frac{\sin^2(\psi)}{\sin^2(\psi) + \frac{\bar{\gamma}}{m}} \right)^m \mathrm{d}\psi. \tag{2.13}$$

The integrand in (2.13) is integrable for integer values of m.

2.6 Performance Analysis of an SSD System

For an arbitrary two-dimensional (2-D) signal constellation, a standard approach of evaluating the error probability of a signal set $\mathcal{S}_M^\theta$ is based on the union bound [42] and the average probability of symbol error P_s is thus upper bounded as

$$P_s \leq P_s^{UB} = \frac{1}{M} \sum_{s \in \mathcal{S}_M^\theta} \sum_{\substack{\hat{s} \in \mathcal{S}_M^\theta \\ s \neq \hat{s}}} P(s \to \hat{s}), \tag{2.14}$$

where $\mathcal{S}_M^\theta$ is the signal constellation of size $|\mathcal{S}_M^\theta| = M = 2^m$ and $P(s \to \hat{s})$ is the pairwise error probability (PEP) that the receiver estimated $\hat{s}$ when s was transmitted; given that s and $\hat{s}$ are the only two signal constellation points under-consideration. The bound can be modified to evaluate the average bit error probability by considering the number of bits per symbol (m) and the mapping rule specifying the Hamming distance associated with each PEP calculation [46]. Let $a(s, \hat{s})$ represent the Hamming distance between the sequences of bits of s and $\hat{s}$ under consideration. Then, P_b can be upper bounded as

$$P_b \leq P_b^{UB} = \frac{1}{m2^m} \sum_{s \in \mathcal{S}_M^\theta} \sum_{\substack{\hat{s} \in \mathcal{S}_M^\theta \\ s \neq \hat{s}}} a(s, \hat{s}) P(s \to \hat{s}). \tag{2.15}$$

If we consider only the nearest neighbors, the P_b can be approximated as

$$P_b \approx P_b^{NN} = \frac{1}{m2^m} \sum_{s \in \mathcal{S}_M^\theta} \sum_{\hat{s} \in \mathcal{N}(s)} a(s, \hat{s}) P(s \to \hat{s}), \tag{2.16}$$

where $\mathcal{N}(s)$ is the set of the nearest neighbors of s in $\mathcal{S}_M^\theta$.

In the literature, for convenience the calculation of PEP is also approximated by using bounds (e.g., Chernoff bound). We, on the other hand in the subsequent analysis, evaluate the exact PEP for MPSK constellations.

2.6.1 Analysis for Rayleigh Fading Channels

In this subsection a closed form expression for an upper bound of P_b of a system employing coordinate interleaving and constellation rotation for M-ary phase shift keying (MPSK) in correlated and uncorrelated Rayleigh fading channels is derived. Previously, in the literature an expression for P_b based on the the nearest neighbor approach was given [29]. In this subsection we show that the results with the nearest neighbor approximation represent an expurgated bound and are only tight for a small range of rotation angles.

The joint PDF of two correlated Rayleigh random variables α_1 and α_2 separated by kT_s is given as [47]

$$p(\alpha_1, \alpha_2) = \frac{4\alpha_1\alpha_2}{1-\rho_k^2} I_o\left(\frac{2|\rho_k|\alpha_1\alpha_2}{1-\rho_k^2}\right) e^{\frac{-(\alpha_1^2+\alpha_2^2)}{1-\rho_k^2}}, \tag{2.17}$$

where

$$\begin{aligned} \rho_k = \rho(kT_s) &= \frac{1}{2} E\{\alpha^*(t)\alpha(t+kTs)\} \\ &= J_o(2\pi f_D T_s k), \end{aligned}$$

is the correlation coefficient with $f_D T_s$ being the normalized Doppler frequency and $|.|$ represents the magnitude. $J_0(.)$ and $I_0(.)$ represent the zero-order Bessel and modified Bessel functions, respectively [12].

Coordinate interleaving is employed so that the I and the Q- channels experience independent fades. Let α_1 and α_2 be Rayleigh distributed random variables with PDF given in equation (2.17). In order to calculate the average probability of error for a system employing coordinate interleaving, the conditional PEP needs to be averaged over α_1 and α_2:

$$P(s \to \hat{s}) = \int_0^\infty \int_0^\infty Q\left(\sqrt{\bar{\gamma}(\alpha_1^2 d_I^2 + \alpha_2^2 d_Q^2)}\right) p(\alpha_1, \alpha_2) \mathrm{d}\alpha_1 \mathrm{d}\alpha_2, \tag{2.18}$$

where $\bar{\gamma} = E_b/N_0$ is the average SNR per bit. Using (2.9) and (2.17) in (2.18) we have

$$\begin{aligned} P(s \to \hat{s}) &= \int_0^\infty \int_0^\infty Q\left(\sqrt{\bar{\gamma}(\alpha_1^2 d_I^2 + \alpha_2^2 d_Q^2)}\right) \frac{4\alpha_1\alpha_2}{(1-\rho_k^2)} I_o\left(\frac{2|\rho_k|\alpha_1\alpha_2}{1-\rho_k^2}\right) \\ &\quad e^{\frac{-(\alpha_1^2+\alpha_2^2)}{1-\rho_k^2}} \mathrm{d}\alpha_1 \mathrm{d}\alpha_2 \\ &= \frac{1}{\pi(1-\rho_k^2)} \int_0^{\pi/2} \int_0^\infty \int_0^\infty e^{-\alpha_1^2\left(\frac{2\sin^2(\psi)+\bar{\gamma}d_I^2(1-\rho_k^2)}{2\sin^2(\psi)(1-\rho_k^2)}\right)} 2\alpha_1 2\alpha_2 \\ &\quad I_0\left(\frac{2|\rho_k|\alpha_1\alpha_2}{1-\rho_k^2}\right) e^{-\alpha_2^2\left(\frac{2\sin^2(\psi)+\bar{\gamma}d_Q^2(1-\rho_k^2)}{2\sin^2(\psi)(1-\rho_k^2)}\right)} \mathrm{d}\alpha_1 \mathrm{d}\alpha_2 \mathrm{d}_\psi. \end{aligned} \tag{2.19}$$

Using the fact [12] that,

$$\int_0^\infty 2x I_0(2bxy)\, e^{-ax^2} dx = \frac{e^{\frac{b^2y^2}{a}}}{a}, \qquad a > 0, \quad b > 0$$

in (2.19) and simplifying we have

$$\begin{aligned} P(s \to \hat{s}) &= \frac{1}{\pi}\int_0^{\pi/2} \frac{2\sin^2(\psi)}{\left(2\sin^2(\psi)+\bar{\gamma}d_I^2(1-\rho_k^2)\right)} \int_0^{\infty} 2\alpha_2 \\ &\quad e^{-\alpha_2^2 \frac{2\sin^2(\psi)+\bar{\gamma}d_Q^2(1-\rho_k^2)}{2\sin^2(\psi)(1-\rho_k^2)}} e^{\alpha_2^2 \frac{2\sin^2(\psi)\rho_k^2}{\left(2\sin^2(\psi)+\bar{\gamma}d_I^2(1-\rho_k^2)\right)(1-\rho_k^2)}} \mathrm{d}\alpha_2 \mathrm{d}\psi \\ &= \frac{1}{\pi}\int_0^{\pi/2}\int_0^{\infty} \frac{2\sin^2(\psi)2\alpha_2 e^{-\alpha_2^2 F(\psi)}}{\left(2\sin^2(\psi)+\bar{\gamma}d_I^2(1-\rho_k^2)\right)} \mathrm{d}\alpha_2 \mathrm{d}\psi, \end{aligned} \tag{2.20}$$

where

$$F(\psi) = \left(\frac{4\sin^4(\psi)+4\bar{\gamma}\sin^2(\psi)+\bar{\gamma}^2 d_I^2 d_Q^2(1-\rho_k^2)}{2\sin^2(\psi)\left(2\sin^2(\psi)+\bar{\gamma}d_I^2(1-\rho_k^2)\right)}\right). \tag{2.21}$$

Inserting $F(\psi)$ in (2.20) and solving we have,

$$\begin{aligned} P(s \to \hat{s}) &= \frac{1}{\pi}\int_0^{\pi/2} \frac{2\sin^2(\psi)}{\left(2\sin^2(\psi)+\bar{\gamma}d_I^2(1-\rho_k^2)\right)} \int_0^{\infty} 2\alpha_2 \\ &\quad e^{-\alpha_2^2\left(\frac{4\sin^2(\psi)\left(\bar{\gamma}+\sin^2(\psi)\right)+\bar{\gamma}^2 d_I^2 d_Q^2(1-\rho_k^2)}{\left(2\sin^2(\psi)\left(\bar{\gamma}d_I^2(1-\rho_k^2)+2\sin^2(\psi)\right)\right)}\right)} \mathrm{d}\alpha_2 \mathrm{d}\psi \\ &= \frac{1}{\pi}\int_0^{\pi/2} \frac{4\sin^4(\psi)}{4\sin^4(\psi)+4\bar{\gamma}\sin^2(\psi)+\bar{\gamma}^2 d_I^2 d_Q^2(1-\rho_k^2)} \mathrm{d}\psi \\ &= \frac{1}{\pi}\int_0^{\pi/2} \frac{\sin^4(\psi)}{\sin^4(\psi)+\bar{\gamma}\sin^2(\psi)+\frac{(\bar{\gamma}^2 d_I^2 d_Q^2)(1-\rho_k^2)}{4}} \mathrm{d}\psi. \end{aligned} \tag{2.22}$$

Solving and simplifying using the identities given in [12], we have

$$\begin{aligned} P(s \to \hat{s}) &= \frac{\Delta_1}{2\left(\Delta_1-\Delta_2\right)}\left(1-\sqrt{\frac{\bar{\gamma}\Delta_1}{2+\bar{\gamma}\Delta_1}}\right) - \\ &\quad \frac{\Delta_2}{2\left(\Delta_1-\Delta_2\right)}\left(1-\sqrt{\frac{\bar{\gamma}\Delta_2}{2+\bar{\gamma}\Delta_2}}\right), \end{aligned} \tag{2.23}$$

where

$$\begin{aligned}\Delta_1 &= 1-\sqrt{1-(1-\rho_k^2)(d_I^2 d_Q^2)},\\ \Delta_2 &= 1+\sqrt{1-(1-\rho_k^2)(d_I^2 d_Q^2)}.\end{aligned} \tag{2.24}$$

When $\rho_k = 0$, i.e., uncorrelated Rayleigh fading channel, (2.23) reduces to

$$\begin{aligned}P(s\to\hat{s}) &= \frac{1}{2}-\frac{d_I^2}{2(2d_I^2-C)}\left(\sqrt{\frac{\bar{\gamma}d_I^2}{2+\bar{\gamma}d_I^2}}\right)+\\ &\quad \frac{C-d_I^2}{2(2d_I^2-C)}\left(\sqrt{\frac{\bar{\gamma}(C-d_I^2)}{2+\bar{\gamma}(C-d_I^2)}}\right),\end{aligned} \tag{2.25}$$

where $C = d_I^2 + d_Q^2$. Also in Appendix A, we present an alternative method to derive (2.23) based on the calculation of the characteristic function of the PDF [48] of the random variable $(\alpha_1 d_I^2 + \alpha_2 d_Q^2)$.

In the subsequent analysis, for simplicity and comparison with previous results in literature, we consider QPSK signal constellation as an example signal constellation from MPSK.

2.6.2 Nearest Neighbor Approximation

The nearest neighbor (NN) approach is exact for a conventional QPSK system. Using (2.25) in (2.16) and with $C = 2$, P_b^{NN} for an SSD system with Gray mapped signal constellation can be given as

$$\begin{aligned}P_b^{NN} &= \frac{1}{4(d_I^2-1)}\left\{d_I^2\left(2-\sqrt{\frac{\bar{\gamma}d_I^2}{(2+\bar{\gamma}d_I^2)}}-\sqrt{\frac{\bar{\gamma}(2-d_I^2)}{(2+\bar{\gamma}(2-d_I^2))}}\right)\right.\\ &\quad \left.-2\left(1-\sqrt{\frac{\bar{\gamma}(2-d_I^2)}{(2+\bar{\gamma}(2-d_I^2))}}\right)\right\}.\end{aligned} \tag{2.26}$$

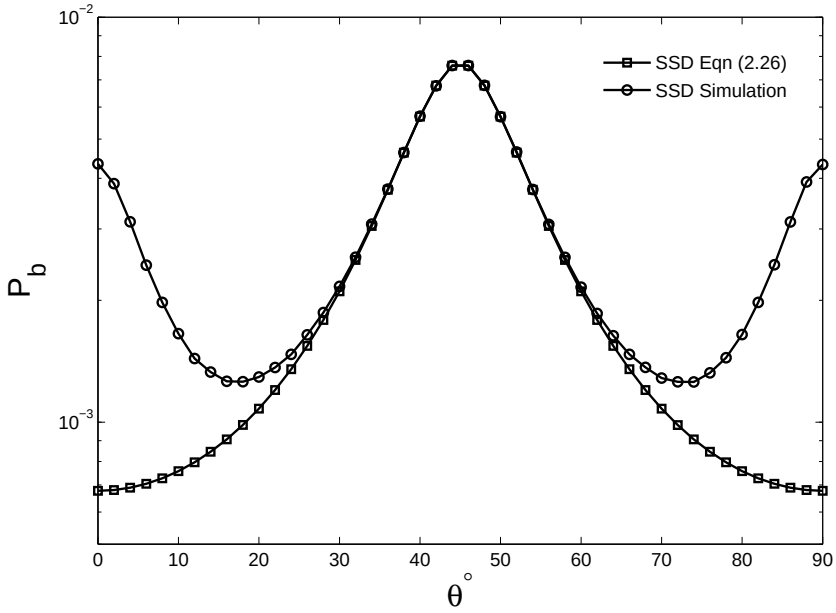

Figure 2.4: *Average probability of error P_b and P_b^{NN} versus rotational angle θ of an SSD system using QPSK signal constellation over Rayleigh fading channel with perfect channel state information at $E_b/N_0 = 15$ dB. Gray signal constellation mapping is used.*

Equation (2.26) is also reported in [29]. Using (2.26), P_b^{NN} is calculated and compared with the simulation results. Figure 2.4 shows the P_b^{NN} versus the rotation angle θ at $E_b/N_0 = 15$ dB for Gray mapped signal constellation. For $\theta = 45°$, P_b^{NN} matches the simulation results. However, apart from $\theta = 45°$, there is a divergence from the simulation results. This divergence is due the NN approximation as not all the error events are considered and also the fact that when I and Q channels experience independent fades the far away neighbors tend to play a more dominant role. This effect was highlighted in Section 2.4. Moreover, we can conclude that the P_b^{NN} reported in [29], in fact, represents an expurgated bound.

Furthermore, the worst case scenario for an SSD system is when one branch

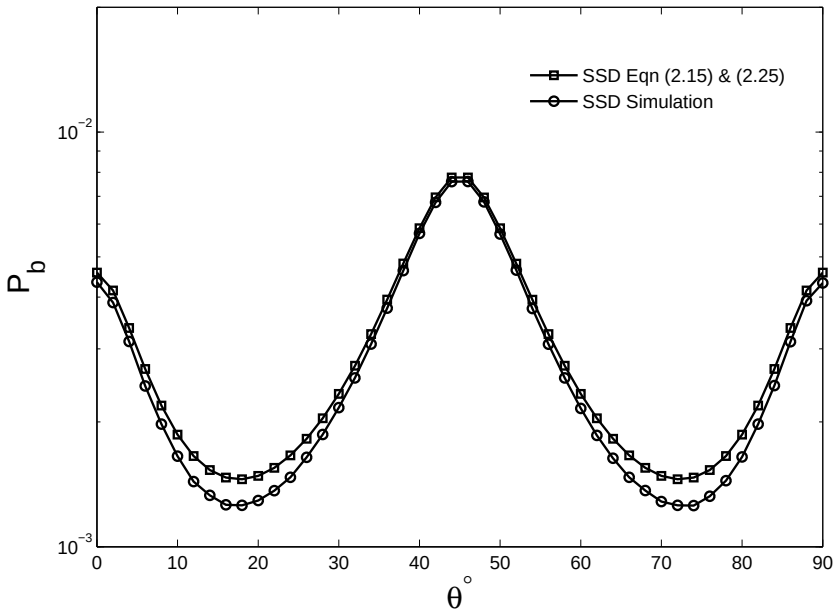

Figure 2.5: *Average probability of error P_b and P_b^{UB} versus rotational angle θ of an SSD system using QPSK signal constellation over Rayleigh fading channel with perfect CSI at $E_b/N_0 = 15$ dB. Gray signal constellation mapping is used.*

has been completely removed, i.e., d_I^2 or $d_Q^2 = 0$. In such a case, (2.26) reduces to the average probability of bit error of a conventional QPSK system (2.11), showing that the choice of the rotation angle plays a very vital role.

2.6.3 Union Bound

In order to calculate (2.15) the squared Euclidean distances (SED) along I and Q- channels, for all possible symbol combinations, need to be calculated. Figure 2.5 shows the upper bound on the average probability of bit error performance calculated by using (2.15) and by simulation. The figure shows that the P_b is upper bounded by the union bound. Gray labeled QPSK signal constellation employing coordinate interleaving and constellation rotation is used. The figure

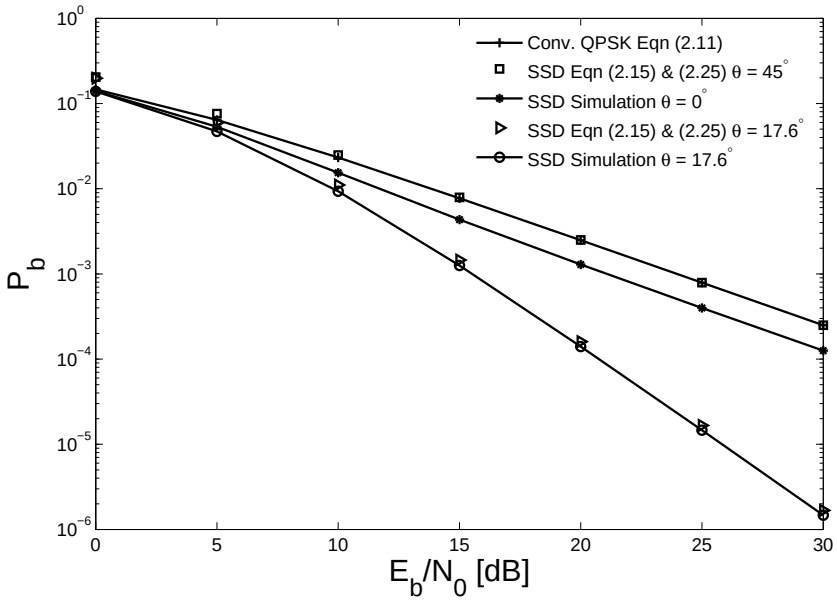

Figure 2.6: *Average probability of error P_b of conventional and SSD systems using QPSK signal constellation over Rayleigh fading channels with perfect CSI. Gray signal constellation mapping is used.*

shows that the bound is tight.

2.6.4 Optimal Rotational Angle

The optimal rotational angle in [29] was based on a symmetry argument and was shown to be 22.5°. The symmetry argument in case of SSD is not valid as highlighted by Section 2.4. We, therefore, present a more general method of determining the optimal rotation angle.

The optimum rotation angle θ for P_b may be found by minimizing (2.15). This can be accomplished by taking the derivative of the objective function (2.15) with respect to θ. In (2.15), we need to take the derivative of (2.25). The derivative

of (2.25) with respect to θ is given as

$$\begin{aligned}\frac{\partial P(s\to\hat{s})}{\partial\theta} &= \frac{-\left(d_I^2\left(\frac{-2\bar{\gamma}^2 d_I^3 d_I'}{(2+\bar{\gamma}d_I^2)^2}+\frac{2\bar{\gamma}d_I d_I'}{2+\bar{\gamma}d_I^2}\right)\right)}{4(-C+2d_I^2)\sqrt{\frac{\bar{\gamma}d_I^2}{2+\bar{\gamma}d_I^2}}}+\frac{2d_I^3\sqrt{\frac{\bar{\gamma}d_I^2}{2+\bar{\gamma}d_I^2}}d_I'}{(-C+2d_I^2)^2}+\\ &\quad\frac{\left((C-d_I^2)\left(\frac{2\bar{\gamma}^2 d_I(C-d_I^2)d_I'}{(2+\bar{\gamma}(C-d_I^2))^2}-\frac{2\bar{\gamma}d_I d_I'}{2+\bar{\gamma}(C-d_I^2)}\right)\right)}{4(-C+2d_I^2)\sqrt{\frac{\bar{\gamma}(C-d_I^2)}{2+\bar{\gamma}(C-d_I^2)}}}-\frac{d_I\sqrt{\frac{\bar{\gamma}d_I^2}{2+\bar{\gamma}d_I^2}}d_I'}{-C+2d_I^2}\\ &\quad-\frac{2d_I(C-d_I^2)\sqrt{\frac{\bar{\gamma}(C-d_I^2)}{2+\bar{\gamma}(C-d_I^2)}}d_I'}{(-C+2d_I^2)^2}-\frac{d_I\sqrt{\frac{\bar{\gamma}(C-d_I^2)}{2+\bar{\gamma}(C-d_I^2)}}d_I'}{(-C+2d_I^2)},\end{aligned}\tag{2.27}$$

where $d_I' = -\sin(\phi_1+\theta)+\sin(\phi_2+\theta)$. The optimal θ can be found by employing the steepest descent algorithm [49] by using (2.15) and (2.27). The optimum rotational angle is found to be $\theta = 17.6°$. In [28], for P_s, the reported angle is $\theta = 31.7°$, however, when translated to our initial QPSK signal constellation represents an angle of $\theta = 13.3°$. In [29], as stated earlier, the reported angle is 22.5°. It is important to state that if only the NN approximation is used the optimum rotation angle should be 0° as shown by Figure 2.4. However, the angle in [29] is chosen based on the symmetry argument, which we have shown in case of a system employing coordinate interleaving is not valid.

2.6.5 Bit Error Rate Performance

Figure 2.6 shows that the optimum rotational angle of $\theta = 17.6°$ leads to a gain of 10.7 dB for SSD over the conventional QPSK system at a bit error rate of 3×10^{-4}. The figure also shows that the worst case scenario for a system employing coordinate interleaving is when one branch is completely removed, i.e., d_I^2 or $d_Q^2 = 0$. In such a case, as shown for $\theta = 45°$, the performance of an SSD

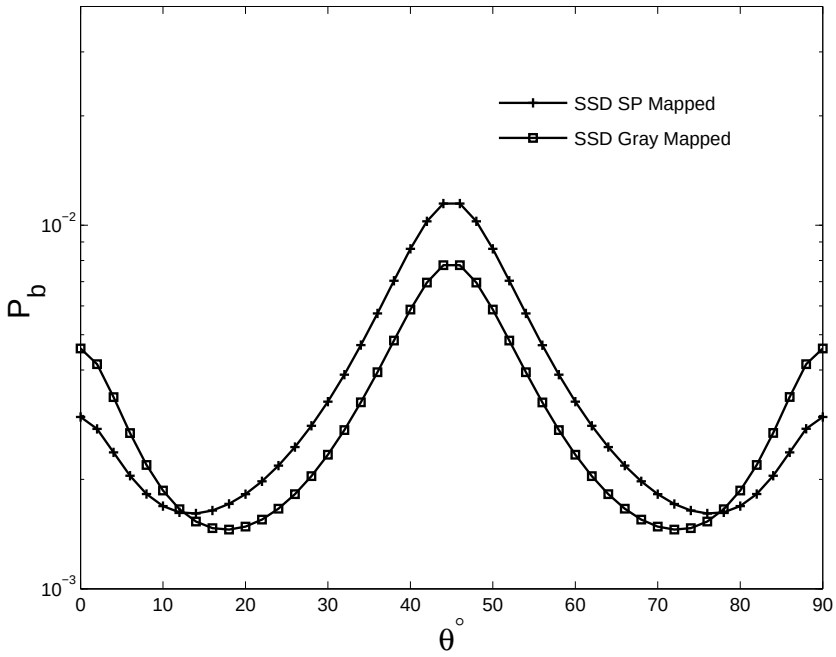

Figure 2.7: *Average probability of error P_b for Gray and Natural mapped QPSK signal constellation over Rayleigh fading channel with perfect CSI at $E_b/N_0 = 15$ dB.*

system reduces to that of a conventional QPSK system (2.11). Hence, showing that the choice of the rotation angle plays a very vital role. Furthermore, the figure shows that the simulation results are in good agreement with the closed form analytical expression (2.15).

2.6.6 Mapping Effect

Figure 2.7 shows the comparison of QPSK with Gray and Natural signal constellation mappings. The figure shows that Gray mapped signal constellation is not necessarily the best choice for the entire θ range. At $\theta = 0°$, for instance, Natural mapped signal constellation outperforms Gray mapped signal constellation. As argued in Section 2.4, the far away neighbors play a more dominant role

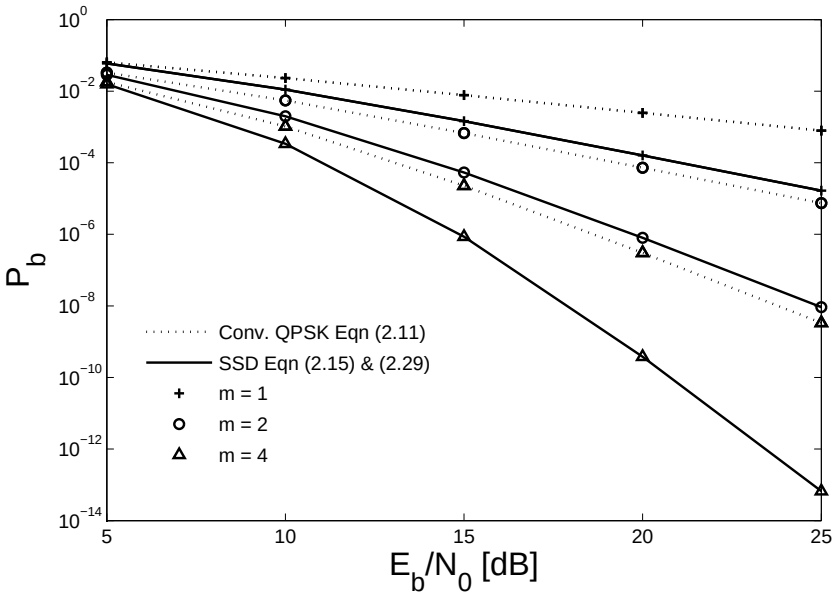

Figure 2.8: *Average probability of error P_b of conventional and SSD systems using QPSK signal constellation over Nakagami-m fading channels with $m = 1$, $m = 2$ and $m = 4$. Perfect CSI is assumed and Gray signal constellation mapping is used.*

when I and $Q-$ channels experience independent fades and therefore, at certain rotational angles Natural mapped signal constellation outperforms Gray mapped signal constellation. Furthermore, this indicates a possibility to design signal constellation mappings for higher MPSK signal constellations which are capable of outperforming Gray signal constellation mapping at a wider range of rotational angle θ.

2.6.7 Analysis for Nakagami-m Fading Channels

In this subsection we extend the analysis from Section 2.6.1 to Nakagami-m fading channels with arbitrary fading parameter for MPSK signal constellations. Let α_1 and α_2 be Nakagami-m distributed random variables with PDF given in (2.12). In order to calculate the P_b for a system employing coordinate interleaving, the

conditional PEP needs to be averaged over α_1 and α_2 as the I and Q channels experience independent fades:

$$\begin{aligned} P(s \to \hat{s}) &= \int_0^\infty \int_0^\infty Q(\sqrt{\bar{\gamma}(\alpha_1^2 d_I^2 + \alpha_2^2 d_Q^2)}) p(\alpha_1) p(\alpha_2) \mathrm{d}\alpha_1 \mathrm{d}\alpha_2 \\ &= \frac{4m^{2m}}{\pi \Gamma^2[m]} \int_0^{\pi/2} \int_0^\infty \int_0^\infty \alpha_1^{2m-1} e^{-\alpha_1^2 \frac{2m \sin^2(\psi) + \bar{\gamma} d_I^2}{2 \sin^2(\psi)}} \\ &\quad \alpha_2^{2m-1} e^{-\alpha_2^2 \frac{2m \sin^2(\psi) + \bar{\gamma} d_Q^2}{2 \sin^2(\psi)}} \mathrm{d}\alpha_1 \mathrm{d}\alpha_2 \mathrm{d}\psi \\ &= \frac{1}{\pi} \int_0^{\pi/2} \left(\frac{\sin^2(\psi)}{\sin^2(\psi) + \frac{\bar{\gamma} d_I^2}{2m}} \right)^m \left(\frac{\sin^2(\psi)}{\sin^2(\psi) + \frac{\bar{\gamma} d_Q^2}{2m}} \right)^m \mathrm{d}\psi, \end{aligned} \quad (2.28)$$

Using the results from [50] we simplify (2.28) when m is an integer as

$$\begin{aligned} P(s \to \hat{s}) &= \frac{\left(\frac{d_I^2}{d_Q^2}\right)^{m-1}}{2\left(1 - \frac{d_I^2}{d_Q^2}\right)^{2m-1}} \left[\sum_{k=0}^{m-1} \left(1 - \frac{d_Q^2}{d_I^2}\right)^k B_k D_k \left(\frac{\bar{\gamma} d_Q^2}{2m}\right) - \right. \\ &\quad \left. \frac{d_I^2}{d_Q^2} \sum_{k=0}^{m-1} \left(1 - \frac{d_I^2}{d_Q^2}\right)^k C_k D_k \left(\frac{\bar{\gamma} d_I^2}{2m}\right) \right], \end{aligned} \quad (2.29)$$

where

$$B_k = \frac{A_k}{\binom{2m-1}{k}}, \quad C_k = \sum_{n=0}^{m-1} \frac{\binom{n}{k}}{\binom{2m-1}{n}} A_n,$$

$$A_k = (-1)^{m-1+k} \frac{\binom{m-1}{k}}{(m-1)!} \prod_{\substack{n=1 \\ n \neq k+1}}^{m} (2m-n),$$

$$\text{and} \qquad D_k(c) \;=\; 1-\sqrt{\frac{c}{1+c}}\left[1+\sum_{n=1}^{k}\frac{(2n-1)!!}{n!2^n(1+c)^n}\right],$$

with the double factorial notation $(2n-1)!!$ denoting the product of only odd integers from 1 to $2n-1$. For $m=1$ (i.e., uncorrelated Rayleigh fading channel), (2.29) reduces to (2.25).

Figure 2.8 shows the performance of SSD system over fading channels with Nakagami distribution with different values of m and QPSK signal constellation. The Nakagami-m distribution spans via the m-parameter the widest range of all the multipath distributions. For further details we refer the reader to Chapter 1. The figure shows that in all varying fading conditions the system employing SSD outperforms the conventional system. For instance, for $m=2$, the SSD system with a rotation angle of $\theta = 17.6^\circ$, has a performance gain of 9.6 dB at a bit error rate of 1×10^{-6} over the conventional QPSK system.

2.7 Analysis of Partially Coherent SSD systems

Coherent detection of MPSK signals requires the generation or extraction of a local carrier phase reference. In most applications, a perfect local reference is not possible and hence, the noise associated with the carrier leads to the degradation of the system performance. The problem arising from phase noise and its effect on the performance of the conventional system has been extensively studied in the literature, e.g., [51–54], and the references therein. In [51], it was shown that the phase error arising from a first-order phase locked loop (PLL) can be modeled by Tikhonov distribution, which is also a good approximation for second-order PLL when the SNR in the loop bandwidth is large. In [52], a BER performance of direct sequence spread spectrum over a Rayleigh fading channel was presented using the

Tikhonov PDF. In [53], the error performance of binary phase shift keying (BPSK) with noisy phase reference having Tikhonov and Gaussian densities are analyzed in Nakagami-m fading channels.

The analysis carried out on systems employing SSD in the literature, e.g., [29,30,36], is under the assumption that a perfect phase reference is available in the receiver for demodulation. In practice, as stated earlier, this is not possible. In this section, we present closed form analytical expressions of the union bound of the P_b for MPSK signal constellations over Nakagami-m fading channels with phase noise. We show that the calculated bound is tight for higher SNRs. Furthermore, it is shown that the optimum rotation angles for a system employing SSD does not change under the influence of phase noise.

Partial coherence implies that the reference phase at the receiver contains a random phase error. Furthermore, it is assumed that the PLL SNR is much greater than $\bar{\gamma}$. This assumption implies that the cosine of the phase estimate can be replaced by a deterministic variable (expected value) in the analysis [52]. This approximation technique is also referred to as linear approximation as it is exact when the function whose expectation is to be approximated is linear, regardless of the variance [52].

A partially coherent receiver provides (via a PLL) a complex reference signal $e^{-j\hat{\phi}}$ whose phase $\hat{\phi}$ is an estimate of the unknown channel phase ϕ. The phase estimation error $\phi_c = \phi - \hat{\phi}$ follows the Tikhonov distribution under the normal operating conditions, i.e., when the PLL's are in lock [52]. The Tikhonov PDF is given as [55][2]

$$p(\phi_c) = \frac{e^{\rho \cos \phi_c}}{2\pi I_0(\rho)}, \tag{2.30}$$

where $I_k(.)$ is the kth-order modified Bessel function of the first kind and ρ is the

[2]The modeling of the phase error PDF was also arrived at independently by [51].

tracking PLL SNR.

Coordinate interleaving is employed so that the I and the Q- channels experience independent fades. Let α_1 and α_2 be Nakagami-m distributed random variables with PDF given by (2.12). In order to calculate the average probability of error P_b, for a system employing coordinate interleaving affected by phase noise and fading, the conditional PEP needs to be averaged over the fading static as well as the phase noise, given as

$$\begin{aligned} P(s \to \hat{s}) &= \int_0^\infty \int_0^\infty \int_{-\pi}^{\pi} Q(\sqrt{\bar{\gamma}(\alpha_1^2 d_I^2 + \alpha_2^2 d_Q^2)} \cos\phi_c) \\ &\quad p(\phi_c)p(\alpha_1)p(\alpha_2)\mathrm{d}\phi_c \mathrm{d}\alpha_1 \mathrm{d}\alpha_2. \end{aligned} \tag{2.31}$$

Using the linear approximation [52], (2.31) can be simplified as

$$\begin{aligned} P(s \to \hat{s}) &= \int_0^\infty \int_0^\infty Q(\sqrt{\bar{\gamma}(\alpha_1^2 d_I^2 + \alpha_2^2 d_Q^2)} I(\rho)) \\ &\quad p(\alpha_1)p(\alpha_2)\mathrm{d}\alpha_1 \mathrm{d}\alpha_2 \end{aligned} \tag{2.32}$$

where $I(\rho) = \frac{I_1(\rho)}{I_0(\rho)}$. Using (2.12), (2.9) in (2.32) we have

$$\begin{aligned} P(s \to \hat{s}) &= \frac{4m^{2m}}{\pi\Gamma^2[m]} \int_0^{\pi/2} \int_0^\infty \int_0^\infty \alpha_1^{2m-1} e^{-\alpha_1^2 \frac{2m\sin^2(\psi) + \bar{\gamma} d_I^2 I(\rho)}{2\sin^2(\psi)}} \alpha_2^{2m-1} \\ &\quad e^{-\alpha_2^2 \frac{2m\sin^2(\psi) + \bar{\gamma} d_Q^2 I(\rho)}{2\sin^2(\psi)}} d\alpha_1 d\alpha_2 d\psi \\ &= \frac{1}{\pi} \int_0^{\pi/2} \left(\frac{\sin^2(\psi)}{\sin^2(\psi) + \frac{\bar{\gamma} d_I^2 I(\rho)}{2m}} \right)^m \left(\frac{\sin^2(\psi)}{\sin^2(\psi) + \frac{\bar{\gamma} d_Q^2 I(\rho)}{2m}} \right)^m d\psi. \end{aligned} \tag{2.33}$$

The above integrand is integrable for integer values of m. For uncorrelated

Rayleigh fading, i.e., $m = 1$, (2.33) reduces to

$$P(s \to \hat{s}) = \frac{1}{2} - \frac{d_I^2}{2(2d_I^2 - C)} \left(\sqrt{\frac{\bar{\gamma} d_I^2 I(\rho)}{2 + \bar{\gamma} d_I^2 I(\rho)}} \right) + \frac{C - d_I^2}{2(2d_I^2 - C)} \left(\sqrt{\frac{\bar{\gamma} I(\rho)(C - d_I^2)}{2 + \bar{\gamma} I(\rho)(C - d_I^2)}} \right), \tag{2.34}$$

where $C = d_I^2 + d_Q^2$.

2.7.1 Optimal Rotational Angle of a Partially Coherent System

As was shown in Section 2.6.4, the optimum rotation angle of a partially coherent SSD system may be found by minimizing the upper bound of (2.15). In (2.15), we need to take the derivative of (2.33) which evaluates to

$$\begin{aligned} \frac{\partial P(s \to \hat{s})}{\partial \theta} = & \frac{-\left(d_I^2 \left(\frac{-2(\bar{\gamma} I(\rho))^2 d_I^3 d_I'}{(2+\bar{\gamma} I(\rho) d_I^2)^2} + \frac{2\bar{\gamma} I(\rho) d_I d_I'}{2+\bar{\gamma} I(\rho) d_I^2} \right) \right)}{4(-C + 2d_I^2)\sqrt{\frac{\bar{\gamma} I(\rho) d_I^2}{2+\bar{\gamma} I(\rho) d_I^2}}} + \frac{2d_I^3 \sqrt{\frac{\bar{\gamma} I(\rho) d_I^2}{2+\bar{\gamma} I(\rho) d_I^2}} d_I'}{(-C + 2d_I^2)^2} + \\ & \frac{\left((C - d_I^2) \left(\frac{2(\bar{\gamma} I(\rho))^2 d_I (C - d_I^2) d_I'}{(2+\bar{\gamma} I(\rho)(C - d_I^2))^2} - \frac{2\bar{\gamma} I(\rho) d_I d_I'}{2+\bar{\gamma} I(\rho)(C - d_I^2)} \right) \right)}{4(-C + 2d_I^2)\sqrt{\frac{\bar{\gamma} I(\rho)(C - d_I^2)}{2+\bar{\gamma} I(\rho)(C - d_I^2)}}} - \\ & \frac{d_I \sqrt{\frac{\bar{\gamma} I(\rho) d_I^2}{2+\bar{\gamma} I(\rho) d_I^2}} d_I'}{-C + 2d_I^2} - \frac{d_I \sqrt{\frac{\bar{\gamma} I(\rho)(C - d_I^2)}{2+\bar{\gamma} I(\rho)(C - d_I^2)}} d_I'}{(-C + 2d_I^2)} \\ & - \frac{2d_I (C - d_I^2) \sqrt{\frac{\bar{\gamma} I(\rho)(C - d_I^2)}{2+\bar{\gamma} I(\rho)(C - d_I^2)}} d_I'}{(-C + 2d_I^2)^2}, \end{aligned} \tag{2.35}$$

where $d_I' = -\sin(\varphi_1 + \theta) + \sin(\varphi_2 + \theta)$. The steepest descent algorithm [49] can be employed using (2.15) and (2.35) to find the optimum rotation angle. The optimum rotation angle calculated for QPSK signal constellation using steepest descent algorithm is 17.6°. The calculated optimum angle for a system affected

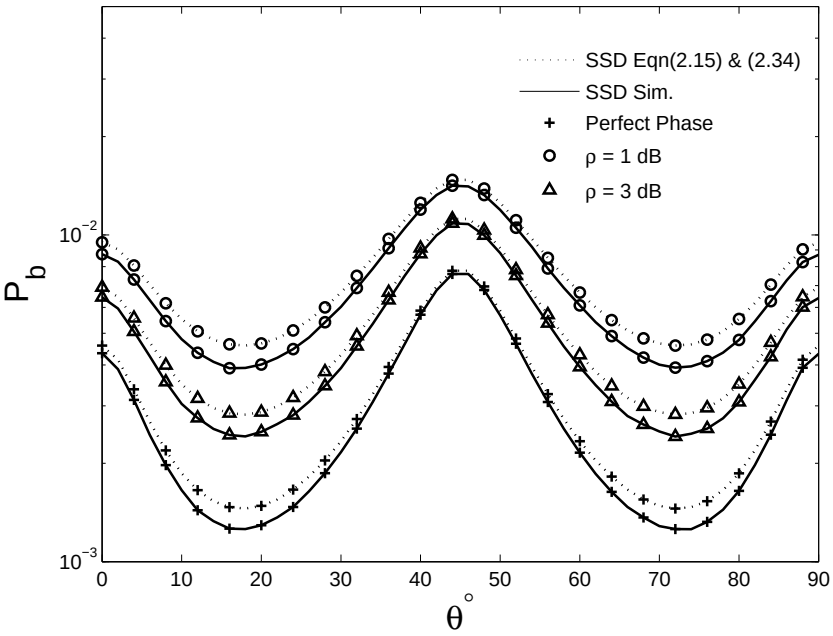

Figure 2.9: *Average probability of error P_b and P_b^{UB} versus rotational angle θ of a system employing coordinate interleaving and constellation rotation using QPSK signal constellation over Rayleigh fading channel at $E_b/N_0 = 15$ dB and in the presence of phase noise. Gray signal constellation mapping is used.*

by phase noise is the same as for a system with perfect phase estimates as shown by Figure 2.9. The figure also shows that the derived bound is tight and is in good agreement with the simulation results at high SNRs.

2.7.2 Phase Error Effect

Figure 2.10 shows the degradation in the performance of an SSD system when the phase noise is taken into account. It is seen that the performance degrades more when the PLL SNR, ρ, is held constant while the system SNR, $\bar{\gamma}$, is increased. This effect is not realistic and can be considered as a worst case scenario. This effect implies that the PLL is generating more noise relative to the rest of the

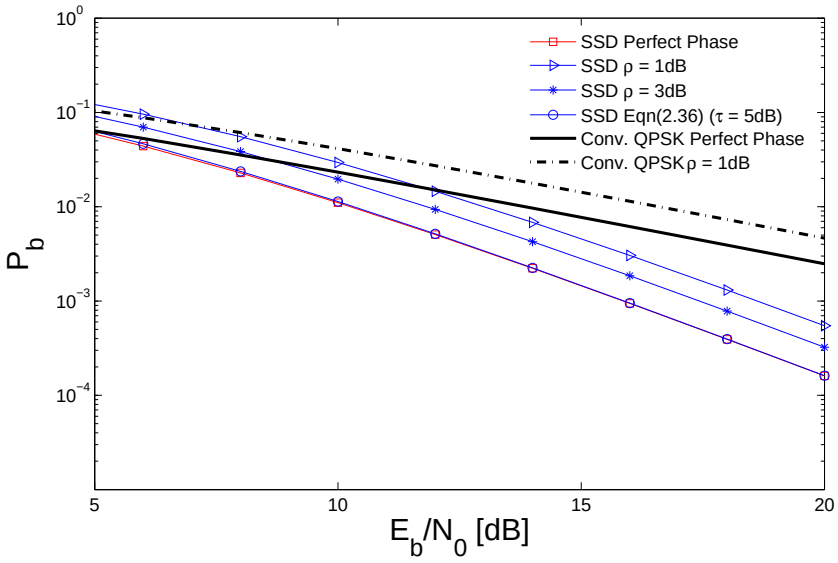

Figure 2.10: *The effect of phase estimation error on the performance of an SSD system at $\theta = 17.6^\circ$ with respect to a conventional QPSK system is shown in Rayleigh fading channel. Gray signal constellation mapping is employed.*

receiver [52]. Figure 2.10, shows that even under such worse conditions the SSD systems' performance is better than a conventional system affected by the same phase noise. ρ being held constant is not realistic as the second-order PLL's ρ is proportional to $\bar{\gamma}$ and as $\bar{\gamma}$ increases PLL performs better and better [52], [53]. A more realistic assignment is as [52],

$$\rho = \tau\bar{\gamma}, \tag{2.36}$$

where τ is a constant. The figure shows that by using the more realistic assignment given by (2.36), the gain at high SNR by SSD becomes more evident. In Figure 2.10, for instance, a curve based on (2.36) is included where $\tau = 5$dB. This curves shows that as $\bar{\gamma}$ increases, ρ increases proportionally and the PLL performs better. Thus, improving the overall system performance and approaching the performance

of a system with perfect phase estimation. Furthermore, the figure also shows that a system employing SSD is more robust than a conventional system even in the worst scenario when the PLL is assumed to be generating more noise.

2.8 Conclusions

In this chapter an introduction to modulation diversity and an intuitive reasoning for the gain provided by a system employing SSD was presented. Closed form expressions for P_b were derived for correlated and uncorrelated Rayleigh fading channels.

It was shown that the previously reported results in the literature represent an expurgated bound and are not valid for the entire range of rotational angle θ. The new derived bound was shown to be tight at high SNR. Optimum rotation angles were found by minimizing the upper bound and they differed to the ones reported in the literature. The effect of signal constellation mapping on the system performance was also highlighted and it was shown that Gray signal constellation mapping is not necessarily the best option for a system employing SSD. Closed form expressions for P_b were also derived for Nakagami multipath fading channels with arbitrary fading parameter. It was shown that SSD systems with a proper choice of rotation angle provide significant performance improvement over the conventional systems.

The performance of SSD systems in the presence of phase noise generated by PLL dynamics was also analyzed. A closed form expression was derived to analyze the performance of SSD systems in the presence of phase noise. It was shown that SSD systems are more robust to phase noise than conventional systems. Lastly, it was also shown that the optimum rotation angles for partially coherent SSD systems do not change.

Chapter 3

Analysis of SSD Systems in Wideband Channels

Performance analysis of a system employing coordinate interleaving and constellation rotation in frequency selective fading channels is presented under the assumption of a single shot transmission. The achievable performance with L-branch microdiversity using maximum ratio combining (MRC) is analyzed and an upper bound on the average probability of bit error (P_b) is derived. Exact closed form expressions for the pairwise error probability (PEP) are derived for correlated Nakagami-m fading channels. Two different correlation models are considered, i.e., the constant (equal) correlation model and the exponential correlation model. Furthermore, the effect of channel estimation error is also investigated and a closed form expression for a system with outdated or imperfect channel estimates is derived.

3.1 Introduction

Wireless communication systems, current and emerging, use diversity in one form or another. It is well-known that diversity can mitigate the performance degradation caused by fading channels [4, 5, 32]. Any diversity technique (e.g., space, time and frequency) attempts to provide statistically independent copies of the transmitted sequence at the receiver to increase the overall received signal-to-noise ratio (SNR) and to reduce the detection error. Diversity tries to exploit the low probability of occurrence of deep fades in all the diversity branches and, therefore, is able to lower the overall probability of error and outage. An attractive option is signal space diversity (SSD), introduced in Chapter 2, that can improve system performance without using extra bandwidth and power expansion [28–31,33]. The basic premise of SSD systems is to use rotated multidimensional signal constellations, where the components of the signal constellation points are sent over independent fading channels. The independence of fading channels can be accomplished by the use of interleavers.

In literature, e.g., [28–30,33], the analysis on systems employing SSD is mostly limited to the case when no other diversity reception technique is employed. For instance, in [28], an upper bound on the average probability of bit error (P_b) is presented for flat Rayleigh fading channels and in [29] P_b was derived based on the nearest neighbor approach for correlated and uncorrelated flat Rayleigh fading channels. In [33], the performance of a bit interleaved coded modulation with iterative decoding (BICM-ID) and signal space diversity in flat Rayleigh fading is shown.

In [31], a Chernoff upper bound on the pairwise error probability (PEP) for an SSD system in frequency-selective channel was presented by assuming no intersymbol interference (ISI) and no co-channel interference (CCI). The entire analysis

was carried out with an assumption of a single symbol transmission; also referred to as one shot transmission. Under this assumption, the frequency selective channel reduces to a multilink fading channel [4]. The emphasis, however, was on the derivation of linear equalization techniques for SSD systems in frequency-selective channels.

Throughout this chapter, we also employ the single symbol transmission assumption. Under the assumption of single symbol transmission, the resulting PEP constitutes a lower bound for continuous transmission since interference from preceding and succeeding symbols is avoided. This approach is similar to the classical matched filter bound method used to analyze the performance limits for transmission over fading ISI channels with diversity [31, 56, 57] and without diversity [58]. Matched filter bound [58] is a simple method that gives the probability of error for the maximum likelihood receiver under the assumption that perfect equalization is achievable. Equivalently, the effects of ISI are ignored by considering the transmission of a single symbol.

In this chapter, we present exact closed form expressions for the PEP over multilink fading channels with signal space diversity for correlated and uncorrelated branches. If the various paths in a system employing multipath diversity are generated by different scatterers, they tend to exhibit negligible correlations [21] and it is therefore reasonable in that case to assume that these paths are statistically independent. However, there are a number of real-life scenarios in which this assumption is not valid [22–24]. Therefore, we consider correlated paths as well. Two correlation models are considered, i.e., the constant (equal) correlation model and the exponential correlation model. The exact PEP is derived for paths with probability density functions (PDF) described by the Nakagami-m distribution. Furthermore, the effect of channel estimation error due to additive noise as

well as channel variation/decorrelation over time is investigated. A closed form expression is derived for the impact of channel estimation error on the performance of maximum ratio combining (MRC) receivers with SSD. It is shown that the system employing SSD is more robust against channel estimation errors than a conventional MRC system. Furthermore, it is shown that the derived upper bounds are tight at high signal-to-noise ratios (SNR). The rotation angles are optimized by minimizing the upper bounds. The optimum rotation angles vary as the number of diversity branches are increased. The effect of signal constellation mapping on the system performance is also presented and it is shown that the Gray signal constellation mapping is not necessarily the best option for optimal system performance over the entire range of signal constellation rotation.

The remainder of the chapter is organized as follows. Section 3.2 briefly outlines the main blocks of the system model. Section 3.3 presents the calculations of the upper bound on bit error probability for a system employing SSD in a multipath uncorrelated Nakagami-m fading channel. Section 3.4, presents the performance analysis of an SSD system with different correlation models. In Section 3.5, performance analysis of an SSD system effected by outdated channel estimates and the associated performance degradation is presented, followed by the conclusions in Section 3.6.

3.2 System Model

The transmitted waveform for the rotated and interleaved system is the same as presented in the system model in Chapter 2. We, therefore, in this section focus on the extensions in the receiver, namely the MRC, and the different fading environments. For further details on the transmitted waveform we refer the reader to Chapter 2. A system employing coordinate interleaving and constellation rotation

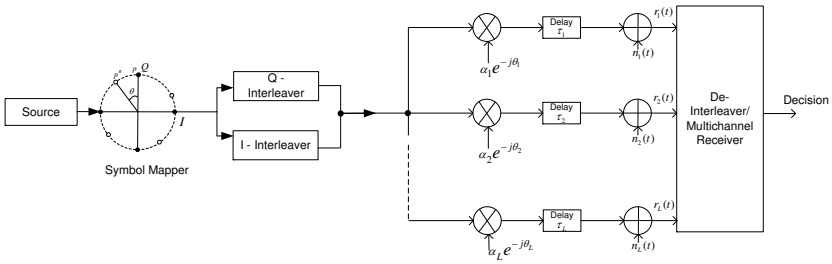

Figure 3.1: *Simplified block diagram of an equivalent baseband transmission model.*

is, hereafter, referred to as an "SSD system". Furthermore, we confine ourselves to MPSK signal constellations and consider both the cases of perfect channel state information (CSI) and imperfect CSI at the receiver.

The fading caused by a frequency selective channel can be modeled as a linear filter characterized by a complex valued low pass equivalent impulse response [4],

$$h(t) = \sum_{l=1}^{L} \alpha_l e^{-j\theta_l} \delta(t - \tau_l), \tag{3.1}$$

where l is the path index, L is the number of resolvable paths, $\delta(\cdot)$ is the Dirac delta function and $\{\alpha\}_{l=1}^{L}$, $\{\theta\}_{l=1}^{L}$ and $\{\tau\}_{l=1}^{L}$ are the random channel amplitudes, phases and delays, respectively. As we assume that there is no CCI and no ISI, the transmitted signal is therefore, sent over L independent and identically distributed (i.i.d) slowly varying flat fading paths as shown in Figure 3.1. Furthermore similar to the analysis of multipath diversity under the assumption of single symbol transmission in the literature, e.g., [4,56,57,59], we assume, without a loss of generality, the first channel with delay $\tau_1 = 0$ to be the reference channel and $\tau_1 < \tau_2 < \cdots < \tau_L$. Also, we assume that the sets $\{\alpha\}_{l=1}^{L}$, $\{\theta\}_{l=1}^{L}$ and $\{\tau\}_{l=1}^{L}$ are mutually independent and are constant over at least a symbol interval. The fading amplitudes, $\{\alpha\}_{l=1}^{L}$, are statistically independent random variables with a

mean-square value $\mathcal{E}[\alpha_l^2] = \Omega_l$, and a PDF described by any of the family of distributions, e.g., Rayleigh, Nakagami-n (Rice) or Nakagami-m. The transmitted signal after passing through the fading channel is perturbed by complex additive white Gaussian noise (AWGN) with a one-sided power spectral density of N_0. The AWGN noise is assumed to be independent of the fading amplitudes and statistically independent from channel to channel. In this chapter, we would confine ourselves to Nakagami-m distribution which for $m \geq 0.5$ is given as [5]

$$p(\gamma_l) = \left(\frac{m}{\bar{\gamma}_l}\right)^m \frac{\gamma_l^{m-1}}{\Gamma(m)} \exp\left(-\frac{m\gamma_l}{\bar{\gamma}_l}\right), \quad \gamma_l \geq 0, \tag{3.2}$$

where $\gamma_l = \alpha_l^2 E_b/N_0$ is the SNR per bit per path, $\bar{\gamma}_l$ is the average SNR per bit per path, m is the Nakagami-m fading parameter which ranges from $\frac{1}{2}$ to ∞ and $\Gamma(\cdot)$ is the gamma function [12]. Furthermore, it is important to state that if the various paths of a given impulse response are generated by different scatterers, they tend to exhibit negligible correlations [21] and it is therefore reasonable in that case to assume that $\{\alpha\}_{l=1}^L$ are statistically independent RVs. However, if the fading is correlated [22–24], the $\{\alpha\}_{l=1}^L$ are considered as correlated RVs.

At the receiver we consider an L-branch maximum ratio combining (MRC) receiver. The performance of MRC receivers has been studied quite extensively in the literature, e.g., [4, 5], and the references therein. MRC, regardless of the fading statistics on various diversity branches, is the optimal multichannel receiver since it results in a maximum likelihood (ML) detection [5]. As CSI is available at the receiver the channel phase shift at all the diversity branches can be removed without any error. Thus, after channel phase removal the samples are de-interleaved and the receiver performs an ML detection. At the output of the MRC the total conditional SNR per bit, γ_t of L i.i.d Rayleigh fading paths is

given as [4, 5]

$$\gamma_t = \sum_{l=1}^{L} \gamma_l, \tag{3.3}$$

and the total average SNR is represented by $\bar{\gamma}$. Finding the PDF of the combined SNR per bit γ_t in a simple form is typically feasible if all the paths are independent and identically distributed. For instance, for Rayleigh fading channel, where γ_t has a chi-square PDF [4, 5]

$$p(\gamma_t) = \frac{1}{(L-1)!\bar{\gamma}^L} \gamma_t^{L-1} e^{\frac{-\gamma_t}{\bar{\gamma}}}. \tag{3.4}$$

Finding γ_t is more difficult if the combined paths have the same fading distribution but have different fading parameters (e.g., different average fading powers).

In this chapter, to analyze the performance of MRC receivers with SSD and multipath diversity we take the approach followed by [60–64]. Similar to the analysis in Chapter 2, we would firstly reintroduce the upper bounds for ease of reading and better comprehension.

3.3 Performance Analysis of an SSD System

A standard approach of evaluating the error probability of a signal set $\mathcal{S}_M^\theta$ is based on the union bound [4]. The average probability of symbol error P_s is thus upper bounded by

$$P_s \leq P_s^{UB} = \frac{1}{M} \sum_{s \in \mathcal{S}_M^\theta} \sum_{\substack{\hat{s} \in \mathcal{S}_M^\theta \\ s \neq \hat{s}}} P(s \to \hat{s}), \tag{3.5}$$

where $\mathcal{S}_M^\theta$ is the signal constellation of size $|\mathcal{S}_M^\theta| = M = 2^m$ and $P(s \to \hat{s})$ is the PEP that the receiver estimated $\hat{s}$ when s was transmitted; given that s and $\hat{s}$ are

the only two signal constellation points under-consideration. The bound can be modified to evaluate the average bit error probability by considering the number of bits per symbol (m) and the mapping rule specifying the Hamming distance associated with each PEP calculation [46]. Let $a(s,\hat{s})$ represent the Hamming distance between the bit sequences of s and $\hat{s}$ under consideration, then

$$P_b \leq P_b^{UB} = \frac{1}{m2^m} \sum_{s \in \mathcal{S}_M^\theta} \sum_{\substack{\hat{s} \in \mathcal{S}_M^\theta \\ s \neq \hat{s}}} a(s,\hat{s}) P(s \rightarrow \hat{s}). \tag{3.6}$$

In the literature, for the convenience of calculation, the PEP is also approximated by using bounds (e.g., Chernoff bound [31]). We, on the other hand in the subsequent analysis, evaluate the exact PEP for MPSK signal constellations and follow the approach given by [4, chapt. 9].

Coordinate interleaving is employed so that the I and the Q- channels experience independent fades. Let γ_{tI} and γ_{tQ} be random variables which effect the system in the I and Q- channels, respectively. In order to calculate the average probability of error P_b, for a system employing coordinate interleaving and multichannel reception, the conditional PEP needs to be averaged over the joint PDF of the instantaneous SNR sequences $\{\gamma_{lI}\}_{l1=1}^{L}$, $\{\gamma_{lQ}\}_{l2=1}^{L}$, given as

$$\begin{aligned} P(s \rightarrow \hat{s}) \quad = \quad & \underbrace{\int_0^\infty \int_0^\infty \cdots \int_0^\infty}_{\text{L-fold}} \underbrace{\int_0^\infty \int_0^\infty \cdots \int_0^\infty}_{\text{L-fold}} \prod_{l=1}^{L} Q\sqrt{\left(\gamma_{lI} d_I^2 + \gamma_{lQ} d_Q^2\right)} \\ & p(\gamma_{lI}) p(\gamma_{lQ}) \mathrm{d}\gamma_{1I} \mathrm{d}\gamma_{2I} \cdots \mathrm{d}\gamma_{LI} \mathrm{d}\gamma_{1Q} \mathrm{d}\gamma_{2Q} \cdots \mathrm{d}\gamma_{LQ}, \end{aligned} \tag{3.7}$$

where $Q(x)$ is the Gaussian Q-function defined as [4]

$$Q(x) = \frac{1}{\pi} \int_0^{\pi/2} e^{\frac{-x^2}{2\sin^2(\psi)}} \mathrm{d}\psi, \qquad x \geq 0, \tag{3.8}$$

and d_I^2 and d_Q^2 are the squared Euclidean distances between two different signal constellation points in the I and Q-directions, respectively. The distances are given as

$$\begin{aligned} d_I^2 &= \left(\cos(\varphi_1+\theta)-\cos(\varphi_2+\theta)\right)^2, \\ d_Q^2 &= \left(\sin(\varphi_1+\theta)-\sin(\varphi_2+\theta)\right)^2, \end{aligned} \tag{3.9}$$

where φ_1, φ_2 represent the phases of the two signal constellation points under consideration, respectively. Using (3.8) in (3.7) we have

$$\begin{aligned} P(s\to\hat{s}) &= \underbrace{\int_0^\infty\int_0^\infty\cdots\int_0^\infty}_{\text{L-fold}}\underbrace{\int_0^\infty\int_0^\infty\cdots\int_0^\infty}_{\text{L-fold}}\frac{1}{\pi}\int_0^{\pi/2}\prod_{l=1}^{L}e^{-\frac{\gamma_{lI}d_I^2+\gamma_{lQ}d_Q^2}{2\sin^2(\psi)}} \\ &\quad p(\gamma_{lI})p(\gamma_{lQ})\mathrm{d}\gamma_{1I}\mathrm{d}\gamma_{2I}\cdots\mathrm{d}\gamma_{LI}\mathrm{d}\gamma_{1Q}\mathrm{d}\gamma_{2Q}\cdots\mathrm{d}\gamma_{LQ}\mathrm{d}\psi. \end{aligned} \tag{3.10}$$

The order of integration can be changed in the above integrand and grouping the terms of lI and lQ together and using (3.2) we have

$$\begin{aligned} P(s\to\hat{s}) &= \frac{1}{\pi}\int_0^{\pi/2}\prod_{l=1}^{L}\left(\frac{m^m}{\bar{\gamma}_l^m\Gamma(m)}\int_0^\infty e^{-\gamma_{lI}\left(\frac{d_I^2}{2\sin^2(\psi)}+\frac{m}{\bar{\gamma}_l}\right)}\gamma_{lI}^{m-1}\mathrm{d}\gamma_{lI}\right) \\ &\quad \left(\frac{m^m}{\bar{\gamma}_l^m\Gamma(m)}\int_0^\infty e^{-\gamma_{lQ}\left(\frac{d_Q^2}{2\sin^2(\psi)}+\frac{m}{\bar{\gamma}_l}\right)}\gamma_{lQ}^{m-1}\mathrm{d}\gamma_{lQ}\right)\mathrm{d}\psi. \end{aligned} \tag{3.11}$$

If fading is assumed to be identically distributed with the same fading parameter and the same average SNR per bit $\bar{\gamma}$ for all L channels, (3.11) reduces to

$$\begin{aligned} P(s\to\hat{s}) &= \frac{1}{\pi}\int_0^{\pi/2}\left(\frac{m^m}{\bar{\gamma}^m\Gamma(m)}\int_0^\infty e^{-\gamma_{lI}\left(\frac{d_I^2}{2\sin^2(\psi)}+\frac{m}{\bar{\gamma}}\right)}\gamma_{lI}^{m-1}\mathrm{d}\gamma_{lI}\right)^L \\ &\quad \left(\frac{m^m}{\bar{\gamma}^m\Gamma(m)}\int_0^\infty e^{-\gamma_{lQ}\left(\frac{d_Q^2}{2\sin^2(\psi)}+\frac{m}{\bar{\gamma}}\right)}\gamma_{lQ}^{m-1}\mathrm{d}\gamma_{lQ}\right)^L\mathrm{d}\psi \end{aligned}$$

$$= \frac{1}{\pi}\int_0^{\pi/2}\left(\frac{\sin^2(\psi)}{\sin^2(\psi)+\frac{\bar{\gamma}d_I^2}{2m}}\right)^{Lm}\left(\frac{\sin^2(\psi)}{\sin^2(\psi)+\frac{\bar{\gamma}d_Q^2}{2m}}\right)^{Lm}\mathrm{d}\psi. \tag{3.12}$$

For $L=1$ and $m=1$ (i.e., Rayleigh fading channel) , (3.12) simplifies as

$$P(s\to\hat{s}) = \frac{1}{2}-\frac{d_I^2}{2(2d_I^2-C)}\left(\sqrt{\frac{\bar{\gamma}d_I^2}{2+\bar{\gamma}d_I^2}}\right)+ \frac{C-d_I^2}{2(2d_I^2-C)}\left(\sqrt{\frac{\bar{\gamma}(C-d_I^2)}{2+\bar{\gamma}(C-d_I^2)}}\right), \tag{3.13}$$

where $C=d_I^2+d_Q^2$. The above equation is reported in Chapter 2 equation (2.25). Using the results from [50] we can simplify (3.12) for integer combinations of Lm as

$$P(s\to\hat{s}) = \frac{(\frac{d_I^2}{d_Q^2})^{mL-1}}{2(1-\frac{d_I^2}{d_Q^2})^{2mL-1}}\left[\sum_{k=0}^{mL-1}\left(1-\frac{d_Q^2}{d_I^2}\right)^k B_k D_k\left(\frac{\bar{\gamma}d_Q^2}{2mL}\right)- \frac{d_I^2}{d_Q^2}\sum_{k=0}^{mL-1}\left(1-\frac{d_I^2}{d_Q^2}\right)^k C_k D_k\left(\frac{\bar{\gamma}d_I^2}{2mL}\right)\right], \tag{3.14}$$

where

$$B_k = \frac{A_k}{\binom{2mL-1}{k}}, \quad C_k=\sum_{n=0}^{mL-1}\frac{\binom{n}{k}}{\binom{2mL-1}{n}}A_n,$$

$$A_k = (-1)^{mL-1+k}\frac{\binom{mL-1}{k}}{(mL-1)!}\prod_{\substack{n=1\\ n\neq k+1}}^{mL}(2mL-n),$$

$$\text{and} \qquad D_k(c) = 1-\sqrt{\frac{c}{1+c}}\left[1+\sum_{n=1}^{k}\frac{(2n-1)!!}{n!2^n(1+c)^n}\right],$$

with the double factorial notation $(2n-1)!!$ denoting the product of only odd integers from 1 to $2n-1$.

The largest diversity gain "jump", in Rayleigh fading channels, between diversity branches is achieved when we add another branch to $L=1$, i.e., we move to $L=2$ from $L=1$ [5]. For $L=2$ evaluation of (3.12) leads to

$$\begin{aligned}
P(s\to\hat{s}) = {} & \frac{1}{4(\frac{\bar{\gamma}}{2}(d_I^2-d_Q^2))^3((\frac{\bar{\gamma}d_I^2}{2}+1)(\frac{\bar{\gamma}d_Q^2}{2}+1))^{3/2}}\left\{-2(\frac{\bar{\gamma}d_Q^2}{2}+1)^{3/2}(\frac{\bar{\gamma}d_I^2}{2})^{9/2}+\right.\\
& 2\sqrt{\left(\frac{\bar{\gamma}d_I^2}{2}+1\right)}(\frac{\bar{\gamma}d_Q^2}{2}+1)^{3/2}(\frac{\bar{\gamma}d_I^2}{2})^4+3\sqrt{\left(\frac{\bar{\gamma}d_Q^2}{2}+1\right)}\left(2(\frac{\bar{\gamma}d_Q^2}{2})^2+\right.\\
& \left.\frac{\bar{\gamma}d_Q^2}{2}-1\right)(\frac{\bar{\gamma}d_I^2}{2})^{7/2}-2\sqrt{(\frac{\bar{\gamma}d_I^2}{2}+1)}\sqrt{(\frac{\bar{\gamma}d_Q^2}{2}+1)}\left(3(\frac{\bar{\gamma}d_Q^2}{2})^2+\right.\\
& \left.2(\frac{\bar{\gamma}d_Q^2}{2})-1\right)(\frac{\bar{\gamma}d_I^2}{2})^3+7(\frac{\bar{\gamma}d_Q^2}{2})(\frac{\bar{\gamma}d_Q^2}{2}+1)^{3/2}(\frac{\bar{\gamma}d_I^2}{2})^{5/2}-\sqrt{\left(\frac{\bar{\gamma}d_I^2}{2}+1\right)}\\
& (\frac{\bar{\gamma}d_Q^2}{2})\left(6(\frac{\bar{\gamma}d_Q^2}{2})^{5/2}-6\sqrt{\left(\frac{\bar{\gamma}d_Q^2}{2}+1\right)}(\frac{\bar{\gamma}d_Q^2}{2})^2+7(\frac{\bar{\gamma}d_Q^2}{2})^{3/2}+\right.\\
& \left.6\sqrt{(\frac{\bar{\gamma}d_Q^2}{2})+1}\right)(\frac{\bar{\gamma}d_I^2}{2})^2+\sqrt{\left(\frac{\bar{\gamma}d_I^2}{2}+1\right)}(\frac{\bar{\gamma}d_Q^2}{2})^2\left(2(\frac{\bar{\gamma}d_Q^2}{2})^{5/2}\right.\\
& \left.-2\sqrt{\left(\frac{\bar{\gamma}d_Q^2}{2}+1\right)}(\frac{\bar{\gamma}d_Q^2}{2})^2-3(\frac{\bar{\gamma}d_Q^2}{2})^{3/2}+4\sqrt{\left(\frac{\bar{\gamma}d_Q^2}{2}+1\right)}(\frac{\bar{\gamma}d_Q^2}{2})-\right.
\end{aligned}$$

$$7\sqrt{(\frac{\bar{\gamma}d_Q^2}{2})}+6\sqrt{\left(\frac{\bar{\gamma}d_Q^2}{2}+1\right)}\,(\frac{\bar{\gamma}d_I^2}{2})+\sqrt{\left(\frac{\bar{\gamma}d_I^2}{2}+1\right)}(\frac{\bar{\gamma}d_Q^2}{2})^3$$
$$\left(2(\frac{\bar{\gamma}d_Q^2}{2})^{3/2}-2\sqrt{\left(\frac{\bar{\gamma}d_Q^2}{2}+1\right)}(\frac{\bar{\gamma}d_Q^2}{2})+3\sqrt{(\frac{\bar{\gamma}d_Q^2}{2})}-\right.$$
$$\left.2\sqrt{\left(\frac{\bar{\gamma}d_Q^2}{2}+1\right)}\right)\Bigg\}, \tag{3.15}$$

In the subsequent analysis we use the QPSK signal constellation as an example and present a performance comparison of an SSD QPSK system with a conventional QPSK system. The average probability of bit error P_b of a conventional QPSK system for i.i.d multipath Rayleigh fading channel using MRC receiver is given as [4, 5]

$$P_b=\left(\frac{1-\mu}{2}\right)^L\sum_{l=0}^{L-1}\left(\begin{array}{c}L-1+l\\ l\end{array}\right)\left(\frac{1+\mu}{2}\right)^l, \tag{3.16}$$

where

$$\mu=\sqrt{\frac{\bar{\gamma}}{1+\bar{\gamma}}}.$$

For i.i.d Nakagami-m fading paths it can be shown, using the same steps as presented in Section 3.3, that the average probability of error P_b can be given as

$$P_b=\frac{1}{\pi}\int_0^{\pi/2}\left(\frac{\sin^2(\psi)}{\sin^2(\psi)+\frac{\bar{\gamma}}{m}}\right)^{Lm}\mathrm{d}\psi,\qquad m\geq 0.5. \tag{3.17}$$

The worst case scenario for a system employing constellation rotation and coordinate interleaving is when one branch has been completely removed, i.e., d_I^2 or $d_Q^2=0$. In such a case, the performance of an SSD system reduces to that of a conventional system.

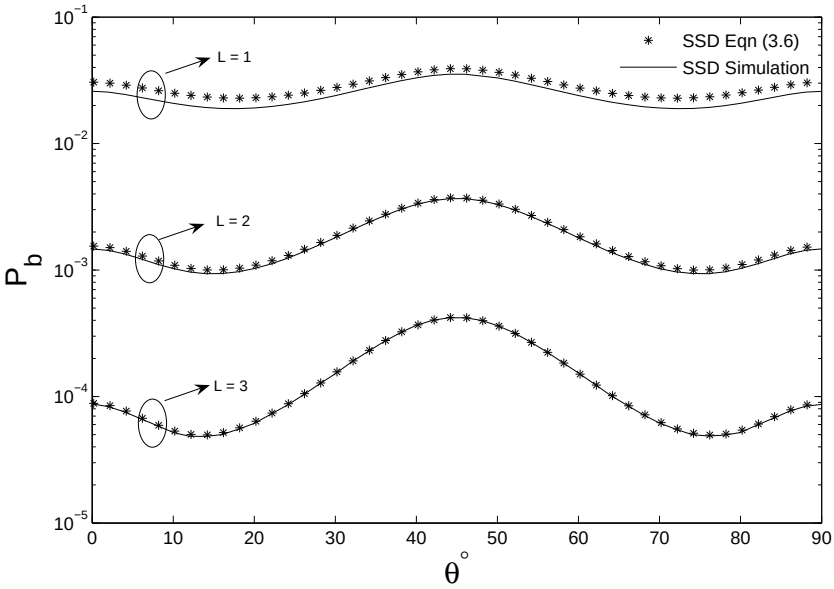

Figure 3.2: *Average probability of error P_b versus rotational angle θ of an SSD system using QPSK signal constellation over Rayleigh fading channel with perfect CSI at $E_b/N_0 = 8$ dB. Gray signal constellation mapping is used.*

3.3.1 Union Bound For Uncorrelated Paths

Using (3.6) and (3.12), the upper bound on P_b for uncorrelated paths in a system employing SSD is evaluated. Figure 3.2 shows the P_b^{UB} calculated using (3.6) and by simulation for $m = 1$ and $L = 1, 2$, and 3 branch MRC receiver using SSD. The figure shows that the upper bound is tight at high SNR and is able to accurately predict the variation in P_b for the entire range of signal constellation rotation for different values of L. Moreover, as expected, there is a performance improvement as the number of branches in an MRC receiver with SSD is increased. Gray labeled QPSK signal constellation is employed.

3.3.2 Optimal Rotational Angle

Figure 3.2 shows that the upper bound is tight for all rotational angles. Therefore, the optimum rotation angle θ for a system using SSD coupled with MRC over uncorrelated paths maybe found by minimizing (3.6). This can be determined by taking the derivative of the objective function (3.6) (i.e. PEP) with respect to θ. In (3.6), for instance, for $L = 1$ and $m = 1$, the derivative of (3.13) is given by

$$\begin{aligned}\frac{\partial P(s \to \hat{s})}{\partial \theta} &= \frac{-\left(d_I^2\left(\frac{-2\bar{\gamma}^2 d_I^3 d_I'}{(2+\bar{\gamma}d_I^2)^2} + \frac{2\bar{\gamma}d_I d_I'}{2+\bar{\gamma}d_I^2}\right)\right)}{4(-C+2d_I^2)\sqrt{\frac{\bar{\gamma}d_I^2}{2+\bar{\gamma}d_I^2}}} + \frac{2d_I^3\sqrt{\frac{\bar{\gamma}d_I^2}{2+\bar{\gamma}d_I^2}}d_I'}{(-C+2d_I^2)^2} + \\ &\quad \frac{\left((C-d_I^2)\left(\frac{2\bar{\gamma}^2 d_I(C-d_I^2)d_I'}{(2+\bar{\gamma}(C-d_I^2))^2} - \frac{2\bar{\gamma}d_I d_I'}{2+\bar{\gamma}(C-d_I^2)}\right)\right)}{4(-C+2d_I^2)\sqrt{\frac{\bar{\gamma}(C-d_I^2)}{2+\bar{\gamma}(C-d_I^2)}}} - \frac{d_I\sqrt{\frac{\bar{\gamma}d_I^2}{2+\bar{\gamma}d_I^2}}d_I'}{-C+2d_I^2} \\ &\quad - \frac{2d_I(C-d_I^2)\sqrt{\frac{\bar{\gamma}(C-d_I^2)}{2+\bar{\gamma}(C-d_I^2)}}d_I'}{(-C+2d_I^2)^2} - \frac{d_I\sqrt{\frac{\bar{\gamma}(C-d_I^2)}{2+\bar{\gamma}(C-d_I^2)}}d_I'}{(-C+2d_I^2)}, \end{aligned} \tag{3.18}$$

where $d_I' = -\sin(\phi_1 + \theta) + \sin(\phi_2 + \theta)$ and $C = d_I^2 + d_Q^2$. The above equation is also reported in Chapter 2 (2.27). Similarly, for integer values of Lm the derivatives can be evaluated. The steepest descent algorithm is used to find the optimum angles. For QPSK signal constellation and $m = 1$ the optimum angle of $\theta = 17.6°$, $15.4°$ and $14.4°$ is calculated for $L = 1, 2$, and 3, respectively. In [29], the reported angle is $22.5°$ based on a symmetry argument and in [28, 31] for P_s the reported angle is $\theta = 31.7°$ for $L = 1$ based on maximizing the product distance of constellations, which when translated to our initial constellation refers to an angle of $13.3°$. For $L = 2$, in [31], the reported angle for P_s is $\theta = 24°$. From our calculations, it is clear that the optimum constellation rotation angle does vary but the variation is very small as the number of branches are increased.

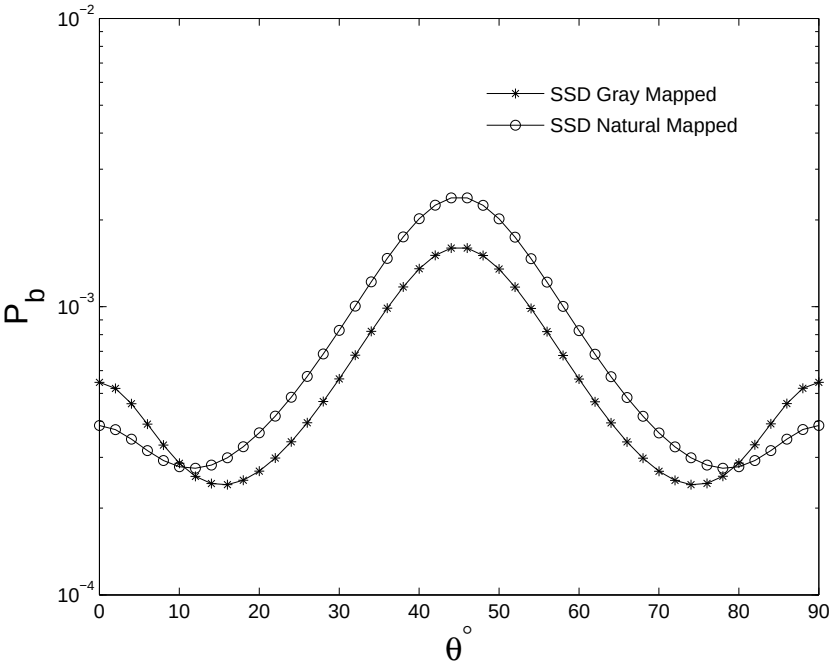

Figure 3.3: *Average probability of error P_b for Gray and Natural mapped QPSK signal constellation over Rayleigh fading channel with $L = 2$ and perfect CSI at $E_b/N_0 = 10$ dB.*

3.3.3 Mapping Effect

Figure 3.3 shows the comparison of QPSK with Gray and Natural signal constellation mappinga with $m = 1$ and $L = 2$ and uncorrelated fading paths. The figure shows that a Gray mapped signal constellation is not necessarily the best choice for the entire θ range. At $\theta = 0°$, for instance, a Natural mapped signal constellation outperforms a Gray mapped signal constellation. As argued in Chapter 2, in an SSD system the far away neighbors tend to play a more dominant role when I and $Q-$ channels experience independent fades and therefore the possi-

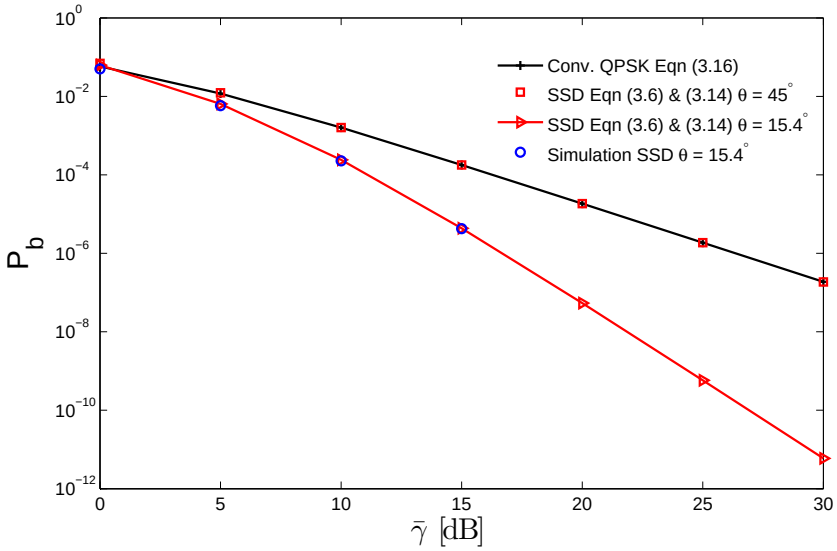

Figure 3.4: *Average probability of error P_b of conventional and SSD systems using QPSK signal constellation over Rayleigh fading channels with $L = 2$ and perfect CSI. Gray signal constellation mapping is used.*

bility of Gray being outperformed by Natural signal constellation mapping arises. Furthermore, this provides a possibility to design signal constellation mapping for higher MPSK signal constellations that are capable of outperforming Gray signal constellation mapping over a wider range of θ.

3.3.4 Performance Gain

Figures 3.4 and 3.5 show the comparison and the performance gain of an SSD system (3.6) over a conventional system (3.16) with multiple diversity branches and $m = 1$. The simulation results are in good agreement with the closed form analytical expression (3.6). Figure 3.4 shows a gain of 9.7 dB for SSD system over the conventional QPSK system at a bit error rate of 1×10^{-6} with $L = 2$. For $L = 3$, SSD systems shows a gain of 5.7 dB over the conventional QPSK system at a bit error rate of 1×10^{-6} as shown in Figure 3.5. Furthermore, simulation

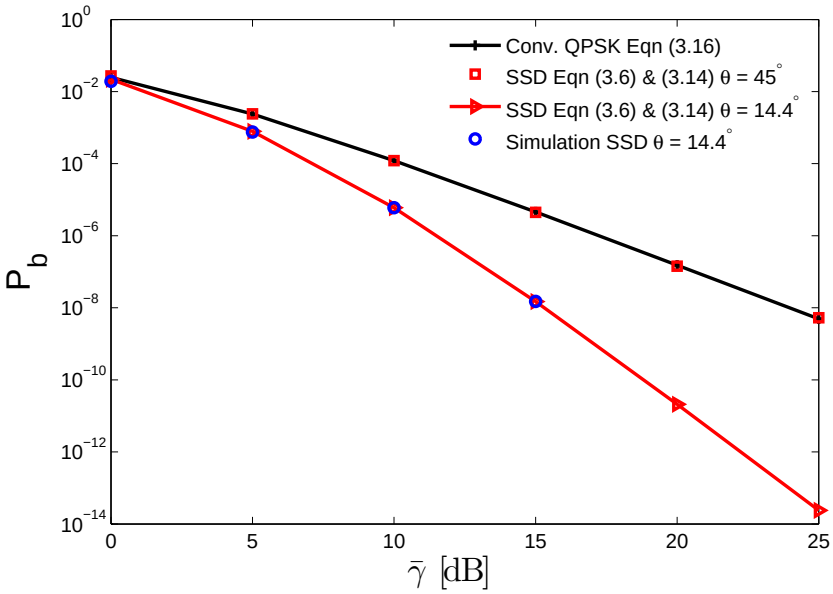

Figure 3.5: *Average probability of error P_b of conventional and SSD systems using QPSK signal constellation over Rayleigh fading channels with $L = 3$ and perfect CSI. Gray signal constellation mapping is used.*

results commensurate the closed form expressions presented for an SSD system.

3.4 Fading Correlation

There are a number of real-life scenarios in which the combined signals are not independent from one another and this occurs, for instance, due to insufficient antenna spacing in small mobile units equipped with space and polarization antenna diversity [65]. Furthermore, for multipath diversity the correlation coefficients can be up to 0.6 between adjacent and second adjacent paths in the channel impulse response of frequency selective channels [22]. As a result, the maximum theoretical diversity gain promised by MRC reception in the previous section cannot be achieved and therefore, the analysis has to be revamped to account for the effect

of correlation between the combined signals.

Several correlation models have been proposed and studied in the literature, e.g., [4, 17, 24, 65]. For instance in [24], a closed form expression for P_b of non-coherent binary frequency shift keying with dual branch MRC reception with nonidentically distributed Nakagami-m fading channel is presented. In [65], the outage probability and P_b for multichannel MRC reception with two correlation models: the constant (equal) correlation model and the exponential correlation is analyzed. We, also follow the same approach and use the same two correlation models for our system. It is to be noted that if two branches are considered the constant correlation model reduces to the case where two correlated branches are nonidentically faded [4, 65].

3.4.1 Identically Distributed Branches with Constant Correlation

This model was proposed in [65] for channels assumed to be having equal average SNR per bit and with the same fading parameter m. The envelope correlation coefficient is assumed to be the same for all channel pairs ($l, \acute{l} = 1, 2, \cdots L$). The envelope correlation coefficient between the signals r_l and $r_{\acute{l}}$ is given as [65]

$$\rho = \rho_{l,\acute{l}} = \frac{\mathrm{cov}(r_l^2, r_{\acute{l}}^2)}{\sqrt{\mathrm{var}(r_l^2)\mathrm{var}(r_{\acute{l}}^2)}}, \quad l \neq \acute{l}, \tag{3.19}$$

where $\mathrm{cov}(\cdot)$ represents the covariance of r_l^2 and $r_{\acute{l}}^2$ and $\mathrm{var}(\cdot)$ represents the variance. A real life scenario for such a model is when diversity antennas are closely placed. For instance, it was shown in [66], that three-element circular symmetric antenna array gives rise to constant correlation matrix.

The PDF of γ_t (defined as per (3.3)) is given as [65]

$$p(\gamma_t) = \frac{\left(\frac{m\gamma_t}{\bar{\gamma}}\right)^{Lm-1} e^{-\frac{m\gamma_t}{(1-\sqrt{\rho})\bar{\gamma}}} {}_1F_1\big(m; Lm; \frac{Lm\sqrt{\rho}\gamma_t}{(1-\sqrt{\rho})(1-\sqrt{\rho}+L\sqrt{\rho})\bar{\gamma}}\big)}{(\frac{\bar{\gamma}}{m})(1-\sqrt{\rho})^{m(L-1)}(1-\sqrt{\rho}+L\sqrt{\rho})^m\Gamma(Lm)}, \qquad \gamma_t \geq 0 \tag{3.20}$$

where ${}_1F_1(\cdot;\cdot;\cdot)$ is the Kummer confluent hypergeometric function [12, Eqn. (13.1.2)].

The unconditional PEP, for a system employing coordinate interleaving is given as

$$\begin{aligned} P(s \to \hat{s}) &= \int_0^\infty \int_0^\infty Q\left(\sqrt{\left(\gamma_{tI} d_I^2 + \gamma_{tQ} d_Q^2\right)}\right) \\ &\quad p(\gamma_{tI}) p(\gamma_{tQ}) \mathrm{d}\gamma_{tI} \mathrm{d}\gamma_{tQ}. \end{aligned} \tag{3.21}$$

Using (3.8) and (3.20) in the above equation we have

$$\begin{aligned} P(s \to \hat{s}) &= \frac{1}{\pi} \int_0^{\pi/2} \int_0^\infty \frac{\left(\frac{m\gamma_{tI}}{\bar{\gamma}}\right)^{Lm-1}}{(\frac{\bar{\gamma}}{m})(1-\sqrt{\rho})^{m(L-1)}(1-\sqrt{\rho}+L\sqrt{\rho})^m\Gamma(Lm)} \\ &\quad e^{-\gamma_{tI}\left(\frac{d_I^2}{2\sin^2(\psi)} + \frac{m}{(1-\sqrt{\rho})\bar{\gamma}}\right)} {}_1F_1\big(m; Lm; \frac{Lm\sqrt{\rho}\gamma_{tI}}{(1-\sqrt{\rho})(1-\sqrt{\rho}+L\sqrt{\rho})\bar{\gamma}}\big) \mathrm{d}\gamma_{tI} \\ &\quad \int_0^\infty \frac{\left(\frac{m\gamma_{tQ}}{\bar{\gamma}}\right)^{Lm-1}}{(\frac{\bar{\gamma}}{m})(1-\sqrt{\rho})^{m(L-1)}(1-\sqrt{\rho}+L\sqrt{\rho})^m\Gamma(Lm)} \\ &\quad e^{-\gamma_{tQ}\left(\frac{d_Q^2}{2\sin^2(\psi)} + \frac{m}{(1-\sqrt{\rho})\bar{\gamma}}\right)} \\ &\quad {}_1F_1\big(m; Lm; \frac{Lm\sqrt{\rho}\gamma_{tQ}}{(1-\sqrt{\rho})(1-\sqrt{\rho}+L\sqrt{\rho})\bar{\gamma}}\big) \mathrm{d}\gamma_{tQ} \mathrm{d}\psi \end{aligned} \tag{3.22}$$

Using the following identities [67, Eq. 4]

$$\int_0^\infty x^{b-1} {}_1F_1(a;c;kx) e^{-sx} \mathrm{d}x = \frac{\Gamma(b)}{s^b} {}_2F_1(a,b;c;\frac{k}{s}), \quad |s| > |k|, b > 0, s > 0, s > k, \tag{3.23}$$

together with the identity [12, Eq. (15.1.8)]

$$ {}_2F_1(a,b;b;z) = (1-z)^{-a}, \tag{3.24} $$

where ${}_2F_1(\cdot,\cdot;\cdot;\cdot)$ is the Gauss hypergeometric function [12, Eq. (15.1.1)], (3.22) can be simplified as

$$ \begin{aligned} P(s \to \hat{s}) \quad = \quad & \frac{1}{\pi}\int_0^{\pi/2} \left(\frac{\sin^2(\psi)}{\sin^2(\psi) + \frac{\bar{\gamma}(1-\sqrt{\rho})d_I^2}{2m}} \right)^{Lm} \\ & \left(\frac{\sin^2(\psi) + \frac{\bar{\gamma}(1-\sqrt{\rho})d_I^2}{2m}}{\sin^2(\psi) + \frac{\bar{\gamma}(1-\sqrt{\rho}+L\sqrt{\rho})d_I^2}{2m}} \right)^{m} \left(\frac{\sin^2(\psi)}{\sin^2(\psi) + \frac{\bar{\gamma}(1-\sqrt{\rho})d_Q^2}{2m}} \right)^{Lm} \\ & \left(\frac{\sin^2(\psi) + \frac{\bar{\gamma}(1-\sqrt{\rho})d_Q^2}{2m}}{\sin^2(\psi) + \frac{\bar{\gamma}(1-\sqrt{\rho}+L\sqrt{\rho})d_Q^2}{2m}} \right)^{m} \mathrm{d}\psi, \end{aligned} \tag{3.25} $$

which for integer values of m and L is integrable. Furthermore, it is important to state that the constant correlation model for $L = 2$, reduces to the model proposed by [17] of two correlated branches with nonidentical fading.

3.4.2 Identically Distributed Branches with Exponential Correlation

This model was also proposed in [65] for all channels having the same $\bar{\gamma}$ (average SNR per bit) and the same fading parameter m. This model assumes an exponential envelope correlation coefficient $\rho_{l,\acute{l}}$ between any pair of channels $(l, \acute{l} = 1, 2, \cdots, L)$ given as [65]

$$ \rho_{l,\acute{l}} = \frac{\mathrm{cov}(r_l^2, r_{\acute{l}}^2)}{\sqrt{\mathrm{var}(r_l^2)\mathrm{var}(r_{\acute{l}}^2)}} = \rho^{|l-\acute{l}|}, \quad l \neq \acute{l}. \tag{3.26} $$

The PDF of γ_t, in this case, is very well approximated by a gamma distribution given as [65]

$$p(\gamma_t) = \frac{\gamma_t^{(mL^2/d_\rho)} e^{\left(-\frac{mL\gamma_t}{d_\rho \bar{\gamma}}\right)}}{\Gamma(\frac{mL^2}{d_\rho}) \left(\frac{d_\rho \bar{\gamma}}{mL}\right)^{mL^2/d_\rho}}, \qquad \gamma_t \geq 0 \tag{3.27}$$

where

$$d_\rho = L + \frac{2\sqrt{\rho}}{1-\sqrt{\rho}} \left(L - \frac{1-\rho^{L/2}}{1-\sqrt{\rho}} \right). \tag{3.28}$$

The unconditional PEP, for a system employing coordinate interleaving is therefore, given as

$$\begin{aligned} P(s \to \hat{s}) &= \int_0^\infty \int_0^\infty Q\left(\sqrt{\left(\gamma_{tI} d_I^2 + \gamma_{tQ} d_Q^2 \right)} \right) \\ &\quad p(\gamma_{tI}) p(\gamma_{tQ}) \mathrm{d}\gamma_{tI} \mathrm{d}\gamma_{tQ}. \end{aligned} \tag{3.29}$$

Using (3.8) and (3.27) in (3.29) we have

$$\begin{aligned} P(s \to \hat{s}) &= \frac{1}{\pi \Gamma^2(\frac{mL^2}{d_\rho}) \left(\frac{d_\rho \bar{\gamma}}{mL}\right)^{\frac{2mL^2}{d_\rho}}} \int_0^{\pi/2} \int_0^\infty \int_0^\infty \gamma_{tI}^{(\frac{mL}{d_\rho}-1)} \\ &\quad e^{-\gamma_{tI}\left(\frac{d_I^2}{2\sin^2(\psi)} + \frac{mL}{d_\rho \bar{\gamma}}\right)} \gamma_{tQ}^{(\frac{mL}{d_\rho}-1)} \\ &\quad e^{-\gamma_{tQ}\left(\frac{d_I^2}{2\sin^2(\psi)} + \frac{mL}{d_\rho \bar{\gamma}}\right)} \mathrm{d}\gamma_{tI} \mathrm{d}\gamma_{tQ} \mathrm{d}\psi, \end{aligned} \tag{3.30}$$

which simplifies to

$$P(s \to \hat{s}) = \frac{1}{\pi} \int_0^{\pi/2} \left(\frac{\sin^2(\psi)}{\sin^2(\psi) + \frac{\bar{\gamma} d_I^2}{2m}} \right)^{\frac{mL^2}{d_\rho}} \left(\frac{\sin^2(\psi)}{\sin^2(\psi) + \frac{\bar{\gamma} d_Q^2}{2m}} \right)^{\frac{mL^2}{d_\rho}} \mathrm{d}\psi. \tag{3.31}$$

The above integrand is integrable for integer values of mL^2/d_ρ.

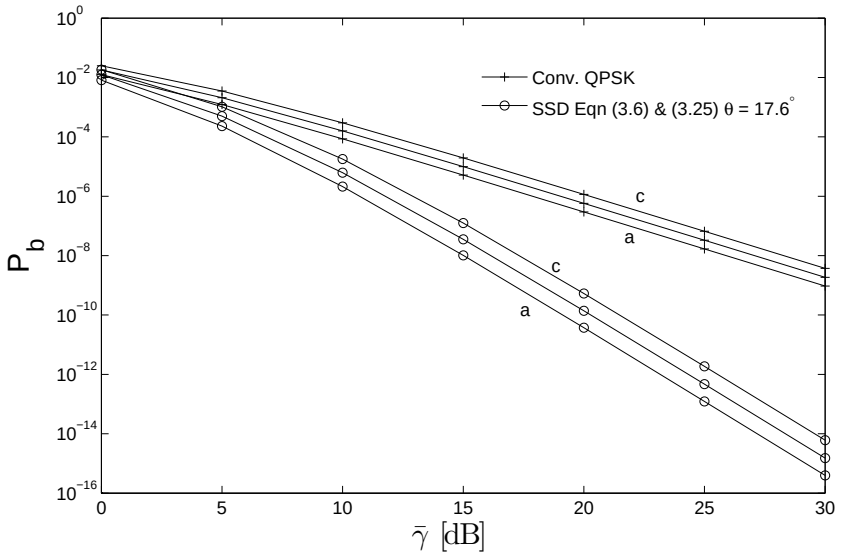

Figure 3.6: *Average probability of error P_b of conventional and SSD systems using QPSK signal constellation for constant correlation profile over Nakagami fading channels with $L = 5$, $m = 0.5$ and perfect CSI. Gray signal constellation mapping is used. The various values of correlation coefficient used are: (a) $\rho = 0$; (b) $\rho = 0.2$; (c) $\rho = 0.4$. $\bar{\gamma}_l = \bar{\gamma}$ for $l = 1, 2, \cdots, L$.*

3.4.3 Union Bound for Correlated Paths

Figures 3.6 and 3.7 show the performance improvement of a system employing SSD over the conventional QPSK system with $L = 5$, $m = 0.5$ and $L = 5$,$m = 2$ for identically distributed branches with constant and exponential correlation, respectively. The figures show that for both the models of correlation (constant and exponential), SSD systems outperform conventional systems even when the correlation between the paths is high. Moreover, from both figures we can also conclude that the constant correlation suffers a minor performance degradation compared to the exponential correlation but the difference is more noticeable for a larger number of diversity branches and higher correlation between the paths.

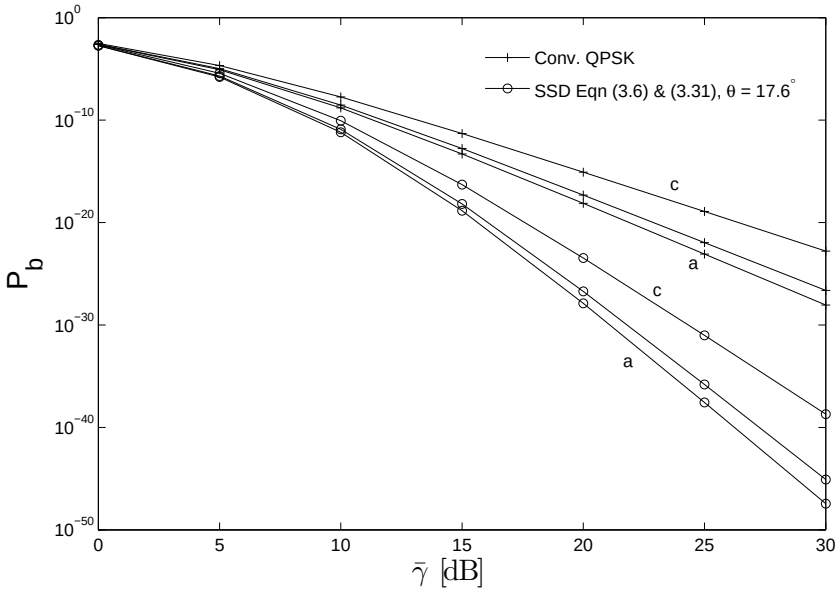

Figure 3.7: *Average probability of error P_b of conventional and SSD systems using QPSK signal constellation for exponential correlation profile over Nakagami fading channels with $L = 5$, $m = 2$ and perfect CSI. Gray signal constellation mapping is used. The various values of correlation coefficient used are: (a) $\rho = 0$; (b) $\rho = 0.2$; (c) $\rho = 0.4$. $\bar{\gamma}_l = \bar{\gamma}$ for $l = 1, 2, \cdots, L$.*

3.5 Impact of Imperfect Channel Estimates

In general, diversity schemes and, in particular, systems employing coordinate interleaving and constellation rotation rely on accurate channel estimation to perform detection at the receiver. However, practical systems suffer from estimation errors due to additive noise as well as channel variation/decorrelation over time. The channel fading extracted, e.g., from pilot symbols differs from the actual fading affecting the data symbols, thereby inducing a performance degradation. The effects of channel estimation on the performance of diversity systems has been studied in the literature [4, 68–70] and the references therein.

It was shown by [68] that the PDF of the combined SNR in the presence of

channel estimation errors for i.i.d Rayleigh fading paths changes from (3.4) to

$$p(\gamma_t) = \frac{(1-\rho_e)^{L-1} e^{(-\frac{\gamma_t}{\bar{\gamma}})}}{\bar{\gamma}} \sum_{l=1}^{L} \frac{\begin{pmatrix} L-1 \\ l-1 \end{pmatrix}}{(l-1)!} \left[\frac{\rho_e \gamma_t}{(1-\rho_e)\bar{\gamma}}\right]^{l-1}, \tag{3.32}$$

where $\rho_e \in [0,1]$ is the power correlation coefficient between the estimated channel fade and the actual fading experienced by the transmitted signal. The coefficient is a measure of the quality of the channel estimation [68, 70] and is related to the time delay τ and the Doppler frequency shift of the channel. It was shown by [70, Eqn. (7)] that (3.32) can be rewritten as

$$p(\gamma_t) = \sum_{l=1}^{L} W(l) \frac{\gamma_t^{l-1} e^{-\frac{\gamma_t}{\bar{\gamma}}}}{(l-1)!\bar{\gamma}^l}, \tag{3.33}$$

where

$$W(l) = \begin{pmatrix} L-1 \\ l-1 \end{pmatrix} (1-\rho_e)^{L-l} \rho_e^{l-1}. \tag{3.34}$$

When $\rho_e = 1$ perfect correlation exists between the estimated channel fading and the actual fading, and perfect MRC combining is achieved. As the correlation between the estimated channel fading and the actual fading decreases (equivalently ρ_e decreases), the performance degrades. Another important aspect is that the weighting coefficients $W(l)$ are independent from γ_t and, therefore, the unconditional PEP for a system employing coordinate interleaving and constellation rotation can be given as

$$\begin{aligned} P(s \to \hat{s}) &= \sum_{l=1}^{L} W(l) \int_0^\infty \int_0^\infty Q\left(\sqrt{\left(\gamma_{tI} d_I^2 + \gamma_{tQ} d_Q^2\right)}\right) \\ &\quad p(\gamma_{tI}) p(\gamma_{tQ}) \mathrm{d}\gamma_{tI} \mathrm{d}\gamma_{tQ}. \end{aligned} \tag{3.35}$$

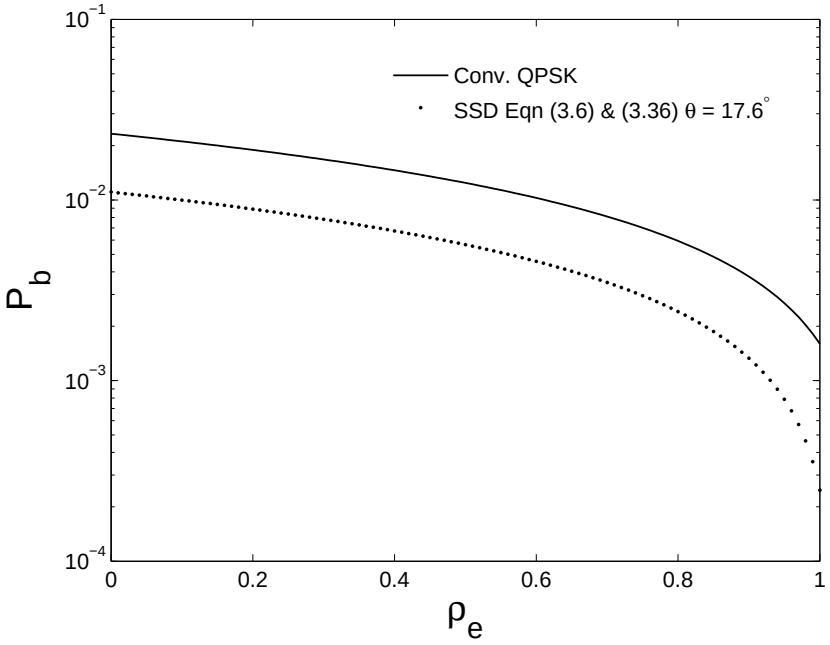

Figure 3.8: *Average probability of error P_b of conventional and SSD systems using QPSK signal constellation for different values of power correlation coefficient ρ_e over Nakagami fading channels with $L = 2$, $m = 1$, $E_b/N_0 = 10$ dB and perfect CSI. Gray signal constellation mapping is used.*

Using the results from Section 3.3 (3.12) we can rewrite the above equation for Nakagami-m fading as

$$P(s \to \hat{s}) = \sum_{l=1}^{L} W(l) \frac{1}{\pi} \int_0^{\pi/2} \left(\frac{\sin^2(\psi)}{\sin^2(\psi) + \frac{\bar{\gamma} d_I^2}{2m}} \right)^{lm} \left(\frac{\sin^2(\psi)}{\sin^2(\psi) + \frac{\bar{\gamma} d_Q^2}{2m}} \right)^{lm} \mathrm{d}\psi, \tag{3.36}$$

which as shown previously (3.14) is integrable for integer values of lm.

3.5.1 Channel Estimation Error

Figure 3.8 illustrates the analysis presented in Section 3.5 by showing the performance degradation due to the correlation coefficient $\rho_e \in [0, 1]$ between the estimated and actual fading for dual branch MRC receiver with SSD and for uncorrelated Rayleigh faded paths. When there is perfect channel estimation $\rho_e = 1$ or, equivalently, perfect correlation between the estimated fading (via e.g., pilots symbols) and the actual fading, MRC with SSD outperforms the conventional system. As ρ_e decreases, the correlation between the estimated fading and the actual fading diminishes and, consequently, the performance of MRC with SSD and conventional MRC systems degrades. However, SSD systems show robustness and even in the limit when $\rho_e \to 0$, i.e., the fading estimate is uncorrelated to the actual fading, SSD outperforms the conventional system. Furthermore, it is important to note that as the $\rho_e \to 0$, the performance of conventional and SSD systems approaches the performance without multipath diversity.

3.6 Conclusions

In this chapter, we have investigated the performance of a system employing signal space diversity using $L-$ branch MRC receiver. An expression for the upper bound of P_b is derived for MPSK signal constellations for uncorrelated and correlated Nakagami-m faded branches. The new derived bound is shown to be tight for the entire range of the constellation rotation angle at high SNRs. The rotation angles are optimized by minimizing the upper bound. Two correlation models are considered, i.e., the constant (equal) correlation model and the exponential correlation model. A closed form expression for a system with outdated or imperfect channel estimation error is derived. It is shown that the system employing SSD is

more robust to channel estimation errors. Furthermore, we have also shown that the Gray mapping in a system employing SSD is not necessarily the best option over the entire range of rotational angle θ.

Chapter 4

Coded SSD Systems

In this chapter an introduction to modulation diversity coupled with channel coding is presented. A brief overview of low density parity check (LDPC) codes and convolutional codes is given and salient features of a coherent wireless communication system employing channel coding and modulation diversity are highlighted. Furthermore, it is shown that with a proper choice of the rotation angle a system employing modulation diversity and channel coding can provide significant performance improvement over an uncoded system using modulation diversity in multipath fading channels.

4.1 Introduction

Diversity coupled with coding has been proposed as a possible solution for next generation wireless communications systems with stringent quality of service (QoS) requirements. Channel coding in last few decades has seen remarkable progress being made towards Shannon's limit [71] by using codes that are termed as turbo codes [72] and codes based on sparse graphs known as low density parity check (LDPC) codes [73]. These codes have dramatically raised the bar for codes to be termed as 'Good' [74] and have the ability to meet the stringent of QoS requirements of the next generation wireless communication systems.

We, in this chapter, and in following chapters, employ these capacity approaching codes as forward error correcting codes in our wireless communication systems. We use practically sized low density parity check (LDPC) codes and recursive systematic convolutional (RSC) codes in combination with signal space diversity (SSD), also known as coordinate interleaving or modulation diversity, to achieve gain in narrow-band wireless communication systems. The main emphasis of the chapter is two fold. Firstly, to introduce a coded system using SSD and to highlight the performance differences from an uncoded system using SSD. Secondly, to lay down the necessary background for cooperative modulation and decoding; also known as iterative demodulation and decoding. Initially, a brief overview of LDPC and RSC codes is presented. SSD[1], coupled with LDPC or RSC codes is proposed as a possible solution for improved performance in fading channels. The performance gain achieved with coded SSD in comparison to the uncoded case is highlighted and it is shown that a system employing coordinate interleaving and constellation rotation exhibits different optimal rotation angles than an uncoded system employing SSD. A symbol-to-bit de-mapper for multi-

[1] See Chapters 2 and 3 for more details on SSD.

level modulation schemes employing SSD is introduced. Furthermore, it is shown that with a proper choice of the rotation angle in coded system using SSD leads to a significant performance improvement over the uncoded case in fading channels.

The rest of the chapter is organized as follows. Sections 4.2 and 4.3 briefly review the basics of LDPC and RSC codes. In Section 4.4 the coded SSD system model is presented and the performance is investigated in Section 4.5 for MPSK signal constellations in frequency flat environments. Lastly, we present the conclusions and the major contributions of the chapter in Section 4.6.

4.2 Low Density Parity-Check Codes

LDPC codes have certain advantages over other codes, e.g., turbo codes. They not only have a simple description of their code structure but can also have a fully parallelizable decoding implementation [73, 75]. LDPC codes with message passing decoding algorithms have achieved excellent performance over the additive white Gaussian noise (AWGN) channel [76, 77]. However, their potential as capacity approaching codes for more realistic wireless channels, has not been established yet. Preliminary results are available which suggest that they can achieve capacity for a wide range of channels [75, 78]. The idiosyncracy of LDPC codes is that if the noise level is smaller than a certain noise threshold, the bit error probability goes to zero as the block size reaches infinity and the codes approach channel capacity [77]. However, these codes have too high complexity to be considered for real-time applications. Random, regular incarnations of LDPC codes provide an alternative where the complexity and the size are reduced with a loss in performance [74]. For a detailed discussion on LPDC codes we refer the reader to [73–79] and the references therein.

4.2.1 Encoder

An LDPC code is a linear block code which is specified by a very sparse parity check matrix H [73]. LDPC codes have an inherent advantage, i.e., the controlled sparseness of the code results in a specified and very small number of non-zero bits in each column. This, not only reduces the number of equations to be solved by the decoder but also results in making decoding feasible by the means of iterative methods similar to turbo codes. LDPC codes can be represented by a bipartite graph. One set of the nodes in the graph corresponds to the elements of the code word referred to as *variable nodes*. The other set of nodes corresponds to the set of parity check constraints and are termed as *check nodes* [79]. An edge exists between the variable and the check node if and only if there is a 1 in the corresponding entry in the parity check matrix. The code word length and the number of parity bits are represented by N and F, respectively, and therefore, the designed code rate R can be expressed as

$$R = 1 - \frac{F}{N} \tag{4.1}$$

There are two main incarnations of LDPC codes, namely, regular and irregular. Regular LDPC codes have the same number of ones in each row (column) of the parity check matrix. Equivalently, the degrees of all the variable nodes (check nodes) are equal, where the degree of any node is the number of edges emanating from or terminating on it. For instance, a $(3, 6)$ regular LDPC has a mathematical representation in which all the variable nodes have degree 3 and all the check nodes have degree 6. The bipartite graph determining such a code is shown in Figure 4.1. Irregular LDPC codes were introduced in [80]. In irregular LDPC codes the variable and the check nodes can have different degrees and their degrees are

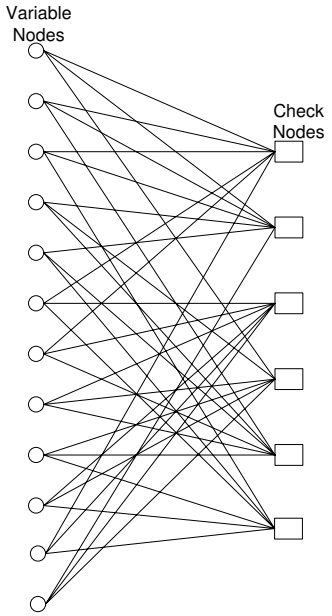

Figure 4.1: *Bi-partite graph representation of a code of length 12 and rate* $1/2$*. There are* 12 *variable nodes and* 6 *check nodes. For each check node, the sum (over GF(2)) of all adjacent variable nodes is equal to zero.*

specified by a degree distribution pair (λ, ρ).

Encoding of linear LDPC codes involves solving a set of linear equations to find the code word. Gaussian elimination and re-ordering of columns can be used to calculate the code word [74]. There are, however, more efficient schemes for reducing the complexity of encoding [81]. We, however, use Gaussian elimination and column reordering which although being less efficient is sill very suitable for codes with small block lengths.

4.2.2 Decoder

One of the most widely used decoding method for LDPC codes is based on belief propagation. It is performed by applying the maximum *a posteriori* (MAP) algorithm [82]. MAP aims at minimizing the bit error rate of the decoded sequence and iteratively calculates the *a posteriori* probabilities [82,83]. Consider a regular (j,k) LDPC code with v as the log-likelihood ratio (LLR) message passed from a variable node of degree j to a check node of degree k, given as [76],

$$v = \Lambda + \sum_{i=1}^{j-1} q_i. \tag{4.2}$$

In (4.2), Λ is the *intrinsic information* conditioned on the channel output, and q_i, for all $i = 1, \ldots, j-1$, is the incoming *extrinsic information* from the neighbors of the variable node except the check node that gets the message v. Extrinsic information is part of the overall LLR stemming from the observation of the received samples.

The check nodes update rule is obtained by noticing the duality between variable and check nodes. It is based upon the well known *tanh* rule and it is given as [83]

$$\tanh \frac{q}{2} = \prod_{i=1}^{k-1} \tanh \frac{v_i}{2}, \tag{4.3}$$

where v_i, for all $i = 1, \ldots, k-1$, are the incoming LLRs from $k-1$ neighbors of a degree-k check node and q is the output LLR message sent to the remaining neighbor.

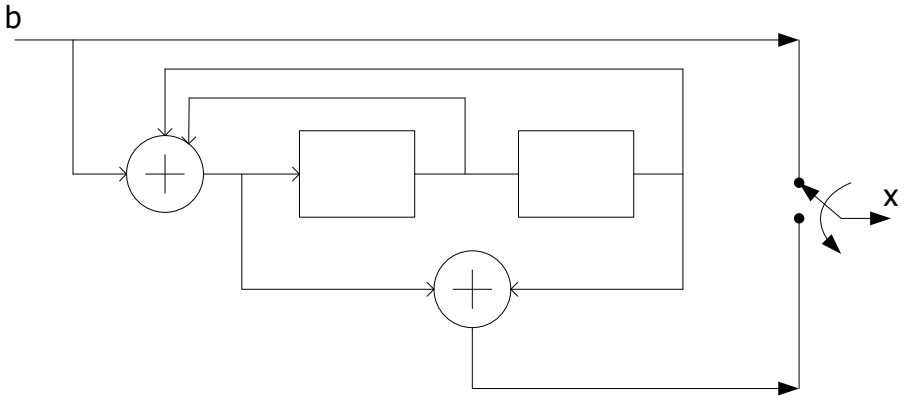

Figure 4.2: *4-state RSC code with rate* $\frac{1}{2}$*, and generator polynomial* $[07, 05]_8$

4.3 Recursive Systematic Convolutional Codes

Convolutional codes are widely used in wireless communication applications. Convolutional codes were introduced in 1954 [84] and the algebraic theory was presented in 1970 [85]. In this section a brief overview of the systematic convolutional codes and a trellis based decoding algorithm based on MAP algorithm, also known as BCJR [82] or APP [86] or sum product algorithm [77] is presented. For a detailed discussion on convolutional codes we refer the reader to [87–91], and the references therein. A binary convolution encoder is a finite-memory system that outputs N binary bits for every K information bits presented at its input. The code rate is defined as $R_c = K/N$. In a convolutional code the N bits generated by the encoder depend not only on the corresponding K message bits but also on the previous $(L-1)K$ bits. Such a code is called an (N, K, L) convolutional code. L is the number of data frames that are retained by the input register. It is also called as the *constraint length* of the code[2].

[2]It is important to note that there is no unique definition of the constraint length in the convolutional code literature.

4.3.1 Systematic Form

In a systematic convolutional code the first K output sequences are the exact replica as of the input information sequences. Figure 4.2, shows an example 4-state RSC encoder of rate $\frac{1}{2}$ with a generator polynomial $[07, 05]_8$. Systematic encoders have a significant advantage over the non-systematic encoders as not only the message sequence is displayed in the encoded output sequence and can be read directly from the received sequence but, also, that the systematic convolutional codes are not *catastrophic*. A catastrophic code causes an infinite number of decoding errors for a finite number of channel errors.

4.3.2 MAP Decoder

MAP algorithm minimizes the symbol (or bit) probability. Let the output code sequence of a convolutional encoder be represented as $\mathbf{x} = (x_1, \cdots, x_N)$ when an input information sequence of $\mathbf{b} = (b_1, \cdots, b_K)$ was given. The associated state sequence $\mathbf{e} = (e_1, \cdots, e_N)$ with an N-stage state trellis, where the state transition (e_{k-1}, e_k) has output/input symbols x_k/b_k at epoch k. The observed (received) sequence is $\mathbf{r} = (r_1, \cdots, r_N)$. At the decoder, the estimate of the information sequence $\mathbf{b}$ is denoted as $\hat{\mathbf{b}} = (\hat{b_1}, \cdots, \hat{b_K})$.

A posteriori probability at epoch k is estimated by the MAP algorithm as [82, 83] ,

$$P(\hat{b_k} = a) = P(b_k = a|\mathbf{r}) = \sum_{(e',e):b_k=a} p(e', e, \mathbf{r})/p(\mathbf{r}), \tag{4.4}$$

where (e', e) is the state transition at epoch k with information symbol $b_k = a$, and a is an 2^m-ary information symbol and m are the number of bits corresponding to a symbol. One elegant representation form of the *a posteriori* probability can

be obtained by splitting the joint probability as [83]

$$\begin{aligned} p(e', e, \mathbf{r}) &= p(e', e, \mathbf{r}_{j<k}, r_k, \mathbf{r}_{j>k}) \\ &= p(e', \mathbf{r}_{j<k}).p(r_k, e|e').p(\mathbf{r}_{j>k}|e) \\ &= \alpha_{k-1}(e').\gamma_k(e', e).\beta_k(e), \end{aligned} \tag{4.5}$$

leading to three branch metrics, i.e., branch metric $\gamma_k(e', e)$, the forward recursion $\alpha_{k-1}(e')$, and the backward recursion $\beta_k(e)$.

The MAP decoding requires large number of operations (multiplications and additions) and memory. The algorithm is considered too complex for implementation at hardware level and therefore, a simplification is by using log-algorithms. Hence, the name Log-MAP algorithm. Even, Log-MAP algorithm has high complexity for many communication devices and therefore, usually its suboptimal variants such as the look-up table Log-MAP and the Max-Log-MAP algorithms are considered for practical applications. Soft output Viterbi algorithm (SOVA) is a desirable alternative as it is simple and has a relation with Viterbi algorithm (VA). However, a finite window SOVA decoding has poor performance compared to the Max-Log-MAP algorithm [92].

Furthermore, it is interesting to note that the MAP algorithm proposed in [82] was also proposed in [93] for the removal of inter-symbol interference. Similarly, in [94] a MAP algorithm was proposed with only the forward recursion. In [95], MAP algorithm was proposed for character recognition. A soft-input soft-output MAP algorithm for serial concatenated codes was reported in [86].

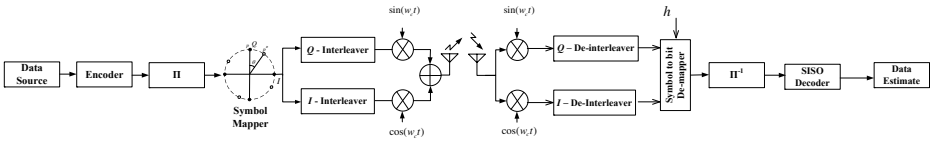

Figure 4.3: *System model of RSC-coded SSD.*

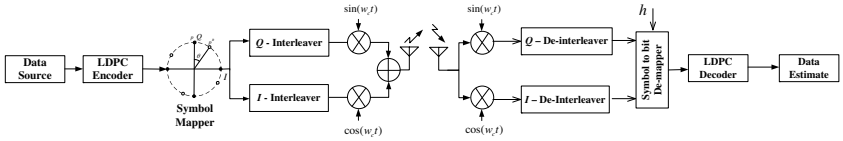

Figure 4.4: *System model of LDPC-coded SSD.*

4.4 System Model

In this section we present RSC and regular, random LDPC codes coupled with SSD and multi-level modulation schemes in a block uncorrelated Rayleigh fading channel. In multi-level modulation schemes, we confine ourselves to MPSK signal constellations and introduce a symbol to bit de-mapper for MPSK modulation schemes employing SSD.

For better comprehension of the analysis presented in this section we repeat certain aspects of the system model already described in Chapter 2 and 3.

Figures 4.3 and 4.4 show RSC and LDPC-coded systems employing coordinate interleaving and constellation rotation. A pseudo-random interleaver, represented by π, is used to break the sequential fading correlation between consecutive bits that are being transmitted. However, an LDPC-coded system is a special instance as shown in Figure 4.4. Contrary to the conventional systems no interleaver (de-interleaver) block is placed between the encoder (decoder) and the symbol mapper (symbol-to-bit demapper). This is due to the fact that the bits are inherently interleaved (de-interleaved) by the LDPC-encoder (decoder) [75]. In the conven-

tional concatenated system's decoding process every bit needs to make use of the information of its neighbor bits to update it's own likelihood information. A channel interleaver is, therefore, introduced to break the correlation of channel fades among the consecutive bits. However, in LDPC decoding, when any bit b updates its related information from a parity check, e.g., check p , it only makes use of the bits participating in check p. As the parity check matrix H of LDPC code is randomly constructed, the probability that these bits will be neighbors of bit b is very small. Therefore, when bit b is in a deep fade, it is very likely that some of the bits that participate in updating the information of bit b will not experience a severe fade and can therefore, provide reliable information for bit b. This inherent interleaving by LDPC codes is a reflection upon the random and sparse structure of it's parity check matrix. This phenomenon is applicable for a fading channel with a coherence time shorter than the length of the code. In [75, 96], it was shown that the LDPC codes due to inherent interleaving are able to achieve good performance over correlated fading channels without the use of an external channel interleaver.

The encoded bits are mapped onto symbols using rotated constellations using pre-defined symbol labeling. The I and Q components of the mapped symbols are then separately interleaved and transmitted through the Rayleigh fading channel which is assumed to be block independent. I and Q interleaving uncorrelates the in-phase and quadrature components. At the receiver, the received I and Q components are de-interleaved. The de-interleaved components along with the channel state information (CSI) are used by the symbol-to-bit de-mapper and the decoder to generate estimates of the transmitted bits. It is important to note that the interleavers shown in the Figures 4.3 and 4.4 after the symbol mapper are symbol coordinate interleavers having smaller depth than a bit interleaver.

Furthermore, since the bit interleaving already breaks the correlation due to fading, the purpose of the coordinate interleaving is to make the I and Q channels uncorrelated implying that the I and Q channel would experience independent fade. A single coordinate interleaver or a delay line introducing a delay that exceeds the coherence time of the channel would have the same effect and can be used instead of the two interleavers.

4.4.1 I and Q Interleaving of Rotated MPSK Constellations

A conventional MPSK signal constellation, using the same notation as Chapters 2 and 3, is denoted by $\mathcal{S}_M = \{s_l = e^{2\pi(l/M)j} : l = 0, 1, \ldots, M-1\}$, where the energy has been constrained to unity and each symbol corresponds to $m = \log_2 M$ bits. Clockwise rotation over an angle θ leads to the constellation

$$\mathcal{S}_M^{\theta} = \{s_l = e^{(2\pi(l/M)-\theta)j} : l = 0, 1, \ldots, M-1\}. \tag{4.6}$$

The symbol mapper can be represented by the one-to-one mapping function $\wp : \{0,1\}^m \rightarrow \mathcal{S}_M^{\theta}, s = \wp(\mathbf{b})$, where, $\mathbf{b} = (b_1, \cdots, b_m), b_j \in \{0,1\}$ represents the binary sequence and s is chosen from the set $\mathcal{S}_M^{\theta}$ consisting of M complex signal points. In case of N symbol transmission each taken from the rotated constellation $\mathcal{S}_M^{\theta}$, let the sequence of I components $\mathbf{x} = (x_0, x_1, \ldots, x_{N-1})$ and the sequence of Q components $\mathbf{y} = (y_0, y_1, \ldots, y_{N-1})$ be interleaved by the I interleaver η and the Q interleaver ρ, respectively, resulting in the sequences $\tilde{\mathbf{x}} = \eta(\mathbf{x}) = (\tilde{x}_0, \tilde{x}_1, \ldots, \tilde{x}_{N-1})$ and $\tilde{\mathbf{y}} = \rho(\mathbf{y}) = (\tilde{y}_0, \tilde{y}_1, \ldots, \tilde{y}_{N-1})$. The transmitted waveform

for the rotated and interleaved system is given by

$$\begin{aligned} s(t) &= \sum_{i=0}^{N-1} \tilde{x}_i p(t - iT_s)\cos(2\pi f_c t) \\ &+ \sum_{i=0}^{N-1} \tilde{y}_i p(t - iT_s)\sin(2\pi f_c t). \end{aligned} \tag{4.7}$$

where

$$p(t) = \begin{cases} 1, & 0 \le t \le T_s, \\ 0, & \text{otherwise}, \end{cases}$$

T_s is the symbol period and f_c is the carrier frequency.

4.4.2 Rayleigh Fading

The transmission is assumed to be over a block independent Rayleigh fading channel with perfect CSI available at the receiver. The baseband input/output relations per channel use are given by

$$\begin{aligned} \tilde{r}_i^I &= \tilde{h}_i \tilde{x}_i + \tilde{n}_i^I, \\ \tilde{r}_i^Q &= \tilde{h}_i \tilde{y}_i + \tilde{n}_i^Q, \end{aligned} \tag{4.8}$$

where the $\tilde{h}_i$ are normalized and independent *Rayleigh fading factors* with a probability density function $p(\alpha) = 2\alpha e^{-\alpha^2}, \alpha > 0$ and thus, $\mathcal{E}\left[(\tilde{h}_i)^2\right] = 1$. The $\tilde{n}_i^I$ and $\tilde{n}_i^Q$ are independent and identically distributed (i.i.d) Gaussian random variables with zero mean and variance $N_0/2$. Separate interleaving of I and Q components thus, results for each symbol in transmitting the I component x_i during one fade interval and the Q component y_i during another fade interval. This kind of interleaving adds diversity to the system as x_i and y_i experience independent fading

as also shown previously for uncoded systems in Chapter 2 and Chapter 3.

4.4.3 Symbol Detection

The received sequences $\tilde{\mathbf{r}}^{\mathbf{I}}$ and $\tilde{\mathbf{r}}^{\mathbf{Q}}$ are de-interleaved resulting in $\mathbf{r}^{\mathbf{I}} = \eta^{-1}(\tilde{\mathbf{r}}^{\mathbf{I}})$ and $\mathbf{r}^{\mathbf{Q}} = \rho^{-1}(\tilde{\mathbf{r}}^{\mathbf{Q}})$. We assume that perfect CSI is available, i.e., the fading sequence $\tilde{\mathbf{h}} = (\tilde{h}_0, \tilde{h}_1, \ldots, \tilde{h}_{N-1})$ and thus the de-interleaved fading component sequences $\mathbf{h}^{\mathbf{I}} = \eta^{-1}(\tilde{\mathbf{h}})$ and $\mathbf{h}^{\mathbf{Q}} = \rho^{-1}(\tilde{\mathbf{h}})$ are known at the receiver. Based on the received symbols we are able to calculate the estimates of the transmitted bit sequence.

4.4.4 Symbol to Bit De-mapping for MPSK Constellations

Assuming perfect CSI, the LLR values for MPSK systems are given in [97, 98] which are modified to incorporate signal space diversity as

$$\begin{aligned}\Lambda\left(b_{i,m}\right) &= \log\left(\frac{\max_{l\in\mathcal{S}_{+m}}\left\{\exp\left(E_{i,l}^{1}+E_{i,l}^{2}\right)\right\}}{\max_{l\in\mathcal{S}_{-m}}\left\{\exp\left(E_{i,l}^{1}+E_{i,l}^{2}\right)\right\}}\right)\\ &= \max_{l\in\mathcal{S}_{+m}}\left\{E_{i,l}^{1}+E_{i,l}^{2}\right\}-\max_{l\in\mathcal{S}_{-m}}\left\{E_{i,l}^{1}+E_{i,l}^{2}\right\},\end{aligned} \tag{4.9}$$

where in the above equation $\Lambda\left(b_{i,m}\right)$ denotes the LLR value and $b_{i,m}$ is bit m of symbol i ($m = 1, 2, \ldots, \log_2 M; i = 0, 1, \ldots, N-1$). In (4.9), $\mathcal{S}_{+m}$ denotes the set of symbols for which the m^{th} bit is 1 and similarly the set $\mathcal{S}_{-m}$ denotes the set of symbols for which the m^{th} bit is 0. $E_{i,l}^{1}$ and $E_{i,l}^{2}$ are defined as:

$$\begin{aligned}E_{i,l}^{1} &= -\frac{1}{N_0}\left|r_i^I - h_i^I s_l^I\right|^2,\\ E_{i,l}^{2} &= -\frac{1}{N_0}\left|r_i^Q - h_i^Q s_l^Q\right|^2.\end{aligned} \tag{4.10}$$

The initial intrinsic LLRs computed by the symbol to bit de-mapper are passed to the decoder.

4.5 Simulation Results And Discussion

In this section, we present the results of a coded SSD system using RSC and LDPC codes as error correcting codes. The effect of the rotational angle (θ) and the performance gain achieved by employing channel coding are highlighted in this section. Regular random $(3, 6)$ LDPC-codes of length 2640, rate $\frac{1}{2}$ and 10 internal iterations and 16-state RSC code with rate $\frac{1}{2}$, information block length of 2600 and generator polynomial $[37, 21]_8$ are considered. QPSK and 8PSK signal constellations are used. Furthermore, frequency flat slowly fading environment with channel amplitudes having Rayleigh distribution and perfect channel state information (CSI) availability at the receiver is assumed. For further information on channel modeling we refer the reader to Chapter 1, and for further details on channel codes being employed we refer the reader to [87–91], and the references therein.

The performance of MPSK signal constellation in frequency flat slowly fading environments was discussed in detail in Chapter 2. It was shown that the average probability of bit error for an uncoded MPSK signal constellation using SSD can be upper bounded as

$$P_b \leq P_b^{UB} = \frac{1}{m2^m} \sum_{s \in \mathcal{S}_M^\theta} \sum_{\substack{\hat{s} \in \mathcal{S}_M^\theta \\ s \neq \hat{s}}} a(s, \hat{s}) P(s \rightarrow \hat{s}), \tag{4.11}$$

where $P(s \rightarrow \hat{s})$ is the pairwise error probability (PEP) that the receiver estimated $\hat{s}$ when s was transmitted; given that s and $\hat{s}$ are the only two signal constellation points under-consideration. $a(s, \hat{s})$ represents the Hamming distance between the bit sequences of s and $\hat{s}$ under consideration. Furthermore it was shown that the $P(s \rightarrow \hat{s})$ for MPSK signal constellations in Rayleigh fading environments can be

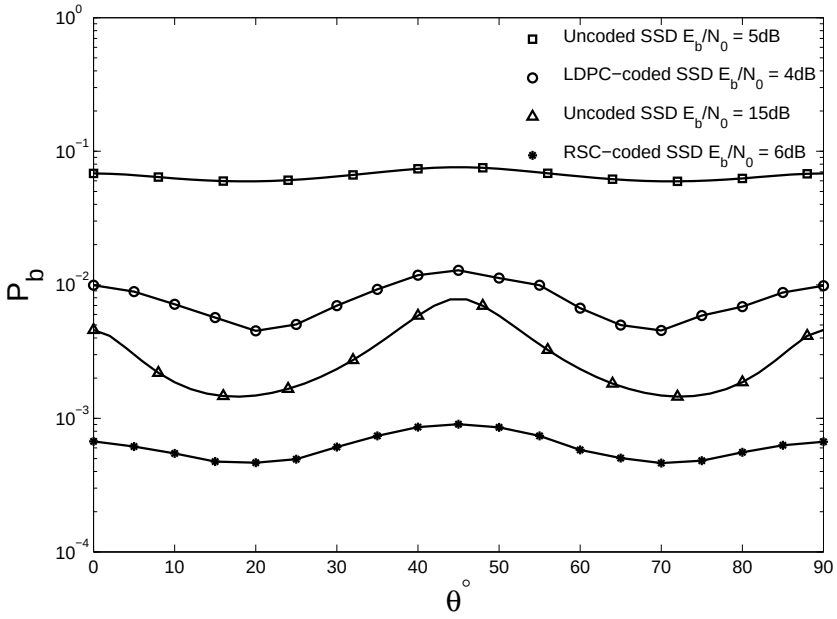

Figure 4.5: *BER performance of QPSK SSD system over different rotation angles. Uncoded and coded (RSC and LDPC coded) SSD system in flat Rayleigh fading channel with perfect CSI. Gray signal constellation mapping is used.*

given as Chapter 2 (2.25)[3]

$$P(s \to \hat{s}) = \frac{1}{2} - \frac{d_I^2}{2(2d_I^2 - C)} \left(\sqrt{\frac{\bar{\gamma} d_I^2}{2 + \bar{\gamma} d_I^2}} \right) + \frac{C - d_I^2}{2(2d_I^2 - C)} \left(\sqrt{\frac{\bar{\gamma}(C - d_I^2)}{2 + \bar{\gamma}(C - d_I^2)}} \right), \tag{4.12}$$

where $C = d_I^2 + d_Q^2$.

[3]Equation (2.25) from Chapter 2 is repeated, intentional, for the sake of better readability.

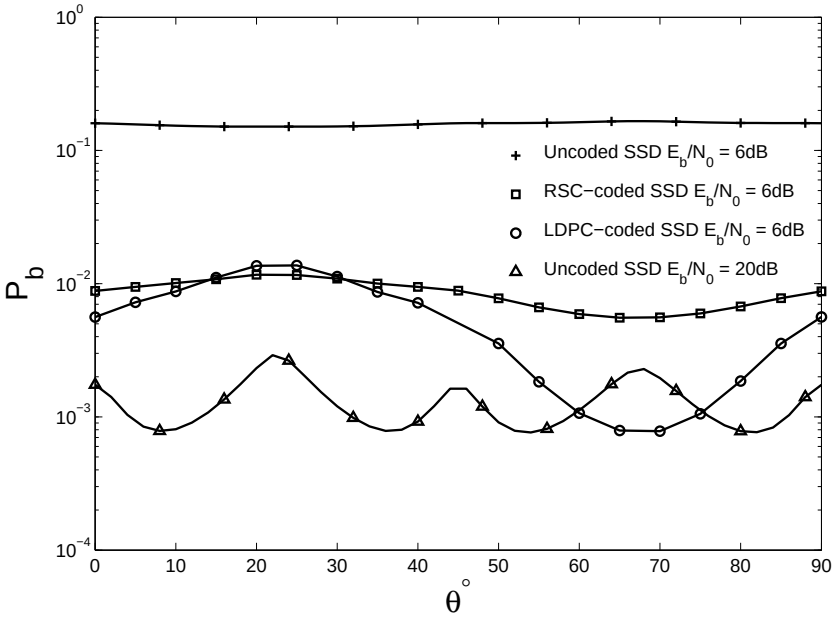

Figure 4.6: *BER performance of 8PSK SSD system over different rotation angles. Uncoded and coded (RSC and LDPC coded) SSD system in flat Rayleigh fading channel with perfect CSI. Gray signal constellation mapping is used.*

4.5.1 QPSK

Rotation Angle

Figure 4.5 depicts the average probability of bit error P_b versus the rotational angle θ for QPSK signal constellation with and without channel coding in multipath Rayleigh fading channels. It is evident from the figure that channel coding provides a significant performance improvement over the uncoded case. Another important aspect highlighted by the figure is that in the uncoded case the optimal rotation angles are different than for a coded system. Both RSC and LDPC codes exhibit different optimal rotation angles and it is possible to suggest that under cooperative demodulation and decoding (also known as iterative demodu-

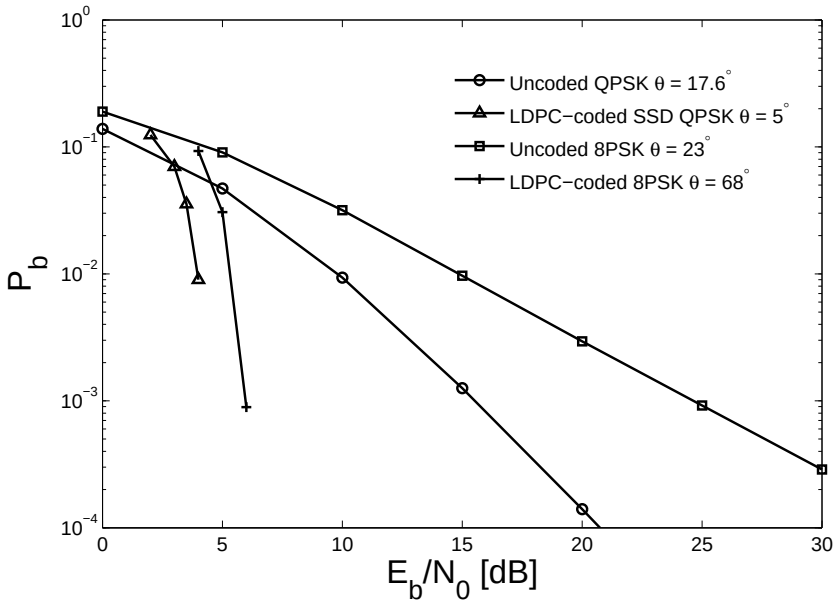

Figure 4.7: *BER performance of uncoded and LDPC-coded QPSK and 8PSK signal constellation in flat Rayleigh fading channel with perfect CSI. Gray signal constellation mapping is used.*

lation and decoding) the optimal rotation angles might change again[4]. Another interesting aspect in the case of QPSK signal constellation is that in all the cases (coded and uncoded) the system shows the worst performance around 45°. This peculiar behavior for an uncoded QPSK case was discussed in Chapter 2. In Chapter 2, it was shown that the worst case scenario for a system employing coordinate interleaving and constellation rotation is when one branch has been completely removed, i.e., d_I^2 or $d_Q^2 = 0$. In such a case, the performance of the system using SSD reduces to the case when coordinate interleaving was not employed. It also shows that the choice of the rotation angle plays a very vital role in a system using coordinate interleaving and constellation rotation. The optimal rotation angle exhibited by the uncoded case is 17° whereas for RSC and LDPC

[4]This phenomenon would be further elaborated upon in Chapter 5.

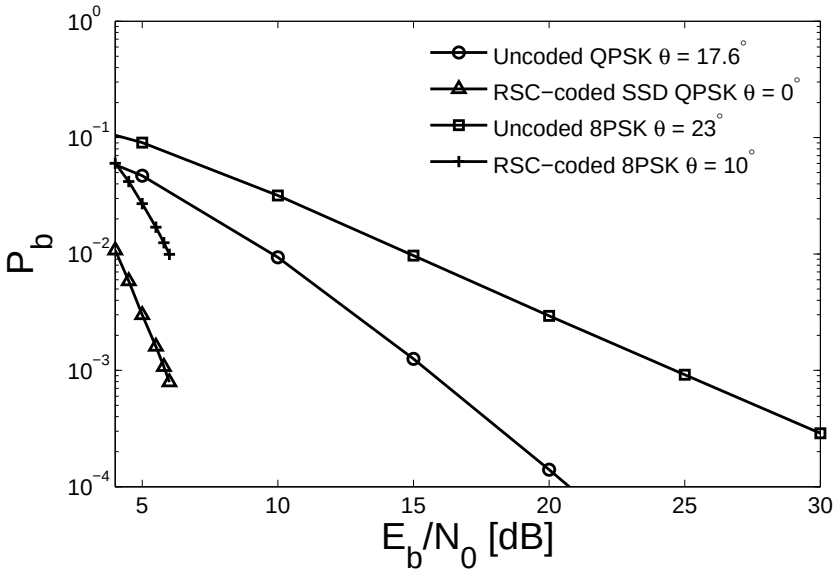

Figure 4.8: *BER performance of uncoded and RSC-coded QPSK and 8PSK signal constellation in flat Rayleigh fading channel with perfect CSI. Gray signal constellation mapping is used.*

codes the optimal rotation angle is around 20°. It is important to state that the optimal rotation angles exhibited for the coded system employing SSD will be further investigated in Chapter 5 using tools, e.g., extrinsic information transfer (EXIT) charts. Furthermore, it is also important to state that Gray-mapped QPSK signal constellation is employed and the rotation angles would vary if the mapping was to be modified. Moreover, the choice of different SNR, for coded and uncoded systems using SSD, is adopted intentionally to easily highlight the effect of the rotational angle on average bit error rate in the figure.

Performance Gain

The performance gain provided by channel coding (RSC and LDPC codes) for QPSK signal constellation is illustrated by Figures 4.7 and 4.8. Figure 4.7 shows

the performance of a RSC-coded SSD system and Figure 4.8 shows the performance an LDPC-coded SSD system. A performance gain of 5.7 dB at a bit error rate (BER) of 1×10^{-2} for LDPC codes using QPSK signal constellation and a gain of 5 dB at a bit error rate (BER) of 1×10^{-2} for RSC codes using QPSK signal constellation is shown in Figures 4.7 and 4.8, respectively. The figures quantify the gain that is achieved by channel coding in a system employing SSD.

4.5.2 8PSK

Rotation Angle θ

Figure 4.6 depicts the average probability of bit error P_b versus rotational angle θ for 8PSK signal constellation with and without channel coding in multipath Rayleigh fading channels. The gain provided by channel coding in comparison to the uncoded case is very evident. The most important aspect highlighted by the figure is that coded system using SSD (either RSC or LDPC codes) exhibits different optimal rotation angles as compared to the uncoded case. For instance, in Figure 4.6, consider $\theta = 70°$, the uncoded case has the worst performance (in terms of average probability of error P_b) whereas for the coded system (both RSC and LDPC codes) have the best performance in the region around $\theta = 70°$. This behavior is very different as compared to the QPSK signal constellation and will be further analyzed in Chapter 5.

Performance Gain

The performance gain provided by channel coding (RSC and LDPC codes) is illustrated by Figures 4.7 and 4.8. A performance gain of 9.4 dB at a bit error rate (BER) of 1×10^{-2} for LDPC codes and a a gain of 8.6 dB at a bit error rate (BER) of 1×10^{-2} for RSC codes is shown in Figures 4.7 and 4.8, respectively. The

figures quantify the gain that is achieved by channel coding in a system employing SSD.

4.6 Conclusions

In this chapter we have introduced a coded SSD system using different error correcting codes, namely, RSC and LDPC codes with MPSK signal constellations. The performance gain achieved by coded SSD in comparison to the uncoded system using SSD is highlighted. A symbol-to-bit demapper for MPSK signal constellations was introduced. It is shown that a system employing coordinate interleaving and constellation rotation exhibits different rotation angle than an uncoded system using SSD. Furthermore, it was shown that the proper choice of a rotation angles plays a vital role in the performance of a system using SSD.

Chapter 5

EXIT Chart Analysis of Coded SSD-ID Systems

This chapter studies the extension of bit interleaved coded modulation schemes with iterative demodulation and decoding (ID) coupled with rotated MPSK signal constellations with different symbol mappings and signal space diversity (SSD). A performance analysis of a system employing SSD with error correcting is presented. Extrinsic information transfer (EXIT) charts are used to analyze the behavior of the system and the factors (degrees of freedom) that can effect the convergence behavior of the iterative demodulation and decoding of the proposed system are identified and their effect is highlighted.

5.1 Introduction

Diversity coupled with coding is an attractive option for systems operating at high data rates and low signal-to-noise ratio (SNR) in severe fading conditions. In this chapter, we extend the analysis presented in Chapter 4 of the use of practically sized error correcting codes (namely, low density parity check (LDPC) codes and convolutional codes) coupled with signal space diversity (SSD) and rotated M-ary phase shift keying (MPSK) constellations to achieve gain in wireless communication channels at low SNRs by the use of iterative demodulation and decoding (ID), also known as cooperative modulation and decoding.

In [99, 100] it was shown that iterative decoding (ID) can increase the minimum intersignal Euclidean distance of bit interleaved coded modulation (BICM), while retaining the desirable Hamming distance. SSD can provide performance improvement over fading channels by maximizing the diversity of a communication system [30]. Also, in [41] it was shown that for a block independent wireless communication link, improved performance can be obtained for a QPSK system without affecting its bandwidth efficiency, by rotating the signal constellation and separately interleaving the in-phase (I) and quadrature phase (Q) components. In [101, 102], this approach was used to increase the diversity by combining with BICM. In [101] and [102], convolutional codes in a BICM system using coordinate interleaving were shown to have improved performance not only over conventional BICM system but also over trellis coded modulation (TCM).

If the noise level is smaller than a certain threshold, LDPC codes show their idiosyncratic behavior to approach channel capacity in an additive white Gaussian noise (AWGN) channel as the block size reaches infinity [77]. However, these LDPC codes with irregular structures have too high complexity to be considered for real-time applications. Random, regular incarnations of LDPC codes pro-

vide an alternative where the complexity and the size are reduced with a loss in performance.

This chapter presents the following. A new system model is proposed based on iterative demodulation and decoding technique using rotated multi-level modulation schemes. LDPC and convolutional codes are used as forward error correcting codes with the proposed scheme. A performance analysis of a system employing coordinate interleaving and constellation rotation with error correction is presented. The effect of different signal mappings, the number of iterations and the effect of iterations on the optimum rotation angles in block Rayleigh fading channels is analyzed. Extrinsic information transfer (EXIT) charts are used to analyze this behavior and to illuminate the effect of optimum rotation on the convergence behavior of iterative demodulation and decoding. A symbol-to-bit de-mapper for multi-level modulation schemes is extended to incorporate iterative demodulation with SSD. Factors (degrees of freedom) which can affect the convergence behavior of the iterative demodulation and decoding are identified and their effect is analyzed by illustrative examples. Different signal mappings for QPSK and 8PSK constellations under various rotation angles are considered. This novel proposed scheme using rotated constellations is shown to outperform conventional BICM-ID.

The chapter is organized as follows. Section 5.2 briefly outlines the main blocks of the system model. Iterative demodulation and decoding is discussed in Section 5.3. Capacity of the system employing SSD is analyzed in Section 5.4. Effect of constellation rotation is discussed in Section 5.5. Sections 5.6, 5.7, 5.8 and 5.9 present the EXIT chart analysis, the transfer characteristics, the convergence behavior and the effect of error correcting codes on the system performance, respectively. Results are presented in Section 5.10 followed by conclusions in

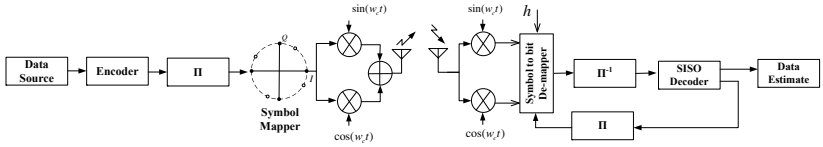

Figure 5.1: *System model of a conventional BICM-ID system.*

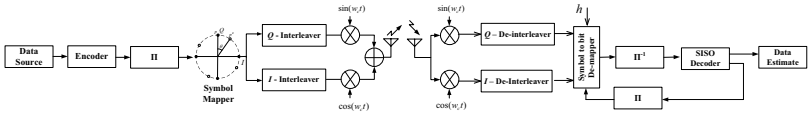

Figure 5.2: *System model of a BICM-ID system with SSD and signal constellation rotation.*

Section 5.11.

5.2 System Model

Figures 5.1, 5.2 and 5.3 depict serially concatenated systems using iterative demodulation and decoding. A generic system block diagram of a conventional BICM-ID system is shown in Figure 5.1. An extension of such a system with SSD (hereafter referred to as SSD-ID) with rotated signal constellation is shown in Figure 5.2. However, an LDPC-coded system is a special instance as shown in Figure 5.3. The transmitted waveform for rotated and interleaved system is the same as presented in the system model in Chapter 4. Therefore, we refer the reader to the system model presented in Chapter 4.

For QPSK only two symbol mappings are possible, i.e., Gray and Natural, which were presented in Chapter 2, whereas for 8PSK we have used Gray, set-partitioned (SP) and semi set-partitioned (SSP) mappings [44,99] in this chapter. Adopting the same method as used in Chapter 2, we for MPSK define an M-element vector $(a_0, \cdots, a_{M-1})$ to represent an MPSK mapper where a_n is the

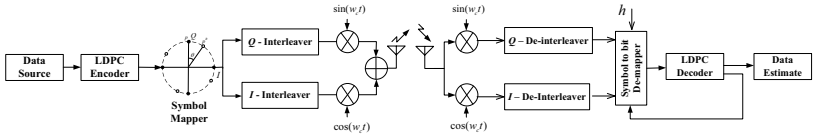

Figure 5.3: *System model of an LDPC-coded BICM-ID system with SSD and signal constellation rotation.*

decimal number of the binary representation of the rotated MPSK signal constellation point. The 8PSK set-partition (SP) mapper is, therefore, given as $(0, 1, 2, 3, 4, 5, 6, 7)$. Whereas, Gray and semi set-partition (SSP) mappings are defined as $(0, 1, 3, 2, 6, 7, 5, 4)$ and $(0, 5, 2, 7, 4, 1, 6, 3)$, respectively.

The transmission is assumed to be over a block independent Rayleigh fading channel with perfect CSI available at the receiver. The baseband input/output relations per channel use are given by

$$\begin{aligned} \tilde{r}_i^I &= \tilde{h}_i \tilde{x}_i + \tilde{n}_i^I, \\ \tilde{r}_i^Q &= \tilde{h}_i \tilde{y}_i + \tilde{n}_i^Q, \end{aligned} \tag{5.1}$$

where the $\tilde{h}_i$ are normalized and independent *Rayleigh fading factors* with a probability density function $p(\alpha) = 2\alpha e^{-\alpha^2}, \alpha > 0$ and thus, $\mathcal{E}\left[(\tilde{h}_i)^2\right] = 1$. The $\tilde{n}_i^I$ and $\tilde{n}_i^Q$ are independent and identically distributed (i.i.d) Gaussian random variables with zero mean and variance $N_0/2$. Separate interleaving of I and Q components thus, results for each symbol in transmitting the I component x_i during one fade interval and the Q component y_i during another fade interval. This kind of interleaving adds diversity to the system as x_i and y_i experience independent fading.

The received sequences $\tilde{\mathbf{r}}^{\mathbf{I}}$ and $\tilde{\mathbf{r}}^{\mathbf{Q}}$ are de-interleaved resulting in $\mathbf{r}^{\mathbf{I}} = \eta^{-1}(\tilde{\mathbf{r}}^{\mathbf{I}})$ and $\mathbf{r}^{\mathbf{Q}} = \rho^{-1}(\tilde{\mathbf{r}}^{\mathbf{Q}})$. We assume that perfect CSI is available, i.e., the fading

sequence $\tilde{\mathbf{h}} = (\tilde{h}_0, \tilde{h}_1, \ldots, \tilde{h}_{N-1})$ and thus the de-interleaved fading component sequences $\mathbf{h^I} = \eta^{-1}(\tilde{\mathbf{h}})$ and $\mathbf{h^Q} = \rho^{-1}(\tilde{\mathbf{h}})$ are known at the receiver. Based on the received symbols we are able to calculate iteratively the estimates of the transmitted bit sequence.

For further details on I and Q interleaving and symbol detection we refer the reader to Chapter 4. The iterative demodulation and decoding process is described in more detail in the next section.

5.3 Iterative Demodulation and Decoding

Figures 5.2 and 5.3 show the serial concatenation of a soft-input soft-output (SISO) symbol-to-bit demodulator (indicated as "symbol-to-bit de-mapper") and a SISO decoder which are employed to iteratively demodulate and decode the received $\mathbf{r^I}$ and $\mathbf{r^Q}$ de-interleaved components. The receiver processes the blocks of received symbols and calculates the estimates of the transmitted data bits by the cooperative assistance of the symbol-to-bit de-mapper and the decoder. The symbol-to-bit de-mapper processes the received symbols to produce the extrinsic information which is passed to the SISO decoder. The demodulator has the CSI information available. The extrinsic information is updated by the SISO decoder and is fed back to the symbol-to-bit demapper. The receiver, thus iterates between the demodulator and the decoder to reliably estimate the transmitted bits. If the code itself does not use iterative decoding, in case of a conventional convolutional code, as shown in Figure 5.2, then there would be a single iteration of decoding for every iteration of demodulation. On the other hand, if the code is iteratively decoded, as it is the case for LDPC codes as shown in Figure 5.3, then for every iteration of demodulation there are a specified number of internal iterations within the decoder before the extrinsic information is updated for feed-back.

The following subsections describe the demodulation and the decoding blocks, for the cases of MPSK constellations and SISO decoding (LDPC and convolutional decoding), in more detail.

5.3.1 Iterative Symbol-to-Bit De-mapping

The symbol-to-bit de-mapper operates on a symbol-by-symbol basis to compute the log likelihood ratio (LLR) of the coded bits associated with each received symbol. The symbol-to-bit de-mapper, with CSI information, computes the LLR at iteration 'q' of $b_{i,j}$ which is the j^{th} bit of the i^{th} received symbol where $j = 1, 2, \ldots, m; i = 0, 1, \ldots, N-1$, denoted by $\lambda^q(b_{i,j})$, as in [98], which is modified to incorporate signal space diversity and feedback from the SISO decoder and is given by

$$\lambda^q(b_{i,j}) = \log \frac{P_r\left(b_{i,j} = 0 \mid r_i, h_i, \omega^{q-1}(b_{i,1}), \cdots, \omega^{q-1}(b_{i,m})\right)}{P_r\left(b_{i,j} = 1 \mid r_i, h_i, \omega^{q-1}(b_{i,1}), \cdots, \omega^{q-1}(b_{i,m})\right)} \tag{5.2}$$

where $\mathbf{r} = (r_0, r_1, \cdots, r_{N-1})$ is the received sequence, $\mathbf{h} = (h_0, h_1, \cdots, h_{N-1})$ is the fading sequence, and ω^{q-1} is the extrinsic information calculated by the SISO decoder in the previous iteration and fed-back as *a priori* information. The equation (5.2) can be rewritten and simplified as

$$\begin{aligned}\lambda^q(b_{i,j}) \approx & \max_{\mathbf{a}\in\{0,1\}^m : a_j = 0} \left\{ E_i(\wp(\mathbf{a})) + \sum_{k=1, k\neq j}^{m} (-1)^{a_k} . \frac{\omega^{q-1}(b_{i,k})}{2} \right\} \\ & - \max_{\mathbf{a}\in\{0,1\}^m : a_j = 1} \left\{ E_i(\wp(\mathbf{a})) + \sum_{k=1, k\neq j}^{m} (-1)^{a_k} . \frac{\omega^{q-1}(b_{i,k})}{2} \right\},\end{aligned} \tag{5.3}$$

where $\wp(.)$ is the mapping function introduced in Chapter 4, subsection 4.4.1 and $E_i(s)$ is defined as

$$E_i(s) = -\frac{1}{N_0}\left(\left|r_i^I - h_i^I s^I\right|^2 + \left|r_i^Q - h_i^Q s^Q\right|^2\right), \tag{5.4}$$

with $s \in \mathcal{S}_M^\theta$. In the first iteration $\omega^0(b_{i,k}) = 0; \forall i,k$, is assumed. On the subsequent passes (i.e., iterations $q \geq 2$), the extrinsic information of the bits $\omega^{q-1}(b_{i,k})$ is used as *a priori* information by the symbol-to-bit de-mapper. Since we have bit interleaving (inherently in LDPC codes), we may assume that the probabilities of the bits that compose the symbol are independent [97, 98]. From (5.3), it is clear that when recalculating the bit metrics for one bit, we only need to use the *a priori* probabilities of the other bits in the same channel symbol.

5.3.2 SISO Decoder

Iterative SISO LDPC decoder [77] and SISO decoder for convolutional codes based on [86] to generate the extrinsic LLR values of the coded bits for iterative demodulation and decoding are considered. After sufficient number of iterations between the symbol-to-bit de-mapper and SISO decoder (LDPC decoder or SISO convolutional decoder), the final decision is based on the *a posteriori* probabilities of the information bits. We refer the reader to Chapter 4, where the salient features of both the decoders are described in detail.

5.4 Capacity

Capacity under uniform input constraints and perfect CSI, in a flat Rayleigh fading channel that is assumed to be memoryless and with continuous-output, is given by the conditional average mutual information. With the help of the

chain rule of mutual information [103], the symbol-wise mutual information can be decomposed into a sum of m bitwise mutual information terms. This implies that there are m-parallel independent channels. Let b denote the binary input and $\mathbf{r}$ the channel output vector. The capacity, therefore, can be given as [104]

$$\begin{aligned} \hat{C} &= I(b;\mathbf{r}) \\ &= 1 - \frac{1}{m}\sum_{i=1}^{m} \mathcal{E}_{b,\mathbf{r}}\left[\log_2 \frac{\sum_{s\in\mathcal{S}_M^{\theta}} P_r\left(\mathbf{r} \mid s\right)}{\sum_{s\in S_b^i} P_r\left(\mathbf{r} \mid s\right)}\right], \end{aligned} \tag{5.5}$$

where, S_b^i is the subset of all the signals in $\mathcal{S}_M^{\theta}$ whose corresponding bit strings have the value $b \in \{0,1\}$ in position i. In general, the expectation in (5.5) cannot be evaluated in closed form. By numerical integration using the Monte Carlo method, the capacity of the BICM system can be evaluated. Figure 5.4 shows the effect of the constellation mapping on the capacity of BICM. Furthermore, the figure also shows that SSD-ID can increase the capacity for a particular signal constellation labeling with a well considered choice of the rotation angle, as indicated by the respective dotted lines. The choice of the rotational angles used would be elaborated upon in the subsequent section.

5.5 Effect of Constellation Rotation

The rotation of the signal constellation has an effect on the overall system performance of SSD-ID. The effect of the rotation of the signal constellation can be visualized by fixing the E_b/N_0-value and observing a system performance parameter, e.g., bit error rate (BER). A block independent Rayleigh fading channel is considered. The observations are parsed for better comprehension on the basis of the error correcting codes being employed.

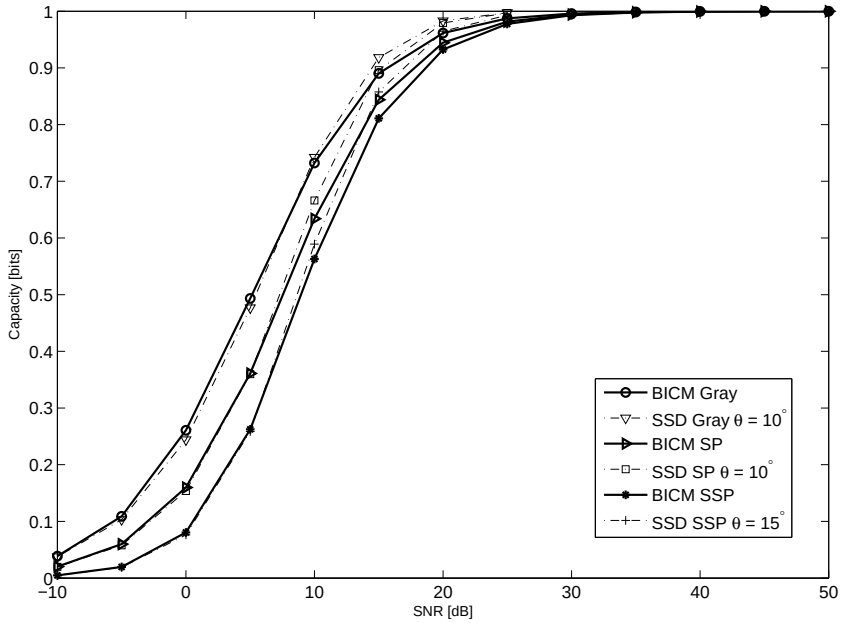

Figure 5.4: *BICM and SSD capacity versus SNR for 8PSK over Rayleigh fading with perfect CSI using different signal constellation labeling.*

5.5.1 Convolutional Codes

16-state, rate $\frac{1}{2}$ and rate $\frac{2}{3}$ recursive systematic convolutional codes (RSC) with a generator polynomial $[37, 21]_8$ are employed in an SSD-ID system. Punctured convolutional codes are employed in which all the transmitted bits are a subset of a lower rate code. This permits an increase in the code redundancy by incremental transmission, and can be combined with ARQ schemes. In punctured convolutional codes only a subset of the coded bits are transmitted while others are removed according to the puncture pattern. The puncture pattern used in our simulation is given in Table 5.1. Each data block contains 2600 information bits. QPSK with Gray and Natural mapping, and 8PSK with Gray, SP and SSP mapping are used. Figures 5.5 and 5.6 show the BER as a function of various rotation angles for QPSK modulation scheme at $E_b/N_0 = 5$ dB, with code rates

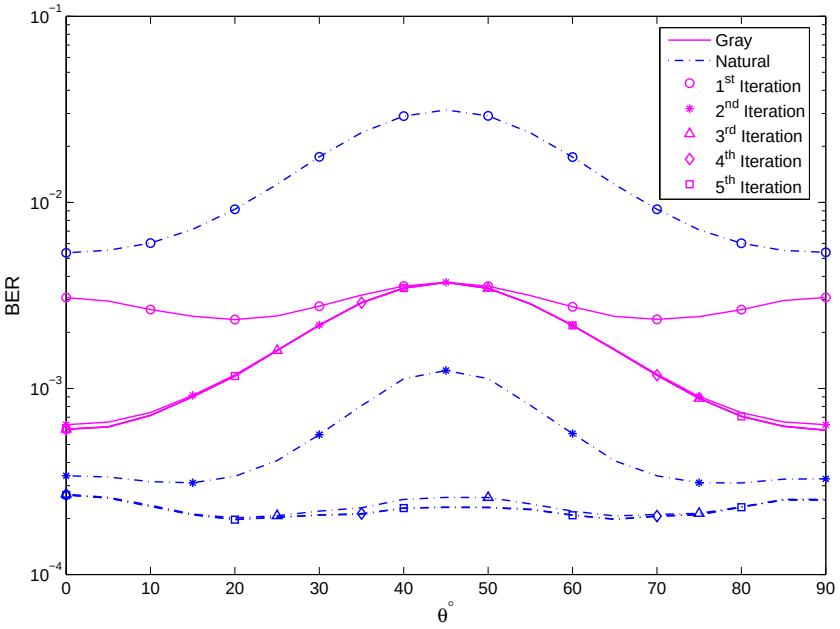

Figure 5.5: *BER performance of QPSK SSD-ID over different rotation angles.* 16-*state, rate* $\frac{1}{2}$ *RSC codes are used with Gray and Natural signal constellation labeling in a Rayleigh fading channel at* $E_b/N_0 = 5$ *dB.*

Table 5.1: *Puncture patterns for the 16-state punctured convolutional codes [88].*

Code Rate (R)	Puncturing Pattern
$\frac{1}{2}$	1111
	1111
$\frac{2}{3}$	1111
	1x1x

$\frac{1}{2}$ and $\frac{2}{3}$, respectively. The figures elucidate that the system performance, i.e., BER is dependent upon the choice of the rotation angle. The system shows best performance at 0° and 20° for Gray and Natural labeling, respectively, when 5 iterations are performed between the demodulator and the decoder. Rotation

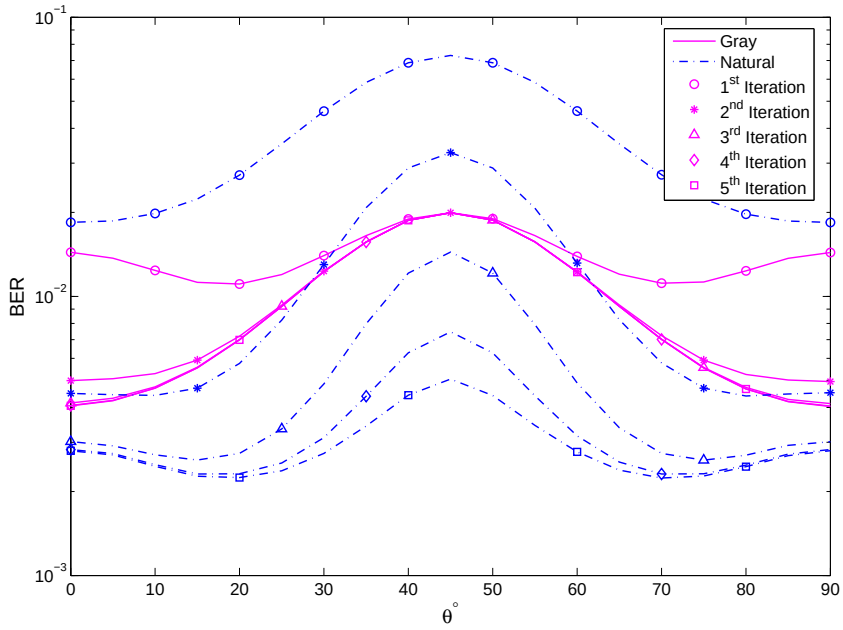

Figure 5.6: *BER performance of QPSK SSD-ID over different rotation angles.* 16-*state, rate* $\frac{2}{3}$ *RSC codes are used with Gray and Natural signal constellation labeling in a Rayleigh fading channel at* $E_b/N_0 = 5$ *dB.*

angles having better BER performance change after the first iteration for both mappings. No further improvement in performance can be obtained with Gray labeled constellation after 2 iterations. This peculiar behavior is further discussed and elaborated upon with the help of EXIT charts. Furthermore, the rotation angles exhibiting better performance for a specific signal constellation are immune to the change in the code rate as depicted in the Figures 5.5 and 5.6. It is due to the fact that the transmitted bits are punctured to a higher rate by removing the parity bits and this lowers the error correcting capability but has no effect on the characteristic features (SSD and signal constellation rotation) of SSD-ID.

Similarly, Figures 5.7 and 5.8 show the BER performance of the 8PSK system as a function of the rotation angle. The figures signify the dependence of

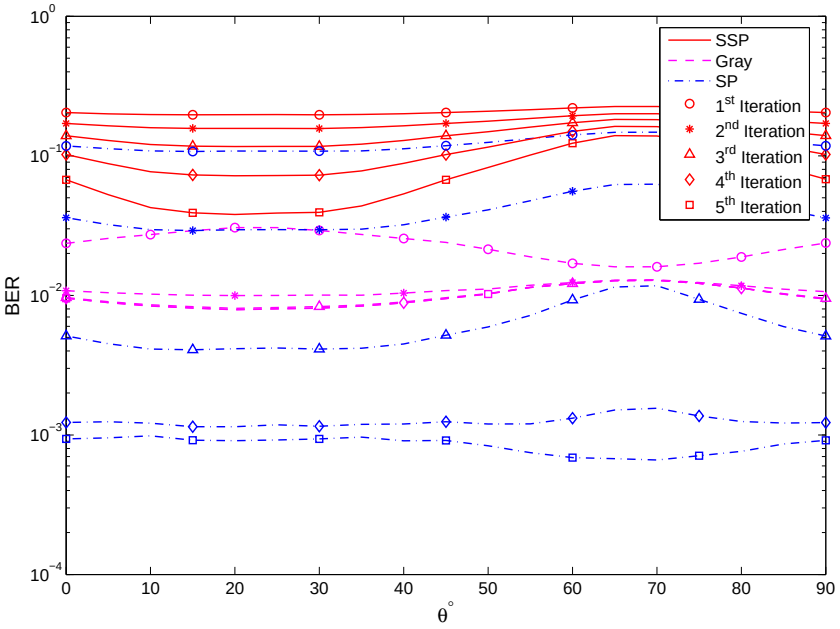

Figure 5.7: *BER performance of 8PSK SSD-ID over different rotation angles.* 16-*state, rate* $\frac{1}{2}$ *RSC codes are used with Gray, SP and SSP signal constellation labeling in a Rayleigh fading channel at* $E_b/N_0 = 5$ *dB.*

the performance of the system on the choice of the rotation angle and the signal constellation labeling. Furthermore, the figures also show that certain signal constellation labeling perform better at higher SNR region. Gray, SP and SSP labeling show best performance at 20°, 70° and 15°, respectively, at the 5^{th} iteration as in comparison to other rotational angles. At higher E_b/N_0-values SSP with an appropriately chosen rotation angle has better performance than Gray and SP labeling when 3 or more iterations are performed between the demodulator and the decoder, as depicted by Figure 5.8.

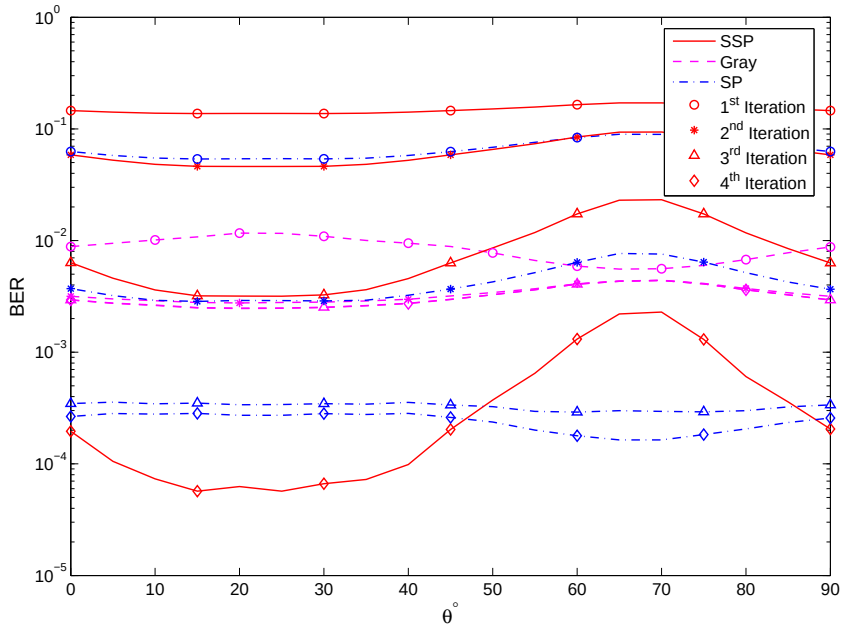

Figure 5.8: *BER performance of 8PSK SSD-ID over different rotation angles.* 16-*state, rate* $\frac{1}{2}$ *RSC codes are used with Gray, SP and SSP signal constellation labeling in a Rayleigh fading channel at* $E_b/N_0 = 6$ *dB.*

5.5.2 LDPC codes

Random, regular $(3, 6)$ LDPC codes of rate $\frac{1}{2}$ and length 2640 with 10 internal iterations are used to observe the dependence of BER on the signal constellation rotation in an SSD-ID system. Figure 5.9 shows the BER performance of QPSK signal constellation as a function of rotation angle using Gray and Natural labeling in an SSD-ID system. Rotation angles of 5° and 0° for Gray and Natural labeling, respectively, have better performance than other rotation angles at the 5^{th} (external) iteration. The BER performance of 8PSK signal constellation, with Gray, SP and SSP labeling, respectively, as a function of rotation angle in SSD-ID system is shown in Figure 5.10.

It is clear from figures for both the error correcting codes being employed that

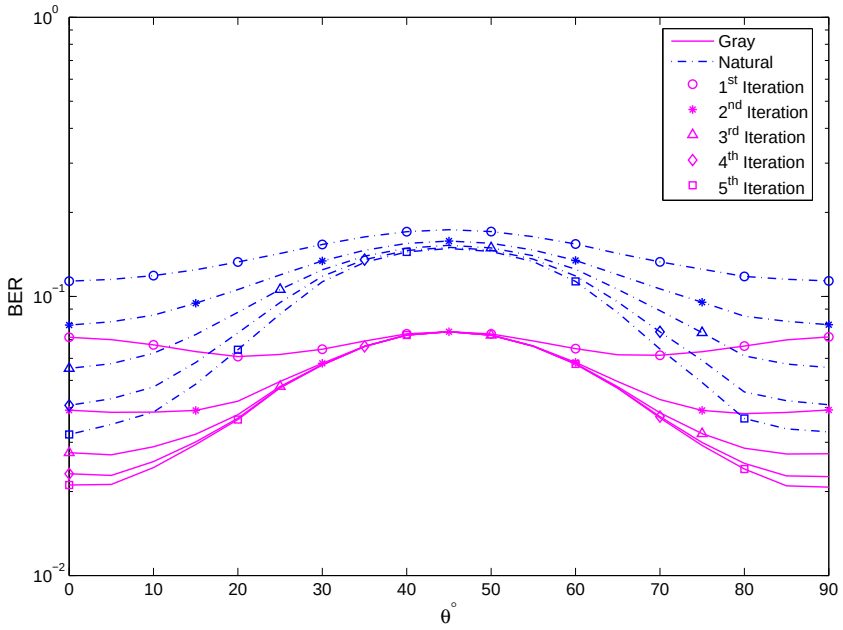

Figure 5.9: *BER performance of QPSK SSD-ID over different rotation angles. Rate* $\frac{1}{2}$ *regular, random* $(3, 6)$ *LDPC codes of length* 2640 *are used with a maximum of 10 internal iterations. Gray and Natural signal constellation labeling in a Rayleigh fading channel at* $E_b/N_0 = 3$ *dB.*

the system performance in terms of BER is dependent upon the signal constellation rotation, the signal constellation labeling, the SNR region of operation and the choice of the error correcting codes being employed.

5.6 EXIT Chart

The convergence behavior of the iterative demodulation and decoding can be analyzed by using mutual information to describe the flow of extrinsic information between the SISO de-mapper and the SISO decoder [105]. In EXIT charts, the exchange of extrinsic information between the symbol-to-bit de-mapper and the SISO decoder is visualized as a decoding trajectory.

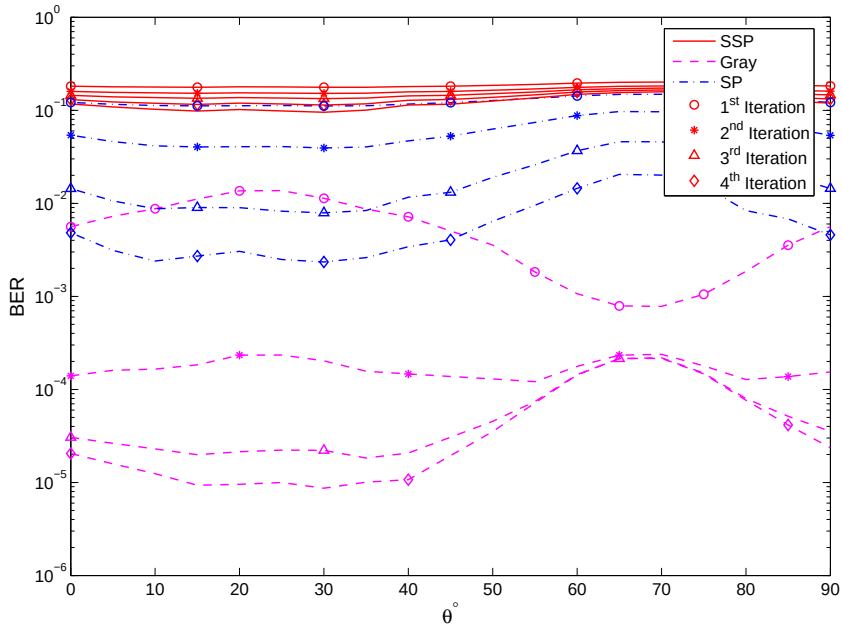

Figure 5.10: *BER performance of 8PSK SSD-ID over different rotation angles. Rate* $\frac{1}{2}$ *regular, random* $(3, 6)$ *LDPC codes of length* 2640 *are used with a maximum of 10 internal iterations. Gray, SP and SSP signal constellation labeling in a Rayleigh fading channel at* $E_b/N_0 = 6$ *dB.*

In EXIT charts we predict the behavior of iterative demodulator (decoder) by solely observing its input/output relations [106]. Constituent element (demodulator/decoder) is represented by an extrinsic information transfer characteristic curve describing the relation to the input *a priori* information to the output extrinsic information. The exchange of extrinsic information between the constituent elements is plotted as a decoding trajectory in EXIT charts. It is, therefore, imperative to separately identify the input(s) and output of the de-mapper and the decoder, respectively. For better comprehension we follow the notations in [106]. *A priori* input and the extrinsic output of the de-mapper is represented as A_1 and E_1, respectively. Similarly, the *a priori* input and the extrinsic output of the SISO decoder is represented as A_2 and E_2, respectively. The variables A_1, E_1, A_2

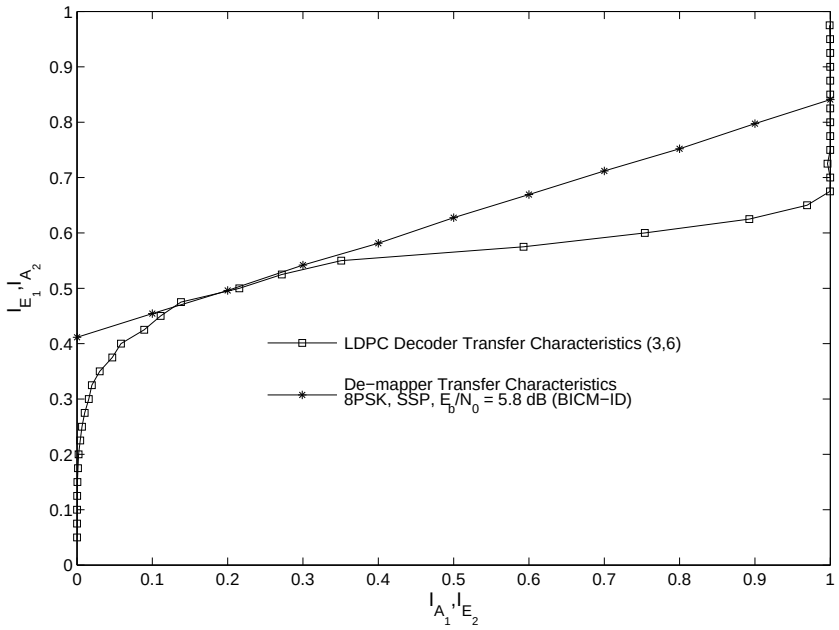

Figure 5.11: *EXIT chart analysis of BICM-ID with 8PSK modulation and SSP labeling at $E_b/N_0 = 5.8$ dB. Rate $\frac{1}{2}$ regular, random $(3, 6)$ LDPC codes of length 2640 are used.*

and E_2 denote the LLR-values. In our analysis, we consider LDPC decoder as a single entity and we will not calculate the flow of extrinsic information within the LDPC decoder (between the variable nodes and the check nodes). The iteration starts at the origin with $q = 1$ and zero *a priori* knowledge. The iterative process stops if an intersection of both characteristic transfer curves occurs in the EXIT chart.

5.7 Transfer Characteristics

A code bit is modeled as an outcome of the binary random variable (RV) B. The LLR-values λ and ω being exchanged between the demodulator and the decoder are modeled as outcomes of the RVs E_1 and E_2, respectively. The RVs are de-

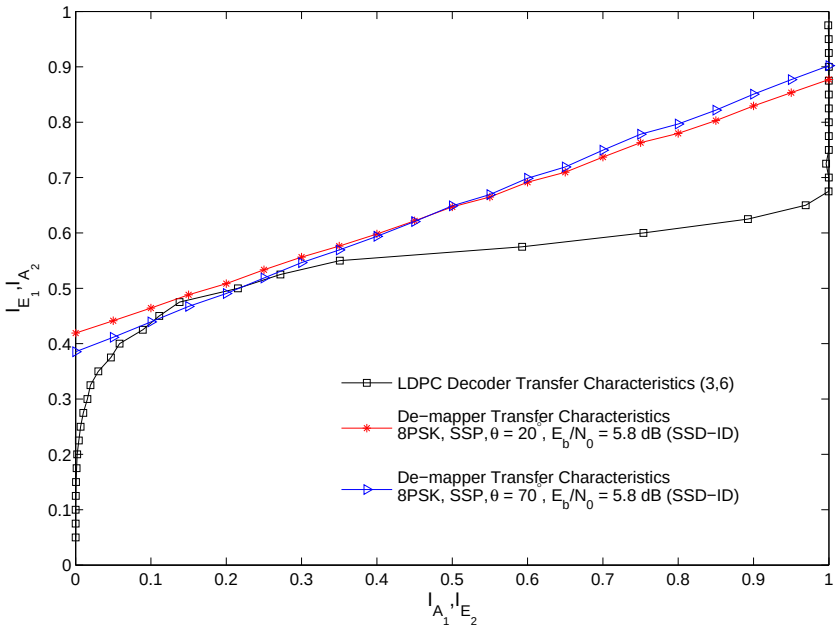

Figure 5.12: *EXIT chart analysis of SSD-ID with 8PSK modulation and SSP labeling with* $\theta = 20°, 70°$ *at* $E_b/N_0 = 5.8$ *dB. Rate* $\frac{1}{2}$ *regular, random* $(3, 6)$ *LDPC codes of length* 2640 *are used.*

scribed with their conditional probability density functions (PDF). The decoding algorithm is analyzed by observing only a single parameter of these PDFs [106], i.e., the mutual information. The information transfer through the de-mapper is controlled by the amount of available *a priori* knowledge A_1 and by the choice of the symbol mapping. Moreover, in SSD the choice of the rotation also plays a critical role as is shown by the EXIT charts in the subsequent subsection. In [106], it has been observed that the extrinsic information LLR-values E_2 (i.e., A_1), fedback from the decoder are Gaussian distributed. Additional, it has also been observed that due to the interleaving *a priori* LLR-values A_1 stay uncorrelated over many iterations. Hence, the *a priori* input A_1 in our calculations is assumed to be Gaussian distributed. The mutual information $I_{A_1} = I(B; A_1)$ between the

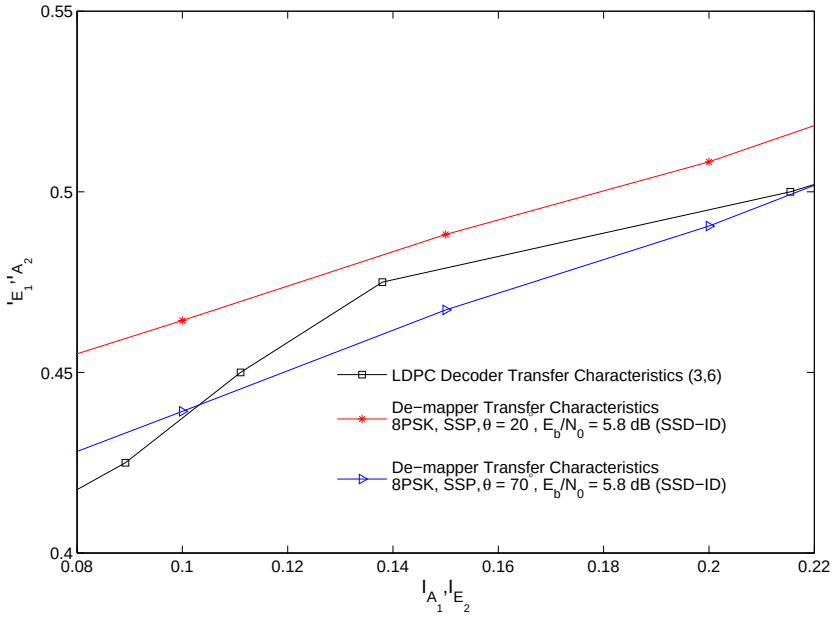

Figure 5.13: *Magnification of the "tunnel" region in Figure 5.12.*

transmitted bits B and the LLR-values A_1 to the de-mapper can be given as

$$I_{A_1} = I(A_1;B) = \frac{1}{2}\sum_{i=0,1}\int_{-\infty}^{\infty} p_{A_1}(\xi \mid B=i) \log_2 \frac{2p_{A_1}(\xi \mid B=i)}{p_{A_1}(\xi \mid B=0)+p_{A_1}(\xi \mid B=1)} d\xi, \quad (5.6)$$

which can be closely approximated with the time average over Nm coded bits [107]

$$I_{A_1} \approx 1 - \frac{1}{Nm}\sum_{n=1}^{Nm} \log_2(1+e^{(-1)^{b_n}\cdot w_n}), \quad (5.7)$$

where b_n is the n^{th} coded bit and w_n is the corresponding *a priori* LLR-value. For a given value of the input mutual information I_{A_1}, the output mutual information I_{E_1} is calculated by Monte Carlo simulations [106]. The mutual information I_{E_1}

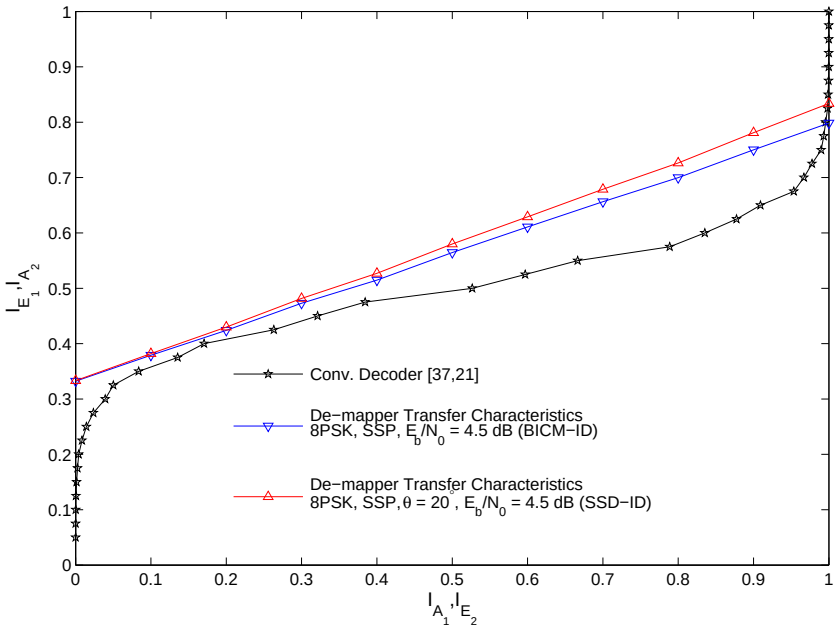

Figure 5.14: *EXIT chart analysis of SSD-ID and BICM-ID with 8PSK modulation and SSP labeling at $E_b/N_0 = 4.5$ dB. RSC code with generator polynomial $(37, 21)_8$ and rate $\frac{1}{2}$ are used.*

can be viewed as a function of I_{A_1}, E_b/N_0 and the rotation angle θ, i.e.,

$$I_{E1} = T_1 \left(I_{A1}, E_b/N_0, \theta \right). \tag{5.8}$$

The extrinsic transfer characteristics of a SISO decoder describe the input/output relationship between the input A_2 and the extrinsic output E_2. It is independent from E_b/N_0 value and can be computed by assuming A_2 to be Gaussian distributed [106]. The transfer characteristic of the SISO decoder is denoted by

$$I_{E_2} = T_2 \left(I_{A_2} \right). \tag{5.9}$$

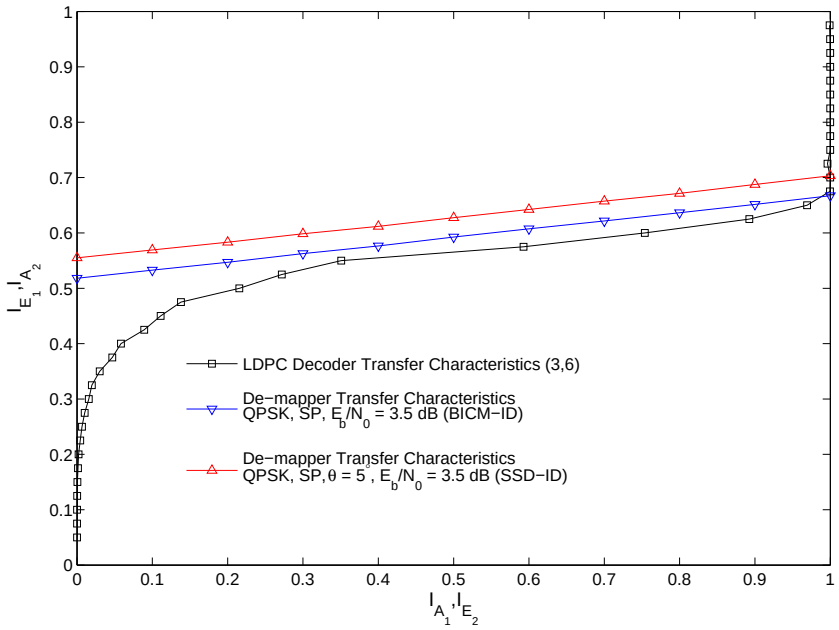

Figure 5.15: *EXIT Chart analysis of BICM-ID and SSD-ID with QPSK modulation and Natural labeling at* $E_b/N_0 = 3.5$ *dB. Rate* $\frac{1}{2}$ *regular, random* $(3, 6)$ *LDPC codes of length* 2640 *are used.*

5.8 EXIT Chart and the Convergence Behavior

An EXIT chart analysis of SSD-ID system, as shown in Figure 5.2 and 5.3, is presented in this section. The purpose is to analyze the effect of the constellation rotation and SSD on the convergence behavior of the system. Illustrative examples are used to identify the degrees of freedom provided by the SSD-ID system.

Figures 5.11 and 5.12 show as an example the performance gain of a system employing SSD-ID over BICM-ID by the use of a proper choice of the rotation angle in a Rayleigh fading channel at $E_b/N_0 = 5.8$ dB with 8PSK modulation and SSP labelling. Regular, random $(3, 6)$ LDPC code of length 2640 and rate $\frac{1}{2}$ is used. In Figure 5.11, the decoding trajectory of BICM-ID gets stuck at low mutual information after a few iterations as the transfer characteristic curves of

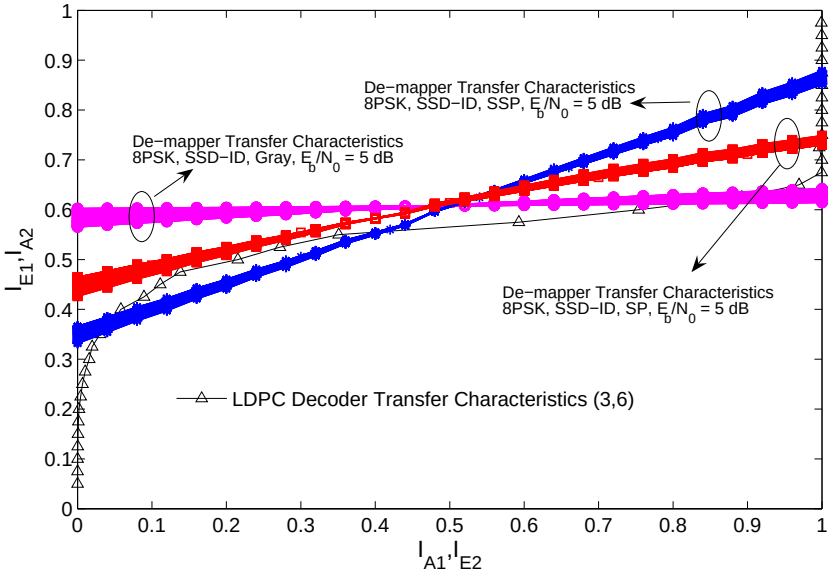

Figure 5.16: *The influence of rotation angle and mapping on the performance of SSD-ID system using 8PSK modulation at* $E_b/N_0 = 5$ *dB. The cloud around each symbol mapping is the effect of rotation angle which vary from* $\theta = 0^\circ$ *to* $\theta = 90^\circ$*. Rate* $\frac{1}{2}$ *regular, random* $(3, 6)$ *LDPC codes of length* 2640 *are used.*

the decoder and de-mapper intersect, whereas in Figure 5.12 for same E_b/N_0-value and a rotation of $\theta = 20^\circ$ SSD-ID is able to open a narrow "tunnel", which is, also, magnified for clarity in the Figure 5.13. This opening of the narrow tunnel allows for the convergence of the iterative decoding towards low bit error rate (BER). This convergence towards low BER, although being slow, is possible since both the decoder and the de-mapper transfer characteristic curves do not intersect anymore. The choice of the rotation angle plays a critical role as illustrated in Figure 5.12, which shows that a rotation angle of $\theta = 70^\circ$ results in decoding trajectory getting stuck after few iterations. The number of iterations performed within the LDPC decoder of length 2640 is 10. The choice of 10 iterations within the LDPC decoder reduces the complexity and time delay of the system. Thus SSD-ID with a proper choice of rotation angle provides an extra degree of freedom

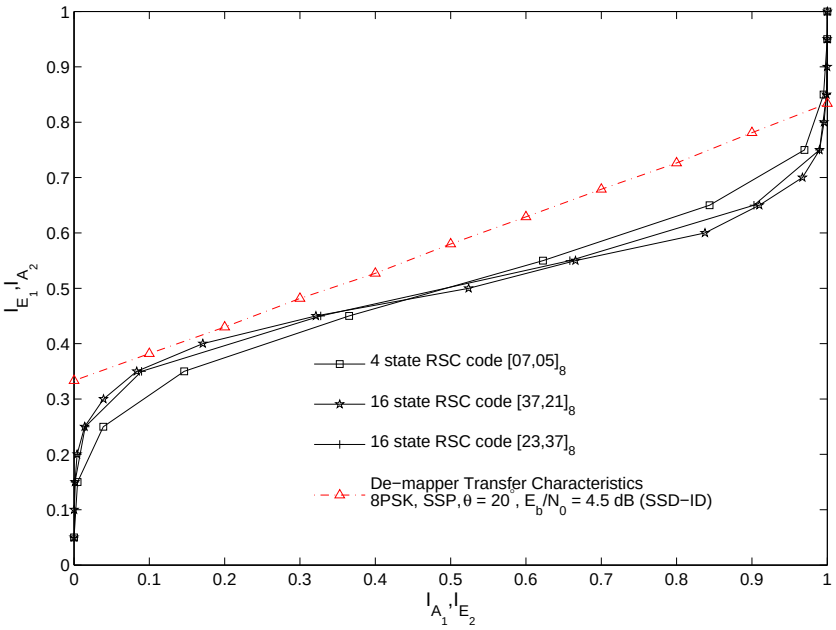

Figure 5.17: *EXIT chart analysis of rate* $\frac{1}{2}$ *RSC codes with 8PSK modulation and SSP labeling,* $\theta = 20^\circ$ *at* $E_b/N_0 = 4.5$ *dB.*

as compared to the conventional BICM-ID system.

Figure 5.14 depicts the same phenomenon with RSC codes. RSC code of information block length 2600 with a generator polynomial $[37, 21]_8$ and rate $\frac{1}{2}$ is used. The figure also shows an additional benefit of SSD-ID as compared to the BICM-ID system, i.e., the early convergence (fewer iterations) of the iterative demodulation and decoding. This is due to the fact that for the same E_b/N_0-value the transfer characteristic curve of the symbol mapper for SSD-ID is always above the symbol mapper characteristic transfer curve for BICM-ID. This results in fewer iterations to achieve the same BER performance. A similar effect is also shown for the QPSK constellation with LDPC codes in Figure 5.15.

Figure 5.16 shows the effect of the signal constellation mapping and rotation by the use of an EXIT chart in an SSD-ID system. Regular, random $(3, 6)$ LDPC

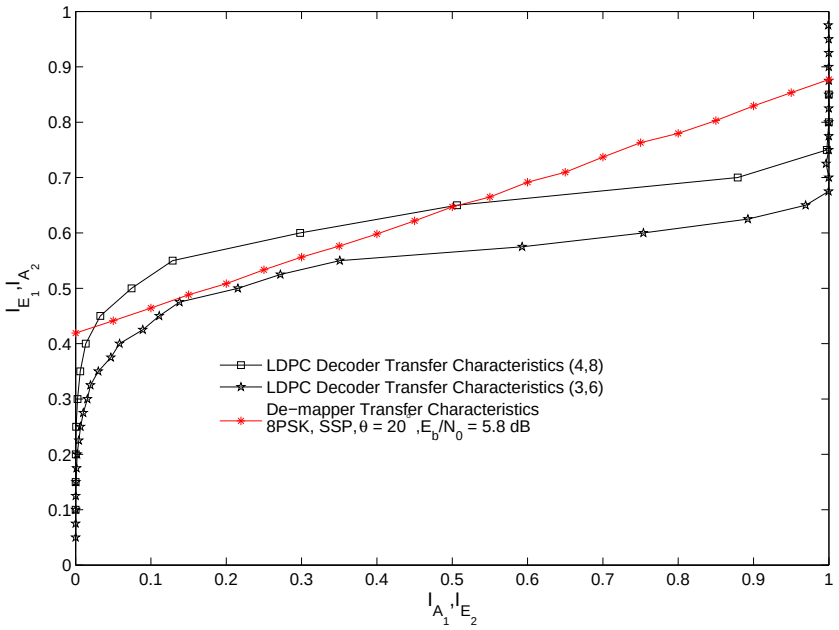

Figure 5.18: *EXIT chart analysis of rate* $\frac{1}{2}$*, regular, random* $(3,6)$ *and* $(4,8)$ *LDPC codes with 8PSK modulation and SSP labeling,* $\theta = 20^\circ$ *at* $E_b/N_0 = 5.8$ *dB.*

code of length 2640 and rate $\frac{1}{2}$ is used. The cloud of lines around a constellation labeling is because of the rotation of that particular constellation from $\theta = 0^\circ$ to $\theta = 90^\circ$. After $\theta = 90^\circ$ the same behavior is periodically repeated. Figure 5.16 commensurate the results shown in Figures 5.7 and 5.8. Figure 5.16, shows that the Gray mapping for 8PSK signal constellation, although, starting at a high mutual information value would converge to a specified BER-value very fast after only a couple of iterations as the extrinsic transfer characteristic curves of the demodulator and the decoder intersect. Multiple iterations after the intersection would not lead to a further gain as substantiated by Figures 5.7 and 5.8. Gray mapping, therefore, is a better candidate for low SNR operation region. Whereas, for SSP labeling at higher SNR would have the capability to converge to a lower BER-value and would have a gain over multiple iterations. The signal constella-

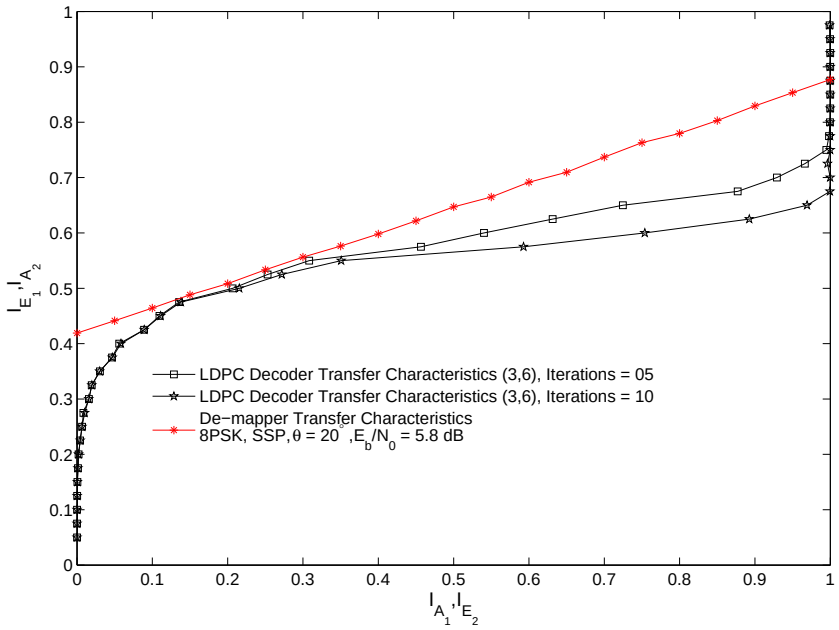

Figure 5.19: *EXIT chart analysis of the impact of the number of iterations performed within rate* $\frac{1}{2}$ *regular, random* $(3, 6)$ *LDPC decoder with 8PSK modulation and SSP labeling,* $\theta = 20^\circ$ *at* $E_b/N_0 = 5.8$ *dB.*

tion labeling and rotation can be optimized by using irregular modulation (also termed as modulation doping) [108, 109] to be used for operation at both low and high SNR regions.

It is important to emphasize the fact that only the benefit of SSD-ID and the degrees of freedom provided by the system are highlighted and no attempt is made to optimize these parameters.

5.9 Effect of different codes

The structure of the error correcting code being employed provides another degree of freedom. In LDPC codes, e.g., the degree distribution of the check and the

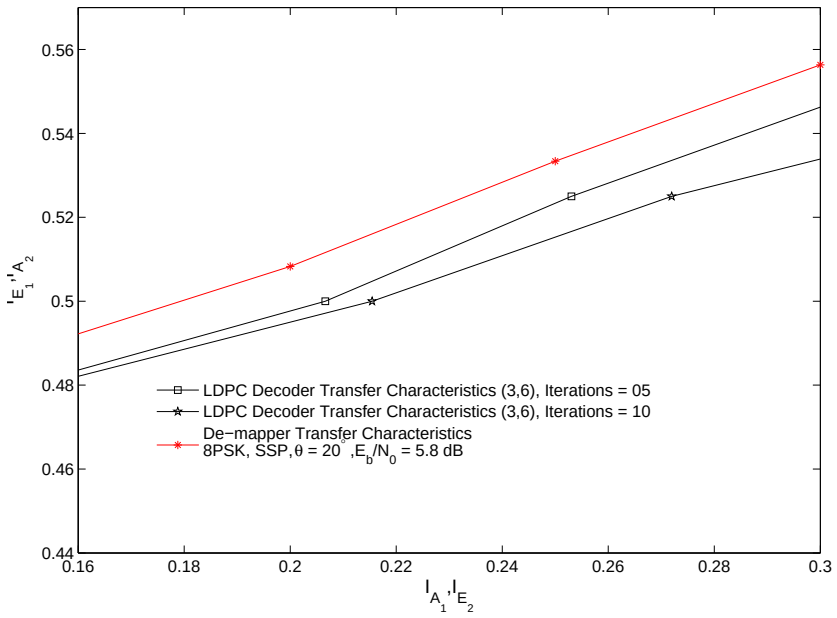

Figure 5.20: *Magnification to show the gain from Figure 5.19.*

variable nodes and the number of iterations performed within the LDPC decoder can be used as a criterium to choose a specific code. Similarly, in RSC codes the generator polynomials can be visualized as a selection criterion. In the context of SSD-ID these selecting criteria are the degrees of freedom to optimally choose the system parameters.

Figure 5.17 shows extrinsic transfer characteristics of rate $\frac{1}{2}$ RSC codes with 8PSK signal constellation, SSP labeling, $E_b/N_0 = 4.5$ dB and a rotation of $\theta = 20°$. It is interesting to see that 4-state RSC code given by the generator polynomial $[07, 05]_8$ has better performance at low mutual information but as the *a priori* information increases their performance is worse than the 16-state RSC codes.

Figure 5.18 shows as an example the comparison of $(3, 6)$ and $(4, 8)$ regular

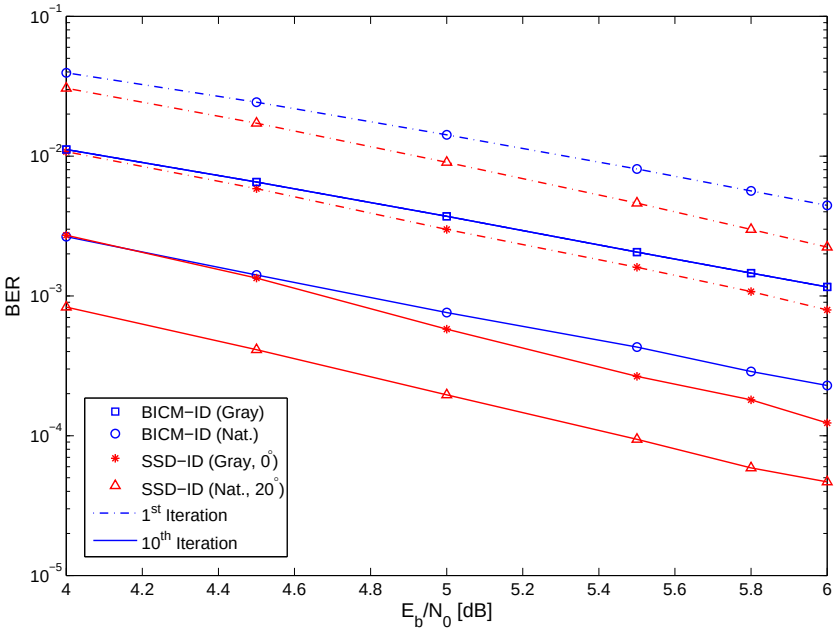

Figure 5.21: *BER performance of SSD-ID and BICM-ID with QPSK signal constellation. Gray and Natural labeling are used.* 16*-state RSC codes of length* 2600 *and rate* $\frac{1}{2}$ *are employed.*

random LDPC codes of length 2640 and 4000, rate $\frac{1}{2}$, respectively, with 8PSK modulation and SSP labeling using SSD-ID at $E_b/N_0 = 5.8$ dB. In Figure 5.18, the decoding trajectory of $(4, 8)$ LDPC decoder gets stuck at low mutual information as the transfer characteristic curves of the decoder and the de-mapper intersect whereas for the same E_b/N_0-value the transfer characteristic curve of $(3, 6)$ LDPC decoder does not intersect. Thus, it provides a possibility for the convergence to a lower BER-value. It is important to stress that this behavior is an indication towards the structure of the parity check matrix being employed. Thus, the degree distribution of the variable and the check nodes is a degree of freedom which can be optimized to achieve better performance.

In the analysis an LDPC decoder is considered as a single entity. The number

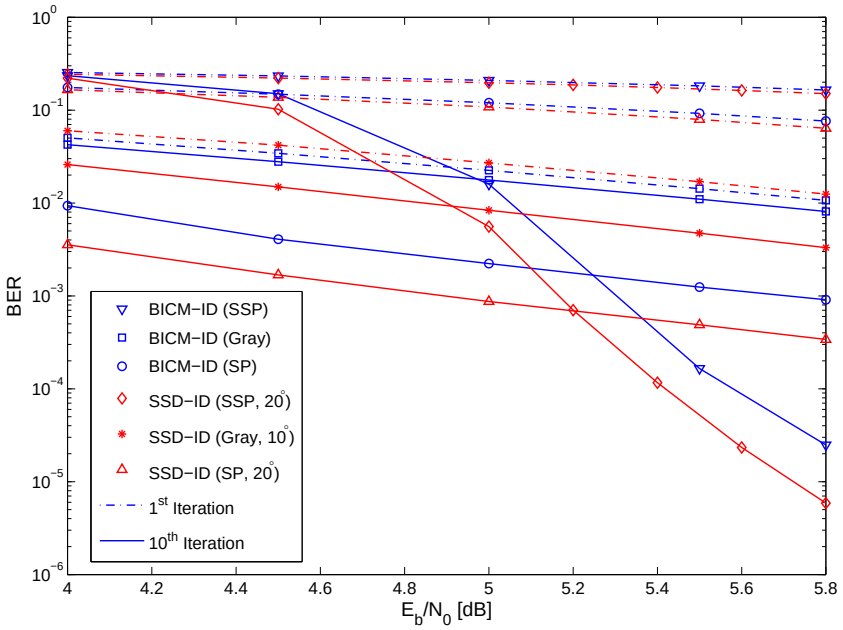

Figure 5.22: *BER performance of SSD-ID and BICM-ID with 8PSK signal constellation. Gray, SP and SSP labeling are used.* 16*-state RSC codes of length* 2600 *and rate* $\frac{1}{2}$ *are employed.*

of iterations performed within the LDPC decoder has an effect on the extrinsic transfer characteristic curve as shown in Figures 5.19 and 5.20. This provides another degree of freedom which can be optimized. Higher number of iterations within the LDPC decoder can lead to a gain but it is on the expense of latency and efficiency.

5.10 Simulation Results And Discussion

Figures 5.21, 5.22, 5.23 and 5.24 quantify the gain that is achieved by using SSD-ID in comparison to BICM-ID. A maximum of 10 iterations between the demodulator and the decoder are performed. The results are parsed on the basis

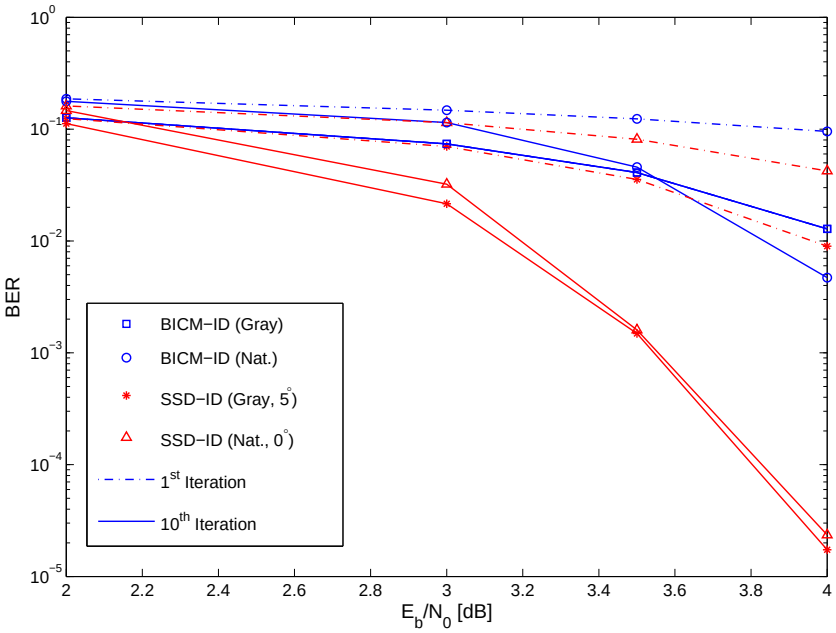

Figure 5.23: *BER performance of SSD-ID and BICM-ID with QPSK signal constellation. Gray and Natural labeling are used. Random, regular* $(3, 6)$ *LDPC-codes of rate* $\frac{1}{2}$ *and length* 2640 *are employed.*

of the error correcting codes being employed. The fading is assumed to be flat and Rayleigh distributed.

5.10.1 RSC Codes

Figures 5.21 and 5.22 show comparative performance gain of SSD-ID over BICM-ID by the use of 16-state RSC code with rate $\frac{1}{2}$, information block length of 2600 and generator polynomial $[37, 21]_8$ with QPSK and 8PSK signal constellations. Figure 5.21 shows the performance of QPSK signal constellation with Gray and Natural mapping. Gray labeled BICM-ID does not show any performance gain after multiple iterations. SSD-ID outperforms BICM-ID over all iterations and all mappings, e.g., the Natural labeled rotated SSD-ID has a performance im-

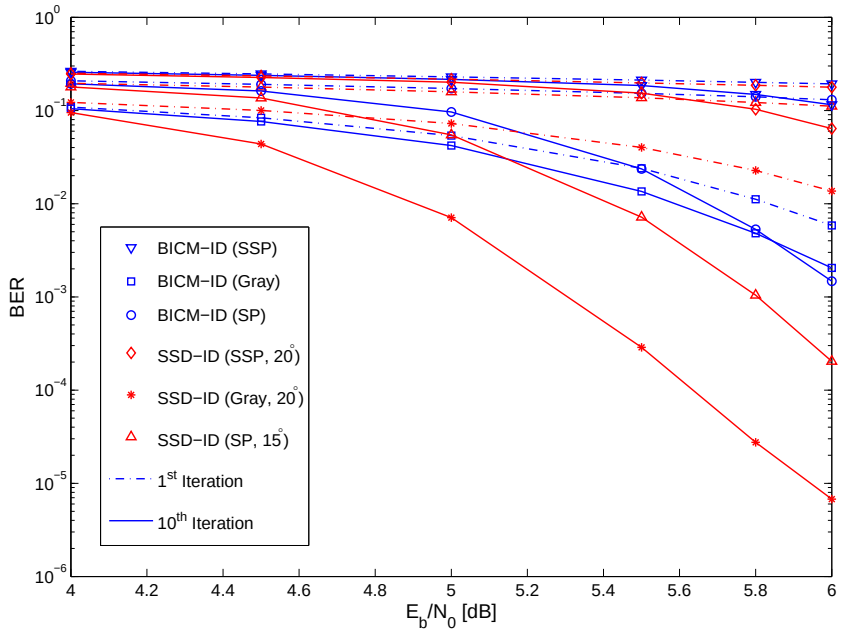

Figure 5.24: *BER performance of SSD-ID and BICM-ID with 8PSK signal constellation. Gray, SP and SSP labeling are used. Random, regular* $(3, 6)$ *LDPC-codes of rate* $\frac{1}{2}$ *and length* 2640 *are employed.*

provement of 1.1 dB at a BER of 2.3×10^{-4} at the 10^{th} iteration as shown in Figure 5.21. Figure 5.22 shows the comparative performance of 8PSK signal constellation with Gray, SP and SSP labeling employed in an SSD-ID and BICM-ID system. In this figure also, SSD-ID outperforms BICM-ID. The performance after 1^{st} iteration is very similar but the gain provided by SSD-ID becomes more clear as more iterations are performed. At the 10^{th} iteration SSD-ID outperforms BICM-ID over all mappings, e.g., SSP labeled rotated SSD-ID has a performance improvement of 0.14 dB at a BER of 1×10^{-3} over BICM-ID.

5.10.2 LDPC Codes

Figures 5.23 and 5.24 quantify the gain that is achieved by using SSD-ID over BICM-ID by the use of regular random $(3, 6)$ LDPC-codes of length 2640, rate $\frac{1}{2}$ and 10 internal iterations. Figure 5.23 shows the performance gain of Gray and Natural labeled QPSK signal constellation. SSD-ID outperforms BICM-ID over all iterations and all mappings, e.g., Gray mapped rotated SSD-ID has a performance gain of 0.93 dB at a BER of 1.3×10^{-2} at 10^{th} iteration over BICM-ID. SSD-ID has a better performance for 8PSK signal constellation as depicted by Figure 5.24. SSD-ID outperforms BICM-ID for Gray, SP and SSP mappings under consideration, e.g., Gray labeled rotated SSD-ID has a performance improvement of 0.8 dB at a BER of 2×10^{-3} over BICM-ID.

The above figures, quantify the gain that is achieved by SSD-ID over BICM-ID. The results commensurate the EXIT chart analysis presented earlier. In EXIT chart analysis it was evident that at any E_b/N_0-value with a well-considered choice of the rotation angle SSD-ID would have a better performance than BICM-ID. This better performance can either be considered as early convergence (fewer iterations required) to achieve a low BER value or eventual (slow with more iterations required) but possible convergence to a low BER value. Both of these criteria are possible due to the fact that the extrinsic information transfer curve of SSD-ID mapper with a well-considered choice of rotation angle is always above the BICM-ID mapper curve for a given decoder extrinsic information transfer curve. The Figures 5.21, 5.22, 5.23 and 5.24, also, show the phenomenon of early convergence that is possible with the SSD-ID system. For instance, in Figure 5.24 Gray mapped 8PSK signal constellation at $\theta = 20°$, with LDPC code at $E_b/N_0 = 6$ dB and 10^{th} iteration has a BER performance of 6.7×10^{-6} whereas for BICM-ID, Gray mapped 8PSK signal constellation has a BER performance

of 2×10^{-3} at the 10^{th} iteration at the same $E_b/N_0 = 6$ dB. BICM-ID would require more iterations to possibly achieve, provided that there is no intersection of extrinsic information transfer curves, a lower BER value.

5.11 Conclusions

In this chapter, we have investigated the performance of SSD-ID system in Rayleigh fading channels. The performance of the proposed scheme was compared with the BICM-ID. A symbol-to-bit de-mapper for multi-level modulation schemes was extended to incorporate iterative demodulation and decoding with SSD. Using EXIT charts an analysis was presented on the effect of the rotation on the overall performance of the system. It was shown that with a well considered choice of the rotation angle the convergence of the iterative demodulation and decoding towards low BER is possible. The choice of the rotation angle was shown to be dependent upon the signal constellation labeling and the choice of the error correcting code being employed. Factors or degrees of freedom which can effect the system performance, such as, the choice of the signal constellation rotation, the signal constellation labeling, the generator polynomial for RSC codes, the degree distribution for LDPC-codes, the number of iterations performed within the LDPC-codes and the SNR region of operation, were discussed with illustrative examples. Furthermore, it was shown that SSD-ID with a well considered choice of the rotation angle and signal constellation labeling provides significant performance improvement over the conventional BICM-ID system.

Chapter 6

Coded SSD-ID Systems with OFDM

This chapter proposes and presents iterative demodulation and decoding of orthogonal frequency division multiplexing (OFDM) with bit interleaved coded modulation (BICM), rotated MPSK constellations and signal space diversity (SSD) in frequency selective fading channels. Practically sized low density parity check (LDPC) and convolutional codes are used as forward error correcting codes. Factors that effect the convergence behavior of iterative demodulation and decoding are identified and their effect is analyzed by extrinsic information transfer (EXIT) charts.

6.1 Introduction

Transmission of signals on land mobile radio channels is marred by various types of impairments such as multipath spread (or delay spread), fading, Doppler spread, nonlinear distortion, frequency offset, phase jitter, impulse noise, thermal noise, and co-channel and adjacent channel interference arising from spectrum sharing. Delay spread causes interference between adjacent symbols, known as intersymbol interference (ISI). In this chapter we focus on a discrete implementation of a multicarrier modulation scheme known as orthogonal frequency division multiplexing (OFDM) by which the ISI can be eliminated by the use of a cyclic prefix. The basic premise of a multicarrier modulation scheme is to break a wideband channel into multiple parallel, typically, orthogonal narrowband channels.

Multicarrier modulation schemes are being currently used in many wireless applications. From the year 1990 [110], multicarrier modulation has been employed in diverse wired and wireless applications. For instance, in digital audio and video broadcasting [111], digital subscriber lines using discrete multitone [112], the wireless LAN systems, such as, IEEE 802.11, HIPERLAN and MMAC [113], wireless broadband services [114] and also is a strong candidate for next generation cellular systems [115, 116]. However, it is not a new technique as it was used in 1950's and early 1960's in military HF radios. It is important to state that a single carrier system employing a minimum mean square error (MMSE) decision feedback equalizer can be theoretically optimum. However, in practice the implementation of this structure is difficult. Multicarrier system's performance is greatly impaired by frequency offset and timing jitter which degrade the orthogonality of the subchannels and in addition peak-to-average power ratio (PAPR) is significantly higher than that of a single carrier systems. For further details on the tradeoffs between single carrier and multicarrier systems we refer the reader

to [117], and the references therein.

Signal space diversity (SSD), also known as co-ordinate interleaving, in combination with bit interleaved coded modulation has been extensively studied and presented for single carrier systems in Chapters 4 and 5. Application of space diversity has also been considered in literature for uncoded OFDM systems, e.g., in [118] and the references therein.

In this chapter we propose and present iterative demodulation and decoding of OFDM with bit interleaved coded modulation (BICM), rotated MPSK constellations and SSD, hereafter referred to as OFDM SSD-ID. Practically sized low density parity check (LDPC) and convolutional codes are used as forward error correcting codes with rotated MPSK constellations over frequency selective fading channels. Factors affecting the performance of iterative demodulation and decoding (ID), such as, symbol mappings, the number of iterations and the effect of iterations on the optimum rotation angles, are analyzed by illustrative examples. The proposed scheme using rotated constellations is shown to outperform conventional BICM-ID OFDM systems. Furthermore, extrinsic information transfer (EXIT) charts are used to analyze and to illuminate the effect of optimum rotation angle on the convergence behavior of iterative demodulation and decoding in frequency selective fading channels.

The outline of the Chapter is as follows. Section 6.2 presents the system model of an OFDM SSD-ID system. Iterative demodulation and decoding of OFDM SSD-ID is presented in Section 6.3. EXIT chart analysis and the degrees of freedom available to the system are presented in Section 6.4. The performance curves of the new concatenated scheme are presented in Section 6.5 followed by the the conclusions in Section 6.6.

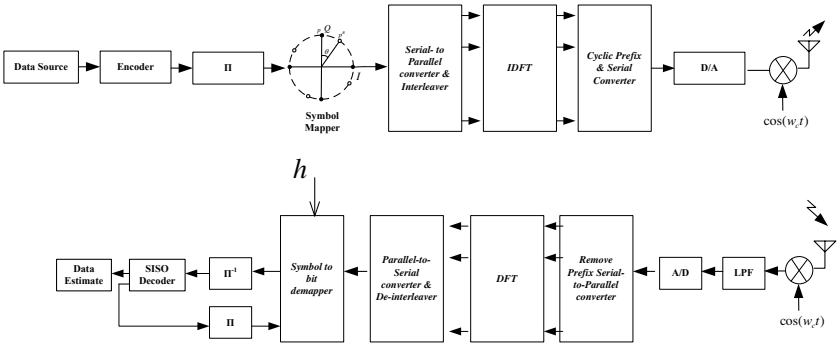

Figure 6.1: *System model of a BICM-ID system with SSD, OFDM and signal constellation rotation.*

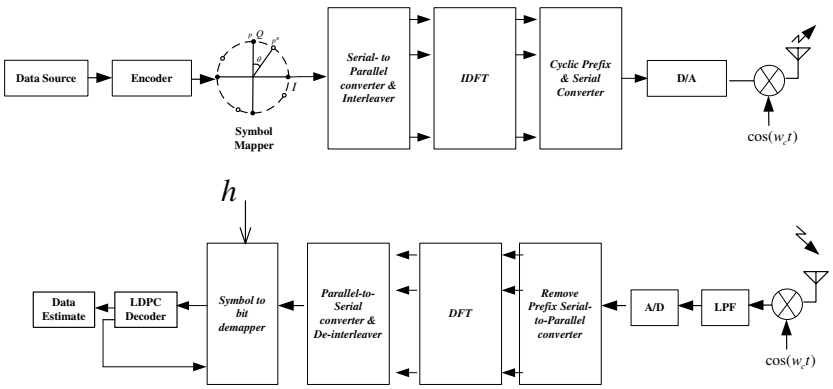

Figure 6.2: *System model of an LDPC-coded BICM-ID system with SSD, OFDM and signal constellation rotation.*

6.2 System Model

Figures 6.1 and 6.2 show the serial concatenated system using iterative demodulation and decoding with OFDM and SSD (hereafter referred to as SSD-ID OFDM). The LDPC-coded SSD-ID OFDM system has no interleaver (de-interleaver) block placed between the encoder (decoder) and the symbol mapper (symbol-to-bit demapper). This is due to the fact that the bits are inherently interleaved (de-interleaved) by the LDPC-encoder (decoder) [75, 96]. In [75, 96], it was shown

that the LDPC codes due to inherent interleaving are able to achieve good performance over correlated fading channels without the use of an external channel interleaver. For further detail we refer the reader to Chapters 4 and 5 and the references therein. We in this section focus mainly on the extensions made to the system model presented earlier in Chapter 5 and repeat certain aspects for better readability.

Clockwise rotation over an angle θ leads to the constellation

$$\mathcal{S}_M^{\theta} = \{s_l = e^{(2\pi(l/M)-\theta)j} : l = 0, 1, \ldots, M-1\}. \tag{6.1}$$

The symbol mapper can be represented by the one-to-one mapping function $\wp : \{0,1\}^m \rightarrow \mathcal{S}_M^{\theta}, s = \wp(\mathbf{b})$, where, $\mathbf{b} = (b_1, \cdots, b_m), b_j \in \{0,1\}$ represents the binary sequence and s is chosen from the set $\mathcal{S}_M^{\theta}$ consisting of M complex signal points.

Consider an OFDM system with N subcarriers. Each group of Nm encoded bits are mapped to an OFDM symbol. Let $\mathbf{x}$ denote the rotated sequence passed to the IDFT block and inserted with cyclic prefix of length L_{cp}. The coordinate interleaving being employed is to make the I and Q channels uncorrelated implying that the I and Q channels experience independent fades. A single coordinate interleaver or a delay line introducing a delay that exceeds the coherence time of the channel would also, have the same effect and can be used instead of the two interleavers. For more details again we refer the reader to Chapters 4 and 5.

The fading caused by a frequency selective channel can be modeled as a linear filter characterized by a complex valued low pass equivalent impulse response [4],

$$h(t) = \sum_{l=1}^{L} \alpha_l e^{-j\theta_l} \delta(t - \tau_l), \tag{6.2}$$

where l is the path index, L is the number of resolvable paths, $\delta(\cdot)$ is the Dirac delta function and $\{\alpha\}_{l=1}^{L}$, $\{\theta\}_{l=1}^{L}$ and $\{\tau\}_{l=1}^{L}$ are the random channel amplitudes, phases and delays, respectively. As we assume that there is no cochannel interference, the transmitted signal is therefore, sent over L independent and identically distributed (i.i.d) slowly varying flat fading paths. Furthermore similar to the analysis of multipath diversity in the literature, e.g., [4, 5], we assume, without loss of generality, the first channel with delay $\tau_1 = 0$ to be the reference channel and $\tau_1 < \tau_2 < \cdots < \tau_L$. Also, we assume that the sets $\{\alpha\}_{l=1}^{L}$, $\{\theta\}_{l=1}^{L}$ and $\{\tau\}_{l=1}^{L}$ are mutually independent and are constant over at least a symbol interval. The fading amplitudes, $\{\alpha\}_{l=1}^{L}$, are statistically independent random variables with a mean-square value $\mathcal{E}[\alpha_l^2] = \Omega_l$, and a PDF described by any of the family of distributions, e.g., Rayleigh, Nakagami-n (Rice) or Nakagami-m. The transmitted signal after passing through the fading channel is perturbed by complex additive white Gaussian noise (AWGN) with a two-sided power spectral density of $N_0/2$. The AWGN noise is assumed to be independent of the fading amplitudes and statistically independent from channel to channel.

The cyclic prefix L_{cp} converts the linear convolution of the transmitted signal and the L-tap channel into a circular convolution. Assuming that the discrete Fourier transform (DFT) and cyclic prefix removal at the receiver with coherent detection are carried out error-free; OFDM converts the frequency selective fading channel into N flat sub-channels. The received signal, $\mathbf{r}$, therefore, can be represented as

$$\mathbf{r} = \mathbf{x}\mathbf{H} + \mathbf{n}, \tag{6.3}$$

where, $\mathbf{n} = [n_0, \ldots, n_{N-1}]$ is a DFT processed complex white Gaussian noise vector with independent components having two-sided spectral density of $N_0/2$. The noise vector is white and Gaussian with same correlation matrix because

the DFT matrix is unitary. OFDM yields a diagonally equivalent channel matrix $\mathbf{H} = diag(H_0, \ldots, H_{N-1})$, where

$$H_i = \frac{1}{\sqrt{N}} \sum_{l=0}^{L-1} \alpha_l e^{-j2\pi il/N}, \qquad 0 \leq i \leq N-1, \tag{6.4}$$

is the frequency response of the underlying FIR channel channel evaluated at the DFT grid.

6.3 Iterative Demodulation and Decoding

Figure 6.1 and 6.2 show the serial concatenation of a soft-input soft-output (SISO) symbol-to-bit demodulator (indicated as "symbol-to-bit de-mapper") and a SISO decoder which are employed to iteratively demodulate and decode the received $\mathbf{r^I}$ and $\mathbf{r^Q}$ de-interleaved components. The receiver processes the blocks of received symbols and calculates the estimates of the transmitted data bits by the cooperative assistance of the symbol-to-bit de-mapper and the decoder. The symbol-to-bit de-mapper processes the received symbols to produce the extrinsic information which is passed to the SISO decoder. It is assumed that the symbol-to-bit de-mapper has the CSI information. The extrinsic information is updated by the SISO decoder and is fed back to the symbol-to-bit demapper. The receiver, thus iterates between the demodulator and the decoder to reliably estimate the transmitted bits. If the code itself does not use iterative decoding, in case of a conventional convolutional code, as shown in Figure 6.1, then there would be a single iteration of decoding for every iteration of demodulation. On the other hand, if the code is iteratively decoded, as it is the case for LDPC codes as shown in Figure 6.2, then for every iteration of demodulation there are a specified number of internal iterations within the decoder before the extrinsic information is updated

for feed-back. For further detail on the demodulation and decoding blocks, for the cases of MPSK constellations and SISO decoding (LDPC and convolutional decoding), we refer the reader to Chapter 5.

6.4 EXIT Chart Analysis & Discussion

The convergence behavior of the iterative demodulation and decoding can be analyzed by using mutual information to describe the flow of extrinsic information between the SISO de-mapper and the SISO decoder [106]. In our analysis, on SSD-ID OFDM we confine ourselves to LDPC decoder as the candidate code and present the analysis. LDPC decoder is considered as a single entity and we will not calculate the flow of extrinsic information within the LDPC decoder (between the variable nodes and the check nodes). The systems are analyzed with $N = 64$ subcarriers and a channel model with root mean square (RMS) delay spread of about 50 nsec, a bandwidth of 50 MHz and a 29-tap power delay profile having an exponentially decaying fading characteristics with each path being assumed to be independently Rayleigh faded. For better comprehension we repeat certain salient features of the EXIT chart analysis and refer the reader to Chapter 5 for more in detail discussion.

6.4.1 Transfer Characteristics

A code bit b_n is modeled as an outcome of the binary random variable (RV) B. The LLR-values λ and ω being exchanged between the demodulator and the decoder are modeled as outcomes of the RVs E_1 and E_2, respectively. The information transfer through the de-mapper is controlled by the amount of available *a priori* knowledge A_1 (i.e., E_2) and by the choice of the symbol mapping.

The mutual information $I_{A_1} = I(B; A_1)$ between the transmitted bits B and the LLR-values A_1 to the de-mapper can be closely approximated with with the time average over Nm coded bits [106]

$$\begin{aligned} I_{A_1} &= 1 - \mathcal{E}\{\log_2(1 + e^{-A_1})\} \\ &\approx 1 - \frac{1}{Nm} \sum_{n=1}^{Nm} \log_2(1 + e^{(-1)^{b_n} \cdot \omega_n}). \end{aligned} \tag{6.5}$$

For a given value of the input mutual information I_{A_1}, the output mutual information I_{E_1} is calculated by Monte Carlo simulations [106]. The mutual information I_{E_1} can be viewed as a function of I_{A_1}, E_b/N_0 and the rotation angle θ, i.e.,

$$I_{E1} = T_1 \left(I_{A1}, E_b/N_0, \theta \right). \tag{6.6}$$

The extrinsic transfer characteristics of a SISO decoder describe the input/output relationship between the input A_2 and the extrinsic output E_2. It is independent from E_b/N_0 value and can be computed by assuming A_2 to be Gaussian distributed [106]. The transfer characteristic of the SISO decoder is denoted by

$$I_{E_2} = T_2 \left(I_{A_2} \right). \tag{6.7}$$

For more details on the transfer characteristics of the LDPC decoder and the demodulator we refer the reader to Chapter 5.

6.4.2 EXIT Chart and the Convergence Behavior

An EXIT chart analysis of the SSD-ID OFDM system is presented in this subsection. The purpose is to analyze the effect of the constellation rotation and SSD on the convergence behavior of the system.

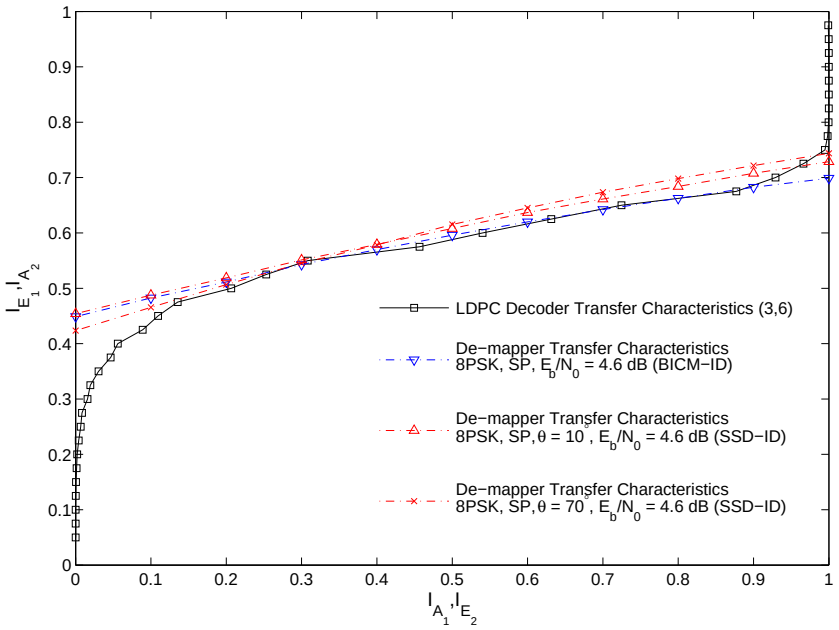

Figure 6.3: *EXIT chart analysis of BICM-ID OFDM and SSD-ID OFDM* ($\theta = 20°, 70°$) *with 8PSK modulation and SP labeling at* $E_b/N_0 = 4.6$ *dB. Rate* $\frac{1}{2}$ *regular, random* $(3, 6)$ *LDPC codes of length* 2640 *are used.*

Figure 6.3 shows as an example the performance gain of a system employing SSD-ID OFDM over BICM-ID OFDM by the use of a proper choice of the rotation angle in a frequency selective fading channel at $E_b/N_0 = 4.6$ dB with 8PSK modulation and SP labeling. Regular, random $(3, 6)$ LDPC code of length 2640 and rate $\frac{1}{2}$ is used. In Figure 6.3, the decoding trajectory of BICM-ID OFDM and SSD-ID OFDM at $\theta = 70°$ gets stuck at low mutual information after a few iterations as the transfer characteristic curves of the decoder and de-mapper intersect, whereas a rotation of $\theta = 10°$ for SSD-ID OFDM is able to open a narrow "tunnel", which is also, magnified for clarity in the Figure 6.4. This opening of the narrow tunnel allows for the convergence of the iterative decoding towards low bit error rate (BER). This convergence towards low BER, although being slow, is

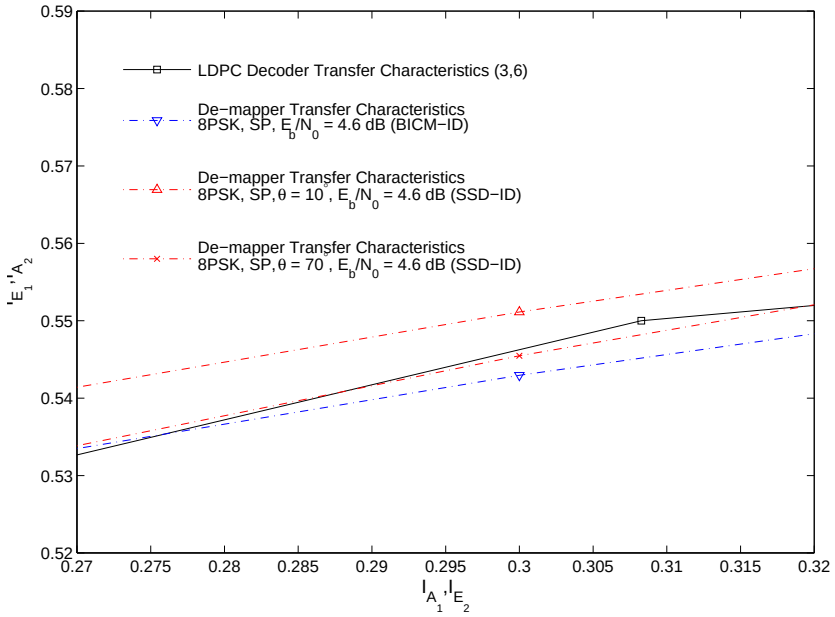

Figure 6.4: *Magnification of the "tunnel" region in Figure 6.3.*

possible since both the decoder and the de-mapper transfer characteristic curves do not intersect anymore. The choice of the rotation angle plays a critical role as illustrated in Figure 6.3. The number of iterations performed within the LDPC decoder of length 2640 is 5. The choice of 5 iterations within the LDPC decoder reduces the complexity and time delay of the system. SSD-ID OFDM, thus with a proper choice of rotation angle provides an extra degree of freedom as compared to the conventional BICM-ID OFDM system.

6.4.3 Effect of Constellation Rotation

Figure 6.5 shows the effect of the signal constellation mapping and rotation by the use of an EXIT chart in an SSD-ID OFDM system. QPSK signal constellation with Gray and Natural labeling is used as an example. The cloud of lines around

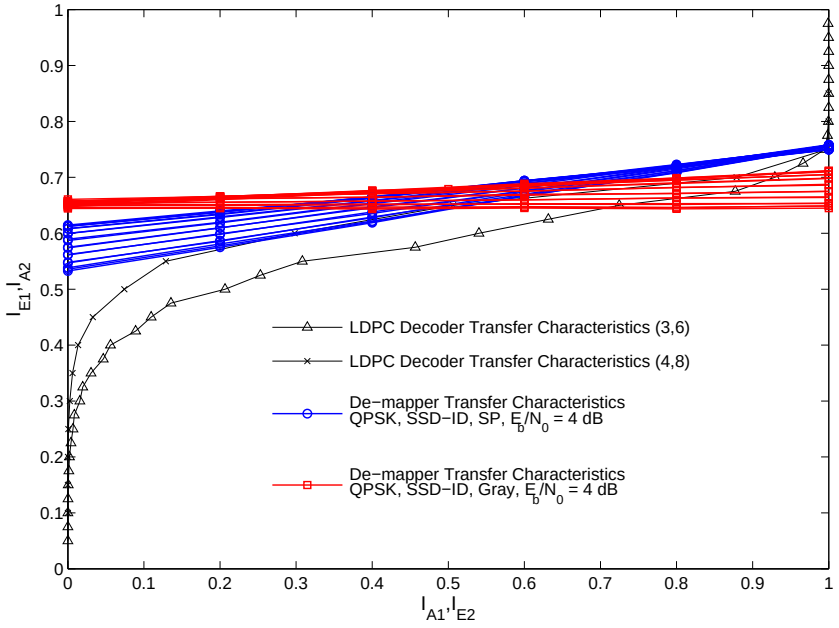

Figure 6.5: *The influence of rotation angle and mapping on the performance of SSD-ID OFDM system using QPSK modulation at* $E_b/N_0 = 4$ *dB. The cloud around each symbol mapping is the effect of rotation angle which vary from* $\theta = 0°$ *to* $\theta = 90°$*. Rate* $\frac{1}{2}$ *regular, random* $(3, 6)$ *and* $(4, 8)$ *LDPC codes of length* 2640 *and* 4000*, respectively are used.*

a constellation labeling is because of the rotation of that particular constellation from $\theta = 0°$ to $\theta = 90°$. After $\theta = 90°$ the same behavior is periodically repeated [34]

In Figure 6.5, also the comparison of $(3, 6)$ and $(4, 8)$ regular random LDPC codes of length 2640 and 4000, rate $\frac{1}{2}$, respectively, is shown. In the figure, the decoding trajectory of $(4, 8)$ LDPC decoder gets stuck at low mutual information as the transfer characteristic curves of the decoder and the de-mapper intersect. It is important to stress that this behavior is an indication towards the structure of the parity check matrix being employed. Thus, the degree distribution of the variable and the check nodes is a degree of freedom which can be optimized to

achieve better performance.

6.5 Simulation Results and Discussion

This section presents simulation results for BICM-ID OFDM and SSD-ID OFDM systems using recursive systematic convolutional (RSC) and LDPC codes. The effect of the rotation of the signal constellation on the overall system performance of SSD-ID OFDM is also presented. The effect of the rotation of the signal constellation can be visualized by fixing the E_b/N_0- value and observing a system performance parameter, e.g., BER. The systems are simulated with $N = 64$ subcarriers and a channel model with root mean square (RMS) delay spread of about 50 nsec, a bandwidth of 50 MHz and a 29-tap power delay profile having an exponentially decaying fading characteristics with each ray being assumed to be independently Rayleigh faded. The simulation results are parsed for better comprehension on the basis of the error correcting codes being employed.

6.5.1 Convolutional Codes

16-state, rate $\frac{1}{2}$ and rate $\frac{2}{3}$ recursive systematic convolutional codes (RSC) with a generator polynomial $[37, 21]_8$ are employed in an SSD-ID system. For further information on puncture pattern employed to achieve a code rate of $\frac{2}{3}$ we refer the reader to Chapter 5. Each data block contains 2600 information bits. QPSK with Gray and Natural mapping, and 8PSK with Gray, SP and SSP mapping are used. Figure 6.6 shows the BER as a function of various rotation angles for QPSK modulation scheme at $E_b/N_0 = 5$ dB, with code rates $\frac{1}{2}$ and $\frac{2}{3}$, respectively. The figure elucidate that the system performance, i.e., BER is dependent upon the choice of the rotation angle. The system shows best performance at 0°

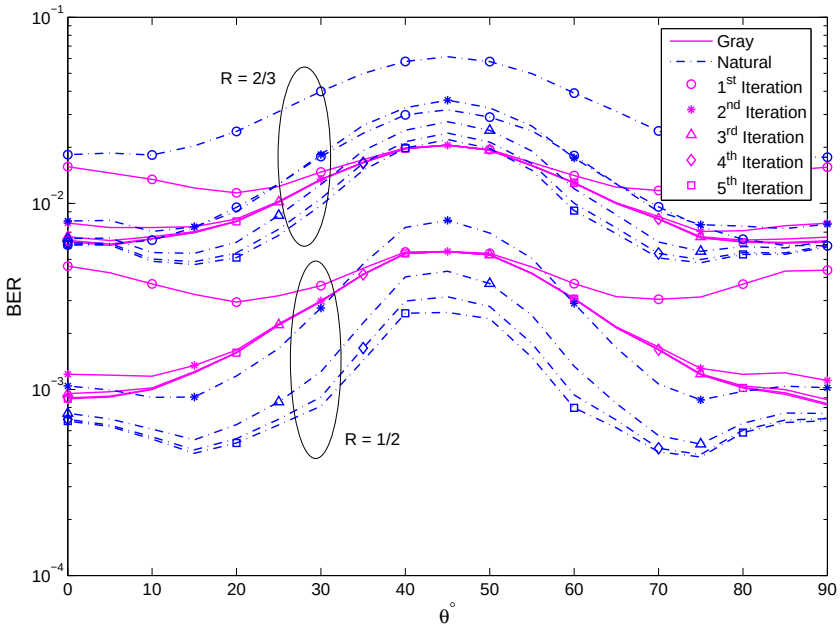

Figure 6.6: *BER performance of QPSK SSD-ID OFDM over different rotation angles. 16-state, rate $\frac{1}{2}$ and $\frac{2}{3}$ RSC codes are used with Gray and Natural signal constellation labeling in a frequency selective fading channel at $E_b/N_0 = 5$ dB.*

and 15° for Gray and Natural labeling, respectively, when 5 iterations are performed between the demodulator and the decoder. Rotation angles having better BER performance change after the first iteration for both mappings. No further improvement in performance can be obtained with Gray labeled constellation after 2 iterations. Furthermore, the rotation angles exhibiting better performance for a specific signal constellation are immune to the change in the code rate as depicted in the Figure 6.6. It is due to the fact that the transmitted bits are punctured to a lower rate by removing the parity bits and this lowers the error correcting capability but has no effect on the characteristic features (SSD and signal constellation rotation) of SSD-ID OFDM.

Similarly, Figures 6.7 and 6.8 show the BER performance of the 8PSK sys-

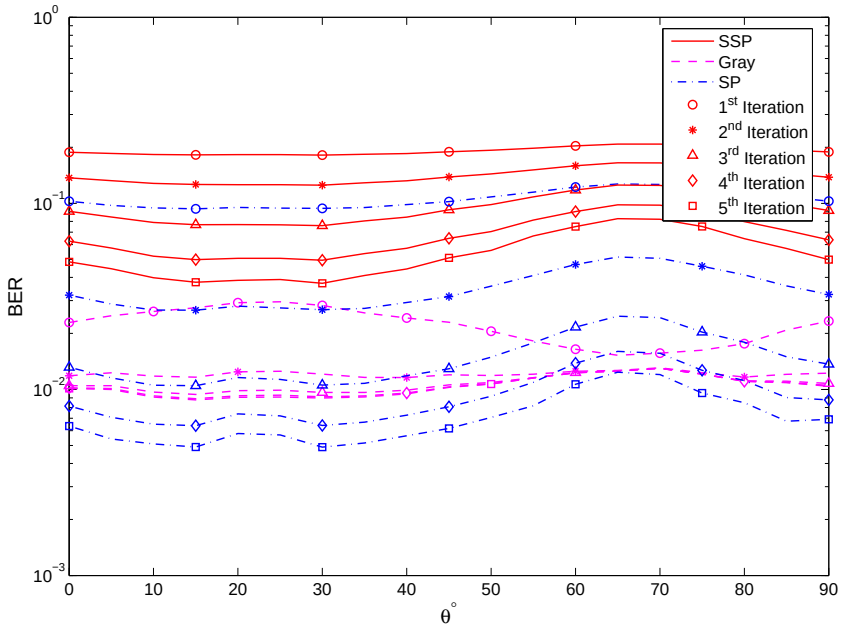

Figure 6.7: *BER performance of 8PSK SSD-ID OFDM over different rotation angles. 16-state, rate $\frac{1}{2}$ RSC codes are used with Gray, SP and SSP signal constellation labeling in a frequency selective fading channel at $E_b/N_0 = 5$ dB.*

tem as a function of the rotation angle. The figures signify the dependence of the performance of the system on the choice of the rotation angle and the signal constellation labeling. Furthermore, the figures also show that certain signal constellation labeling perform better at higher SNR region. Gray, SP and SSP labeling show best performance at 10°, 15° and 15°, respectively, at the 5^{th} iteration as in comparison to other rotational angles. At higher E_b/N_0-values SSP with an appropriately chosen rotation angle has better performance than Gray labeling when 3 or more iterations are performed between the demodulator and the decoder, as depicted by Figure 6.8.

Figures 6.9 and 6.10 show comparative performance gain of SSD-ID OFDM over BICM-ID OFDM with QPSK and 8PSK signal constellations. Figure 6.9

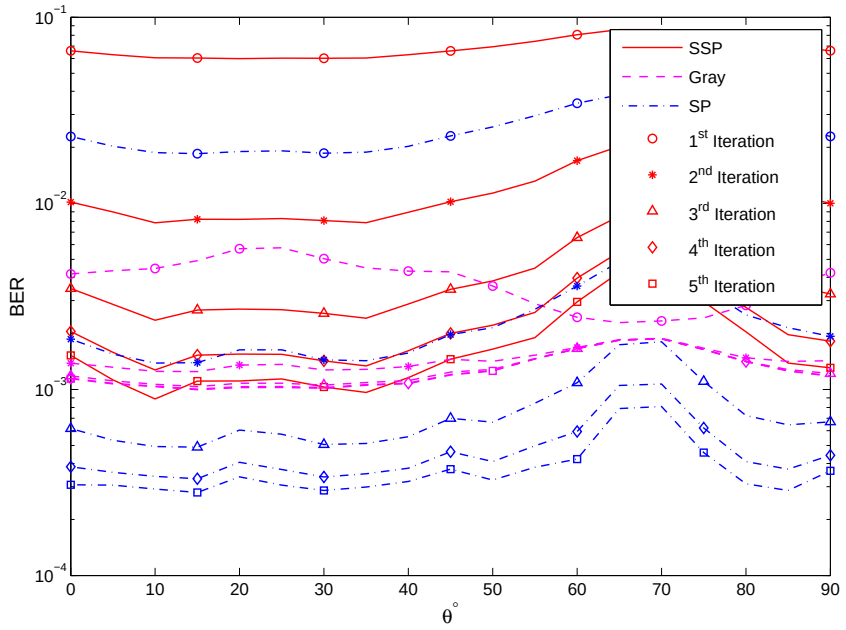

Figure 6.8: *BER performance of 8PSK SSD-ID OFDM over different rotation angles. 16-state, rate $\frac{1}{2}$ RSC codes are used with Gray, SP and SSP signal constellation labeling in a frequency selective fading channel at $E_b/N_0 = 7$ dB.*

shows the performance of QPSK signal constellation with Gray and Natural mapping. Gray labeled BICM-ID OFDM does not show any performance gain after multiple iterations. SSD-ID OFDM outperforms BICM-ID OFDM over all iterations and all mappings, e.g., the Natural labeled rotated SSD-ID OFDM has a performance improvement of 2.7 dB at a BER of 3×10^{-5} at the 5^{th} iteration as shown in Figure 6.9. Figure 6.10 shows the comparative performance of 8PSK signal constellation with Gray, SP and SSP labeling employed in an SSD-ID OFDM and BICM-ID OFDM system. In this figure also, SSD-ID OFDM outperforms BICM-ID OFDM. At the 5^{th} iteration SSD-ID OFDM outperforms BICM-ID OFDM over all mappings, e.g., SSP labeled rotated SSD-ID has a performance improvement of 1.2 dB at a BER of 2.6×10^{-4} over BICM-ID OFDM.

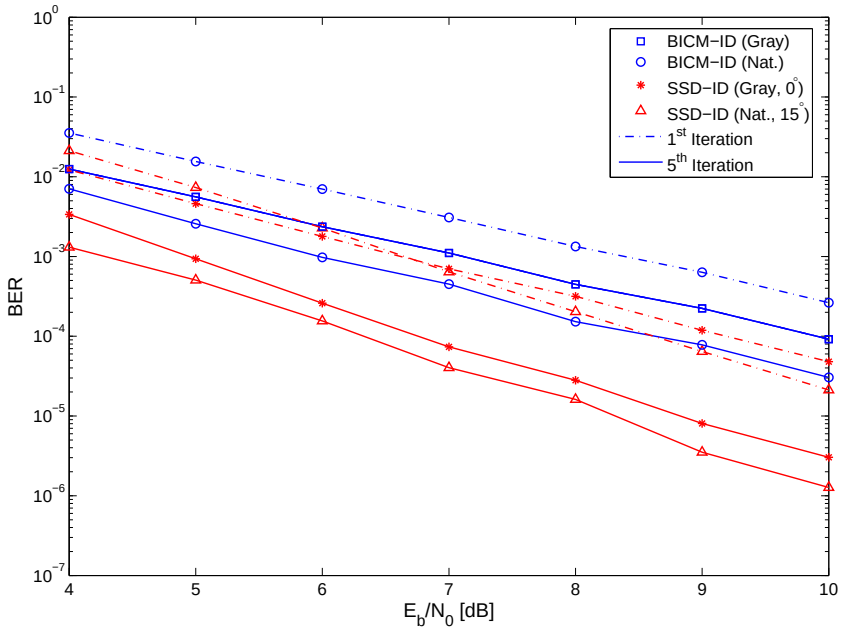

Figure 6.9: *BER performance of SSD-ID OFDM and BICM-ID OFDM with QPSK signal constellation. Gray and Natural labeling are used.* 16*-state RSC codes of length* 2600 *and rate* $\frac{1}{2}$ *are employed in a frequency selective fading channel.*

6.5.2 LDPC Codes

Random, regular $(3, 6)$ LDPC codes of rate $\frac{1}{2}$ and length 2640 with 5 internal iterations are used. Higher number of internal iterations within the LDPC decoder can lead to a gain but it is on the expense of latency and efficiency. Furthermore, the purpose was to observe the dependence of BER on the signal constellation rotation in an SSD-ID OFDM system. Figure 6.11 shows the BER performance of QPSK signal constellation as a function of rotation angle using Gray and Natural labeling in an SSD-ID system. Rotation angles of 10° and 15° for Gray and Natural labeling, respectively, have better performance than other rotation angles at the 5^{th} (external) iteration. The BER performance of 8PSK signal constellation, with Gray, SP and SSP labeling, respectively, as a function of rotation angle in

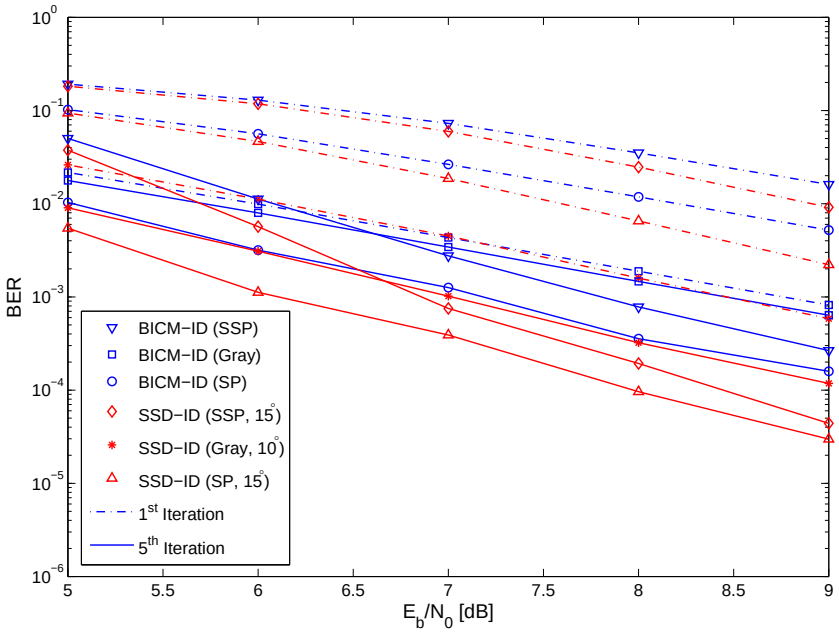

Figure 6.10: *BER performance of SSD-ID OFDM and BICM-ID OFDM with 8PSK signal constellation. Gray, SP and SSP labeling are used.* 16*-state RSC codes of length* 2600 *and rate* $\frac{1}{2}$ *are employed in a frequency selective fading channel.*

SSD-ID OFDM system is shown in Figure 6.12.

Figures 6.13 and 6.14 quantify the gain that is achieved by using SSD-ID OFDM over BICM-ID OFDM by the use of regular random $(3, 6)$ LDPC-codes of length 2640, rate $\frac{1}{2}$ and 5 internal iterations. Figure 6.13 shows the performance gain of Gray and Natural labeled QPSK signal constellation. SSD-ID OFDM outperforms BICM-ID OFDM over all iterations and all mappings, e.g., Natural mapped rotated SSD-ID OFDM has a performance gain of 2.8 dB at a BER of 5.5×10^{-4} at 4^{th} iteration over BICM-ID OFDM. Similarly, SSD-ID OFDM has a better performance for 8PSK signal constellation as depicted by Figure 6.14. SSD-ID OFDM outperforms BICM-ID OFDM for Gray, SP and SSP mappings under consideration, e.g., Gray labeled rotated SSD-ID OFDM has a performance

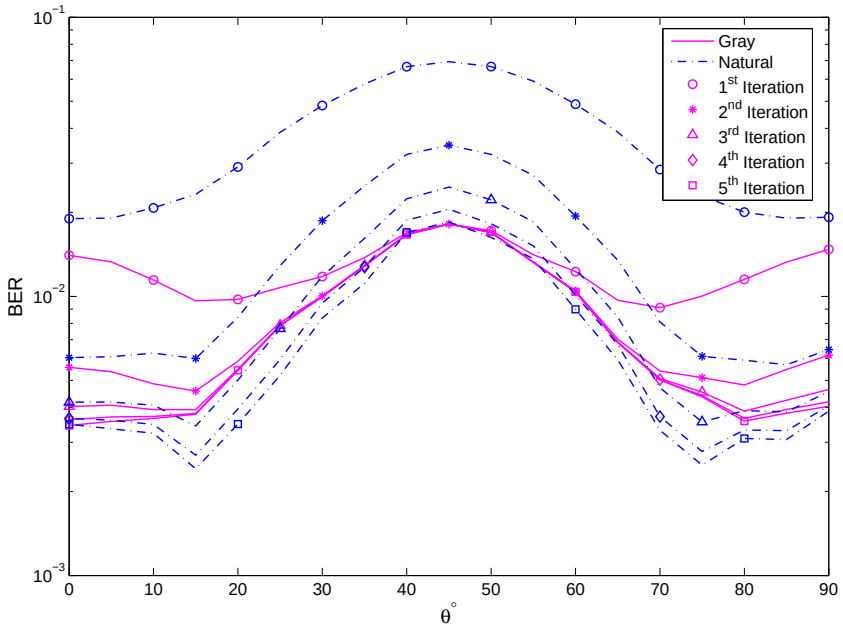

Figure 6.11: *BER performance of QPSK SSD-ID OFDM over different rotation angles. Rate* $\frac{1}{2}$ *regular random LDPC codes of length* 2640 *with a maximum of 5 internal iterations. Gray and Natural signal constellation labeling are used in a frequency selective fading channel at* $E_b/N_0 = 5$ *dB.*

improvement of 1.4 dB at a BER of 2.18×10^{-3} over BICM-ID OFDM.

It is clear that the system performance in terms of BER is dependent upon the signal constellation rotation, the signal constellation labeling, the SNR region of operation and the choice of the error correcting codes being employed.

6.6 Conclusions

In this chapter, we have presented the performance of RSC and LDPC codes over frequency selective fading channels using SSD, rotated MPSK constellations and OFDM. A symbol-to-bit de-mapper for iterative demodulation was introduced. The performance of the proposed scheme was compared with the BICM-ID OFDM

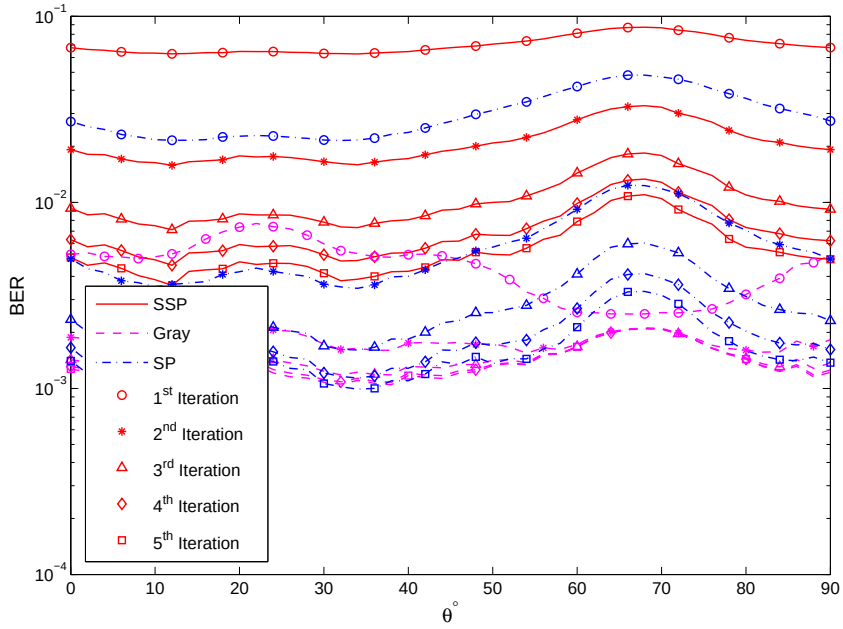

Figure 6.12: *BER performance of 8PSK SSD-ID OFDM over different rotation angles. Rate* $\frac{1}{2}$ *regular random LDPC codes of length* 2640 *are used with a maximum of 5 internal iterations. Gray, SP and SSP signal constellation labeling are used in a frequency selective fading channel at* $E_b/N_0 = 8$ *dB.*

by employing rotated MPSK constellations and different symbol-to-bit mappings. It was shown that a well considered choice of rotation angle and signal constellation labeling can provide significant performance improvement over the conventional BICM-ID OFDM system. The choice of the rotation angle was seen to be dependent on the signal constellation mapping and quite interestingly on the number of iterations performed at the receiver. Furthermore, it was also shown that the BER performance is dependent upon the signal constellation labeling, the SNR region of operation, a well considered choice of the rotation angle and the choice of the error correcting codes being employed. Using EXIT charts an analysis was presented on the effect of the signal constellation rotation on the overall performance of the system. It was shown that with a well considered choice of

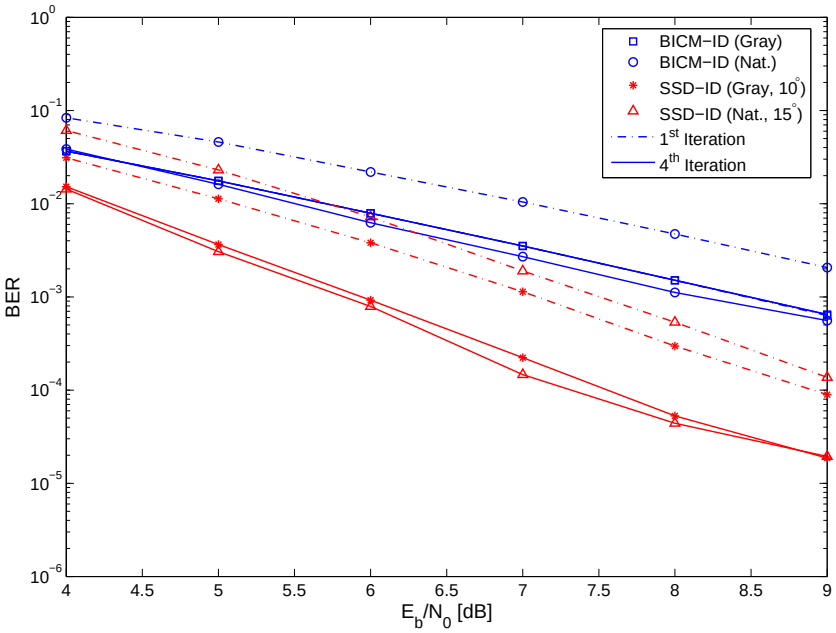

Figure 6.13: *BER performance of SSD-ID OFDM and BICM-ID OFDM with QPSK signal constellation. Gray and Natural labeling are used. Random, regular* $(3, 6)$ *LDPC-codes of rate* $\frac{1}{2}$ *and length* 2640 *are employed with 5 internal iterations in a frequency selective fading channel.*

the rotation angle the convergence of the iterative demodulation and decoding towards low BER is possible. Factors or degrees of freedom which can effect the system performance, such as, the constellation mapping, the rotation angle and the structure of LDPC codes, were discussed with illustrative examples.

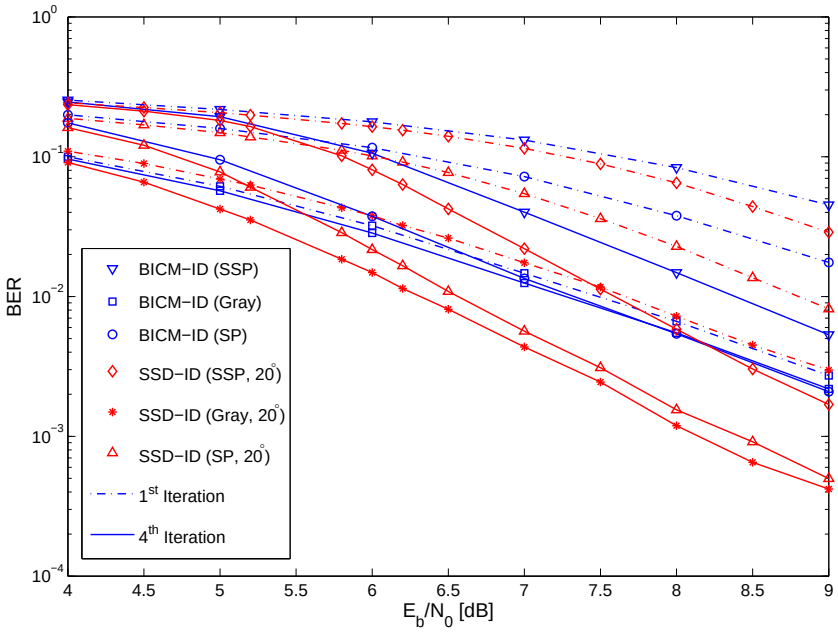

Figure 6.14: *BER performance of SSD-ID OFDM and BICM-ID OFDM with 8PSK signal constellation. Gray, SP and SSP labeling are used. Random, regular* $(3, 6)$ *LDPC-codes of rate* $\frac{1}{2}$ *and length* 2640 *are employed with 5 internal iterations in a frequency selective fading channel.*

Chapter 7

Conclusions and Recommendations

In this chapter, a short summary of the major contributions of each of the previous chapters is presented. Furthermore, the chapter highlights a number of issues which remain unsolved and may constitute a possible list of topics for future research.

The aim of the dissertation was to propose novel digital modulation and coding algorithms for systems that can adapt to different environments and still can maintain and provide the required quality of service (QoS). Thereby, resulting in systems that either consume less power for a given performance or offer more performance for a given amount of average energy than a conventional system. The algorithms had to be versatile and suitable for both narrowband as well as wideband wireless communication systems for indoor and low-mobility outdoor scenarios. In this dissertation we also focused on wireless communication systems employing diversity and multicarrier modulation schemes, specifically, orthogonal frequency division multiplexing (OFDM). In the subsequent sections we parse the major results of the dissertation on the basis of the uncoded and coded systems and furthermore we include suggestions, wherever applicable, based on unsolved problems which may constitute a possible list of topics for future research.

7.1 Uncoded Systems

Chapters 2 and 3 presented the results for uncoded wireless communication systems using modulation diversity, also known as signal space diversity in narrowband and wideband channels. The major contributions are as follows:

7.1.1 Narrowband Channels

In Chapter 2, a closed form expression for average bit error probability (BEP) in terms of average signal-to-noise ratio (SNR) for a system employing modulation diversity in Nakagami multipath fading channels with arbitrary fading parameter was derived. Correlated Rayleigh fading channels were also considered.

It was shown that the nearest neighbor approach, previously used in the literature for the analysis of modulation diversity systems, represents an expurgated bound and is only valid for a limited range of rotational angles.

It was shown that Gray signal constellation mapping is not necessarily the best option for a system employing modulation diversity.

Moreover, it was shown that the new derived upper bound is tight at high SNRs. Performance degradation due to imperfect receiver phase estimates was also considered. A closed form expression was derived for imperfect phase estimates caused by phase locked loop (PLL) dynamics having Tikhonov distribution.

It was shown that in the presence of phase noise the optimum rotation angle does not change for Nakagami fading channels with arbitrary fading parameter.

It was also shown that a system employing modulation diversity is more robust against phase estimation errors than a conventional system.

There are certain aspects of importance that have not been considered in Chapter 2 and would be interesting to solve for the completion of analysis. These aspects include the calculation of outage probability for a system employing modulation diversity in Nakagami multipath fading channels. Phase noise was explicitly considered in the analysis but noise due to analog-to-digital and digital-to-analog converters, mixer noise, power amplifier imperfections were not considered which would result in the degradation of the maximum achievable performance promised by Chapter 2. Furthermore, it would also be interesting to consider other modulation techniques, for instance, minimum shift keying (MSK), frequency shift keying (FSK) etc., to be exploited with modulation diversity and degrees of freedom identified for performance improvement in narrowband channels.

7.1.2 Wideband Channels

In Chapter 3, we investigated the performance of a system employing modulation diversity using $L-$ branch maximum ratio combining (MRC) receiver in a frequency selective channel under the assumption of a single symbol transmission. A closed form expression for average BEP in terms of the average SNR was derived for MPSK signal constellations for uncorrelated and correlated Nakagami-m faded paths. The new derived bound was shown to be tight for the entire range of the constellation rotation angle at high SNRs. The optimum rotation angles were found by minimizing the upper bound. Two correlation models were considered, i.e., the constant (equal) correlation model and the exponential correlation model.

It was shown that a system employing modulation diversity and MRC in correlated or uncorrelated frequency selective channels has significantly improved performance than a conventional $L-$ branch MRC receiver.

It was shown that the optimum rotation angles change as the number of diversity branches is increased.

A closed form expression for a system with outdated or imperfect channel estimation error was derived.

It was shown that the system employing SSD is robust to channel estimation errors.

It was also shown that the Gray mapping in a system employing SSD is not necessarily the best option over the entire range of rotational angle in frequency selective fading channels.

Equal gain combining (EGC), although suboptimal is a very attractive technique which does not require the estimation of channel fading amplitudes and hence results in reduced complexity relative to the optimum MRC scheme considered in Chapter 3 and can present an interesting problem to analyze for future

research for systems employing modulation diversity. Similarly, the analysis could also be extended to other known techniques, for instance, selection combining (SC), switch and stay combining (SSC) and hybrid combining techniques. Furthermore, the analysis of systems employing modulation diversity with optimum combining schemes that cater for co-channel interferers (CCI) and inter symbol interference (ISI) are interesting problems to be solved.

7.2 Coded Systems

Chapters 4, 5 and 6 presented results for coded systems using modulation diversity in narrowband and wideband multipath fading channels. The major contributions are as follows:

7.2.1 Narrowband Channels

In Chapters 4 and 5 coded modulation diversity systems' performance in narrowband channels was analyzed. In Chapter 4, modulation diversity coupled with regular, random low density parity check (LDPC) and convolutional codes was analyzed in comparison to uncoded systems in Rayleigh fading channels. A symbol-to-bit demapper for MPSK signal constellations was introduced.

It was shown that a system employing modulation diversity and channel coding exhibits different optimum rotation angles than an uncoded system.

In Chapter 5, the performance of modulation diversity system with iterative demodulation and decoding (ID) coupled with LDPC and convolutional codes (SSD-ID) was analyzed in Rayleigh fading channels. The performance of the proposed scheme was compared with the conventional bit interleaved coded modulation with iterative demodulation and decoding (BICM-ID) systems. A symbol-

to-bit de-mapper for multi-level modulation schemes was extended to incorporate iterative demodulation and decoding with SSD. Using EXIT charts an analysis was presented on the effect of the rotation on the overall performance of the system.

It was shown that with a well considered choice of the rotation angle the convergence of the iterative demodulation and decoding towards low bit error rate (BER) is possible.

The choice of the rotation angle was shown to be dependent upon the signal constellation labeling and the choice of the error correcting code being employed.

Factors or degrees of freedom which can effect the system performance, such as, the choice of the signal constellation rotation, the signal constellation labeling, the generator polynomial for recursive systematic convolutional (RSC) codes, the degree distribution for LDPC codes, the number of iterations performed within the LDPC codes and the SNR region of operation, were identified.

It was shown that SSD-ID systems with a well considered choice of the rotation angle and signal constellation labeling provides significant performance improvement over the conventional BICM-ID systems.

The extension of the entire results to more general Nakagami multipath fading channel with arbitrary fading parameter would be an interesting problem for future research. Moreover, the closed form expressions are derivable in the form of a true upper bound for average BEP in terms of SNR which can be approximated, for instance, by saddle point approximation to yield fairly accurate results and this extension would be a valuable addition to the entire analysis for coded systems using modulation diversity in different multipath fading environments.

7.2.2 Wideband Channels

In Chapter 6, we analyzed the performance of RSC and LDPC codes over frequency selective fading channels using SSD, rotated MPSK constellations and OFDM. A symbol-to-bit de-mapper for iterative demodulation was introduced. The performance of the proposed scheme was compared with the conventional BICM-ID OFDM by employing rotated MPSK constellations and different symbol-to-bit mappings.

It was shown that a well considered choice of rotation angle and signal constellation labeling can provide significant performance improvement over the conventional BICM-ID OFDM system.

The choice of the rotation angle was seen to be dependent on the signal constellation mapping and quite interestingly on the number of iterations performed at the receiver.

Furthermore, it was also shown that the BER performance is dependent upon the signal constellation labeling, the SNR region of operation, a well considered choice of the rotation angle and the choice of the error correcting codes being employed. Using EXIT charts an analysis was presented on the effect of the signal constellation rotation on the overall performance of the system.

It was shown that with a well considered choice of the rotation angle the convergence of the iterative demodulation and decoding towards low BER is possible.

Factors or degrees of freedom which can effect the system performance, such as, the constellation mapping, the rotation angle and the structure of LDPC codes, were also identified.

When the sinusoidal signals of the N sub-carriers add constructively, the peak power can be N- times the mean power, i.e., the peak-to-average power ratio

(PAPR) of the transmitted signal can be as large as N. Some initial work has been done on PAPR issues of OFDM systems using modulation diversity by us but still it is an open area which requires more research and insight. Similarly, at the receiver, synchronization issues are of prime importance and the exact location of the sub- carrier frequencies have to be found to be able to receive the data symbols. Any possible differences due to carrier frequencies or phase distortion causes inter carrier interference (ICI) and hence a degradation in performance. An interesting research problem would be to formulate a joint approach to mitigate the effects of ICI and PAPR for systems employing modulation diversity. Furthermore, investigation of power allocation methods, linear constellation precoding and extension to multiple input multiple output (MIMO) systems can present interesting research questions to be answered. Lastly, a practical working demonstrator for proof of ideas can also present a challenging task and can provide valuable insight to practical implementation issues for system employing modulation diversity.

Appendix A

An Alternative Derivation of PEP in Correlated Rayleigh Fading

We present an alternative method for the derivation of pairwise error probability (PEP) in correlated Rayleigh fading channel as given in Chapter 2 Section 2.6.1 equation (2.25). The method provides a simplification for the calculation of the PEP of correlated Rayleigh fading channels by using the alternative approach to calculate the pdf of $(\alpha_1^2 d_I^2 + \alpha_2^2 d_Q^2)$ and then employing the PDF in equation (2.18). Let $f = \alpha_1^2 d_I^2 + \alpha_2^2 d_Q^2$ be the random variable, the characteristic function [48, 119]

of which can be derived by using (2.17) and (2.9) as

$$\begin{aligned}
\Phi(\omega) &= E\{e^{j\omega f}\} \\
&= \int_0^\infty p(f)e^{j\omega f}\mathrm{d}f \\
&= \int_0^\infty \int_0^\infty e^{j\omega\left(\alpha_1^2 d_I^2+\alpha_2^2 d_Q^2\right)} \frac{4\alpha_1\alpha_2}{1-\rho_k^2} I_o\left(\frac{2|\rho_k|\alpha_1\alpha_2}{1-\rho_k^2}\right) e^{\frac{-(\alpha_1^2+\alpha_2^2)}{1-\rho_k^2}} \mathrm{d}\alpha_1\mathrm{d}\alpha_2 \\
&= \frac{1}{(1-\rho_k^2)} \int_0^\infty \int_0^\infty 2\alpha_1 e^{-\alpha_1^2\left(\frac{1-j\omega d_I^2(1-\rho_k^2)}{(1-\rho_k^2)}\right)} I_o\left(\frac{2|\rho_k|\alpha_1\alpha_2}{1-\rho_k^2}\right) \\
&\quad 2\alpha_2 e^{-\alpha_2^2\left(\frac{1-j\omega d_Q^2(1-\rho_k^2)}{(1-\rho_k^2)}\right)} \mathrm{d}\alpha_1\mathrm{d}\alpha_2. \qquad \text{(A.1)}
\end{aligned}$$

Simplifying we have

$$\begin{aligned}
\Phi(\omega) &= \int_0^\infty \frac{e^{\alpha_2^2\left(\frac{\rho_k^2}{\left(1-j\omega d_I^2(1-\rho_k^2)\right)(1-\rho_k^2)}\right)}}{(1-j\omega d_I^2(1-\rho_k^2))} 2\alpha_2 e^{-\alpha_2^2\left(\frac{1-j\omega d_Q^2(1-\rho_k^2)}{(1-\rho_k^2)}\right)} \mathrm{d}\alpha_2 \\
&= \frac{1}{(1-j\omega d_I^2(1-\rho_k^2))} \int_0^\infty 2\alpha_2 \\
&\quad e^{-\alpha_2^2\left(\frac{-\rho_k^2+\left(1-j\omega d_Q^2(1-\rho_k^2)\right)\left(1-j\omega d_I^2(1-\rho_k^2)\right)}{(1-\rho_k^2)\left(1-j\omega d_I^2(1-\rho_k^2)\right)}\right)} \mathrm{d}\alpha_2 \\
&= \frac{(1-\rho_k^2)}{(1-\rho_k^2)\left(1-(1-\rho_k^2)(\omega^2 d_I^2 d_Q^2)-j\omega d_I^2-j\omega d_Q^2\right)} \\
&= \frac{1}{\left(1+(j\omega)^2(1-\rho_k^2)(d_I^2 d_Q^2)-2j\omega\right)}. \qquad \text{(A.2)}
\end{aligned}$$

Completing the square in the denominator of (A.2) we have

$$\Phi(\omega) = \frac{1}{(1-j\omega\Delta_1)\,(1-j\omega\Delta_2)} \qquad \text{(A.3)}$$

where,

$$\begin{aligned}\Delta_1 &= 1-\sqrt{1-(1-\rho_k^2)(d_I^2 d_Q^2)},\\ \Delta_2 &= 1+\sqrt{1-(1-\rho_k^2)(d_I^2 d_Q^2)}.\end{aligned} \tag{A.4}$$

Taking the inverse of (A.3) we have

$$\begin{aligned}p(f) &= \frac{1}{2\pi}\int_{-\infty}^{\infty} e^{j\omega f}\Phi_F(\omega)\mathrm{d}\omega\\ &= \frac{1}{2\pi}\int_{-\infty}^{\infty} e^{j\omega f}\frac{1}{(1-j\omega\Delta_1)(1-j\omega\Delta_2)}\mathrm{d}\omega\\ &= \frac{-1}{2\pi}2\pi\frac{\left(-e^{\frac{-f}{\Delta_1}}+e^{\frac{-f}{\Delta_2}}\right)}{\Delta_1-\Delta_2}\\ &= \frac{e^{\frac{-f}{\Delta_1}}}{\Delta_1-\Delta_2}-\frac{e^{\frac{-f}{\Delta_2}}}{\Delta_1-\Delta_2}.\end{aligned} \tag{A.5}$$

Using (2.9) & (A.5) in (2.18) and rewriting we have

$$\begin{aligned}P(s\to\hat{s}) &= \frac{1}{\pi(\Delta_1-\Delta_2)}\int_0^{\pi/2}\int_0^{\infty} e^{\frac{-\bar{\gamma}f}{2\sin^2(\psi)}}\left(e^{\frac{-f}{\Delta_1}}-e^{\frac{-f}{\Delta_2}}\right)\mathrm{d}f\mathrm{d}\psi\\ &= \frac{1}{\pi(\Delta_1-\Delta_2)}\int_0^{\pi/2}\left(\frac{2\Delta_1\sin^2(\psi)}{\bar{\gamma}\Delta_1+2\sin^(\psi)}-\frac{2\Delta_2\sin^2(\psi)}{\bar{\gamma}\Delta_2+2\sin^(\psi)}\right)\mathrm{d}\psi\\ &= \frac{1}{\pi(\Delta_1-\Delta_2)}\int_0^{\pi/2}\left(\frac{\Delta_1\sin^2(\psi)}{\frac{\bar{\gamma}\Delta_1}{2}+\sin^(\psi)}-\frac{\Delta_2\sin^2(\psi)}{\frac{\bar{\gamma}\Delta_2}{2}+\sin^(\psi)}\right)\mathrm{d}\psi\\ &= \frac{\Delta_1}{2(\Delta_1-\Delta_2)}\left(1-\sqrt{\frac{\bar{\gamma}\Delta_1}{2+\bar{\gamma}\Delta_1}}\right)-\\ &\quad \frac{\Delta_2}{2(\Delta_1-\Delta_2)}\left(1-\sqrt{\frac{\bar{\gamma}\Delta_2}{2+\bar{\gamma}\Delta_2}}\right)\end{aligned} \tag{A.6}$$

The above result matches to the one obtained in (2.23) and if $\rho_k = 0$ which implies an uncorrelated Rayleigh fading case (A.6) reduces to the form given in (2.25).

Bibliography

[1] M. Zeng, A. Annamalasi, and V. Bhargava, "Recent advances in cellular wireless communications," *IEEE Commun. Mag.*, no. 9, pp. 128–138, Sept. 1999.

[2] S. Ohmori, Y. Yamao, and N. Nakajima, "The future generations of mobile communications based on broadband access technologies," *IEEE Commun. Mag.*, pp. 134–142, Dec. 2000.

[3] S. Jun-Zhao, J. Sauvola, and D. Howie, "Features in future: 4G visions from a technical perspective," *Proc. IEEE Global Telecomm. Conf.*, pp. 3533–3537, Nov. 2001.

[4] M. K. Simon and M. S. Alouini, *Digital Communication over Fading Channels - A Unified Approach to Performance Analysis.* New York, NY: John Wiley & Sons, 2000.

[5] G. L. Stüber, *Principles of Mobile communications*, 2nd ed. Norwell, USA: Kluwer academic publishers, 2001.

[6] A. Goldsmith, *Wireless Communications*. New York, NY: Cambridge University Press, 2005.

[7] J. G. Proakis, *Digital Communications*. New York, NY: McGraw-Hill, 2001.

[8] T. S. Rappaport, *Wireless Communications: Principles and Practice*. Upper Saddle River, NJ: Prentice Hall, 1996.

[9] D. Tse and P. Viswanath, *Fundamentals of Wireless Communication*. New York, NY: Cambridge University Press, 2005.

[10] L. J. Mason, "Error probability evaluation of systems employing differential detection in a Rician fading environment and gaussian noise," *IEEE Trans. Commun.*, pp. 39–46, May 1987.

[11] U. Charash, "Reception through Nakagami fading multipath channels with random delays," *IEEE Trans. Commun.*, vol. 27, pp. 657–670, Apr. 1979.

[12] M. Abramowitz and I. A. Stegun, *Handbook of Mathematical Functions*. New York, NY: Dover Publications, 1972.

[13] H. B. James and P. I. Wells, "Some tropospheric scatter propagation measurements near the radio-horizon," *Proc. IRE*, pp. 1336–1340, Oct. 1955.

[14] G. R. Sugar, "Some fading characteristics of regular VHF ionospheric propagation," *Proc. IRE*, pp. 1432–1436, Oct. 1955.

[15] T. L. Staley, R. C. North, W. H. Ku, and J. R. Zeidler, "250 MHz/GHz scintillation parameters in the equatorial, polar and aural environments," *IEEE J. Select. Areas Commun.*, pp. 102–115, Feb. 1987.

[16] S. O. Rice, "Statistical properties of a sine wave plus random noise," *Bell Syst. Tech. J.*, vol. 27, pp. 109–157, Jan. 1948.

[17] M. Nakagami, "The m-distribution: A general formula for intensity distribution of rapid fading," in *Statistical Methods in Radio Wave Propogation*, 1960, pp. 3–36.

[18] H. Suzuki, "A statistical model for urban multipath propagation," *IEEE Trans. Commun.*, pp. 673–680, July 1977.

[19] T. Aulin, "Characteristics of a digital mobile radio channel," *IEEE Trans. Veh. Technol.*, vol. VT-40, pp. 45–53, May 1991.

[20] A. U. Sheikh, M. Handforth, and M. Abdi, "Indoor mobile radio channel at 946 MHz: measurements and modeling," *IEEE Veh. Technol. Conf.*, pp. 73–76, May 1993.

[21] H. Hashemi, "Impulse response modeling of indoor radio propagation channels," *IEEE J. Select. Areas Commun.*, pp. 967–978, Sept. 1993.

[22] A. S. Bajwa, "UHF wideband statistical model and simulation of mobile radio multipath propagation effects," *IEE Proc.*, pp. 327–333, Aug. 1985.

[23] F. Patenaude, J. Lodge, and Y.-Y. Chouinard, "Temporal correlation analysis of frequency selective fading channels," *6th Annu. Int. Conf. Wireless Comm.*, pp. 134–139, July 1994.

[24] E. K. Al-Hussaini and A. M. Al-Bassiouni, "Performance of MRC diversity systems for the detection of signals with Nakagami fading," *IEEE Trans. Commun.*, pp. 1315–1319, Dec. 1985.

[25] G. L. Turin, F. D. Clapp, T. L. Johnston, S. B. Fine, and D. Lavry, "A statistical model of urban multipath propagation," *IEEE Trans. Veh. Technol.*, pp. 1–9, Feb. 1972.

[26] W. R. Braun and U. Dersch, "A physical mobile radio channel model," *IEEE Trans. Veh. Technol.*, vol. VT-40, pp. 472–482, May 1991.

[27] S. A. Abbas and A. U. Sheikh, "A geometric theory of Nakagami fading multipath mobile radio channel with physical interpretations," *IEEE Veh. Technol. Conf.*, pp. 637–641, April 1996.

[28] G. Taricco and E. Viterbo, "Performance of component interleaved signal sets for fading channels," *Electronics Lett.*, vol. 32, no. 13, pp. 1170–1172, April 1996.

[29] S. B. Slimane, "An improved PSK scheme for fading channels," *IEEE Trans. Veh. Technol.*, vol. 47, no. 2, pp. 703–710, May 1998.

[30] J. Boutros and E. Viterbo, "Signal space diversity: a power and bandwidth-efficient technique for the Rayleigh fading channel," *IEEE Trans. Inform. Theory*, vol. 44, no. 4, pp. 1453–1467, July 1998.

[31] R. Schober, L. H.-J. Lampe, W. H. Gerstacker, and S. Pasupathy, "Modulation diversity for frequency-selective channels," *IEEE Trans. Inform. Theory*, no. 9, pp. 2268–2276, Sept. 2003.

[32] D. Brennan, "Linear diversity combining techniques," *Proc. IRE*, pp. 1075–1102, June 1959.

[33] N. F. Kiyani and J. H. Weber, "Iterative demodulation and decoding for rotated MPSK constellations with convolutional coding and signal space diversity," *IEEE Veh. Technol. Conf.*, pp. 1712–1716, Oct. 2007.

[34] N. F. Kiyani, U. H. Rizvi, J. H. Weber, and G. J. M. Janssen, "Optimized rotations for LDPC-coded MPSK constellations with signal space diversity," *Proc. IEEE Wireless Comm. and Networking Conf.*, pp. 677–681, Mar. 2007.

[35] ——, "Rotation optimization for MPSK/MQAM signal constellations with LDPC coding over Rayleigh fading channels," *IEEE Symposium on Commun. and Veh. Technol.*, pp. 77–80, Nov. 2006.

[36] N. F. Kiyani, J. H. Weber, A. G. Zajić, and G. L. Stüber, "Performance analysis of a system using coordinate interleaving and constellation rotation in Rayleigh fading channels," *IEEE Veh. Technol. Conf.*, Sept. 2008.

[37] N. F. Kiyani and J. H. Weber, "A novel iterative demodulation and decoding scheme with convolutional coding and co-ordinate interleaving," *28th Symposium on Information Theory in the Benelux*, pp. 11–17, May 2007.

[38] ——, "OFDM with BICM-ID and rotated MPSK constellations and signal space diversity," *IEEE Symposium on Commun. and Veh. Technol.*, pp. 1–4, Nov. 2007.

[39] ——, "Performance analysis of a partially coherent system using constellation rotation and coordinate interleaving," {*accepted*}*IEEE Global Comm. Conf.*, Dec. 2008.

[40] ——, "Performance analysis of coordinate interleaved systems over Rayleigh fading channels," *29th Symposium on Information Theory in the Benelux*, pp. 69–76, May 2008.

[41] C. Schlegel and D. J. Costello Jr., "Bandwidth efficient coding for fading channels: Code construction and performance analysis," *IEEE J. Select. Areas Commun.*, vol. 7, no. 9, pp. 1356–1368, Dec. 1989.

[42] M. K. Simon, S. M. Hinedi, and W. C. Lindsey, *Digital Communication Techniques: Signal Design and Detection.* Upper Saddle River, NJ: Prentice Hall, 1995.

[43] J. K. Cavers, "An analysis of pilot symbol assisted modulation for Rayleigh fading channels," *IEEE Trans. Commun.*, pp. 686–693, Nov. 1991.

[44] J. Tan and G. L. Stüber, "Analysis and design of symbol mappers for iteratively decoded BICM," *IEEE Trans. Wireless Commun.*, vol. 4, no. 2, pp. 662–672, Mar. 2005.

[45] M. K. Simon and D. Divsalar, "Some new twists to problems involving the Gaussian probability integral," *IEEE Trans. Commun.*, vol. 46, no. 2, pp. 200–210, Feb. 1998.

[46] P. J. Lee, "Computation of the bit error rate of coherent M-ary PSK with Gray code bit mapping," *IEEE Trans. Commun.*, vol. 32, no. 5, pp. 488–491, May 1982.

[47] W. C. Jakes, *Microwave Mobile Communications.* New York, NY: John Wiley & Sons, 1974.

[48] A. L.-Garcia, *Probability and random processes for electrical engineering.* Addison-wesley publishing company, 1989.

[49] G. J. Foschini, R. D. Gitlin, and S. B. Weinstein, "Optimization of two-dimensional signal constellations in the presence of Gaussian noise," *IEEE Trans. Commun.*, vol. 22, no. 1, pp. 28–38, Jan. 1974.

[50] E. Villier, "Performance analysis of optimum combining with multiple interferers in flat Rayleigh fading," *IEEE Trans. Commun.*, vol. 47, no. 2, pp. 1503–1510, Oct. 1999.

[51] A. J. Viterbi, "Phase-locked loop dynamics in the presence of noise by Fokker-Planck techniques," *Proc. IEEE*, vol. 51, pp. 1737–1753, Dec. 1963.

[52] T. Engg and L. B. Milstein, "Partially coherent DS-SS performance in frequency selective multipath fading," *IEEE Trans. Commun.*, vol. 45, no. 1, pp. 110–118, Jan. 1997.

[53] C. M. Lo and W. H. Lam, "Error probability of binary phase shift keying in Nakagami-m fading channel with phase noise," *Electronics Lett.*, vol. 36, pp. 1773–1774, Oct. 2000.

[54] M. K. Simon and D. Divsalar, "Multiple symbol partially coherent detection of MPSK," *IEEE Trans. Commun.*, vol. 42, pp. 430–439, Feb-Apr. 1994.

[55] V. I. Tikhonov, "The effect of noise on phase-locked oscillator operation," *Autom. Remote Control*, vol. 20, pp. 1160–1168, 1959.

[56] M. V. Clark, L. J. Greenstein, W. K. Kennedy, and M. Shafi, "Matched filter performance bounds for diversity combining receivers in digital mobile radio," *IEEE Trans. Veh. Technol.*, vol. 41, pp. 356–362, Nov. 1992.

[57] R. Visoz and E. Bejjani, "Matched filter bound for multichannel diversity over frequency-selective Rayleigh fading mobile channels," *IEEE Trans. Veh. Technol.*, vol. 49, pp. 1832–1845, Sept. 2000.

[58] J. E. Mazo, "Exact match filter bound for two-beam Rayleigh fading," *IEEE Trans. Commun.*, vol. 39, pp. 1027–1030, July 1991.

[59] R. Schober, W. H. Gerstacker, and L. H.-J. Lampe, "Perfomance analysis and design of STBCs for frequency-selective fading channels," *IEEE Trans. Wireless Commun.*, no. 9, pp. 734–744, May 2004.

[60] M. K. Simon and M. S. Alouini, "A unified approach to the performance analysis of digital communication over generalized fading channels," *Proc. IEEE*, vol. 86, no. 9, pp. 1860–1877, Sept. 1998.

[61] M. S. Alouini and A. J. Goldsmith, "A unified approach for calculating the error rates of linearly modulatted signal over generalized fading channels," *IEEE Trans. Commun.*, vol. COM-47, pp. 1324–1334, Sept. 1999.

[62] A. Annamalai, C. Tellambura, and V. K. Bhargava, "Analysis of M-ary phase shift keying with diversity reception for land-mbile satellite channels," *IEEE Trans. Veh. Technol.*, vol. VT-46, pp. 910–922, Nov. 1997.

[63] ——, "Exact evaluation of maximal-ratio and equal-gain diversity receivers for M-ary QAM on Nakagami fading channels," *IEEE Trans. Commun.*, vol. COM-47, pp. 1335–1344, Sept. 1999.

[64] X. Dong, N. C. Beaulieu, and P. H. Wittke, "Signalling constellations for fading channels," *IEEE Trans. Commun.*, vol. COM-47, pp. 703–714, May 1999.

[65] V. A. Aalo, "Performance of maximum-ratio diversity systems in a correlated Nakagami-fading environment," *IEEE Trans. Commun.*, pp. 2360–2369, Aug. 1995.

[66] R. G. Vaughan and J. B. Anderson, "Antenna diversity in mobile communications," *IEEE Trans. Veh. Technol.*, pp. 149–172, Nov. 1987.

[67] I. S. Gradshteyn and I. M. Ryzhik, *Table of Integrals, Series and Products*, 5th ed. San Diego, CA: Academic Press, 1994.

[68] M. J. Gans, "The effect of Gaussian error in maximum-ratio combiners," *IEEE Trans. Commun.*, pp. 492–500, Aug. 1971.

[69] M. S. Alouini, S.-W. Kim, and A. Goldsmith, "RAKE reception with maximum-ratio and equal-gain combining for CDMA systems in Nakagami fading," *IEEE Int. Conf. Univ. Personal Comm.*, pp. 708–712, Oct. 1997.

[70] B. R. Tomiuk, N. C. Beaulieu, and A. A. Abu-Dayya, "General forms for maximal ratio diversity with weighting errors," *IEEE Trans. Commun.*, pp. 488–492, Apr. 1999.

[71] C. E. Shannon, "A mathematical theory of communication," *Bell Sys. Tech. Journal*, vol. 27, pp. 379–423, 623–656, Jul. Oct. 1948.

[72] C. Berrou, A. Glavieux, and P. Thitimajshima, "Near Shannon limit error-correcting coding and decoding: Turbo-codes," in *Proc. ICC'93*, May 1993, pp. 1064–1070.

[73] R. G. Gallager, *Low density parity check code.* Cambridge: MA:MIT Press, 1963.

[74] D. J. C. Mackay, "Good error correcting codes based on very sparse matrices," *IEEE Trans. Inform. Theory*, no. 2, pp. 399–431, Mar. 1999.

[75] J. Hou, P. H. Siegel, and L. B. Milstein, "Performance analysis and code optimization of low density parity-check codes on Rayleigh fading channels," *IEEE J. Select. Areas Commun.*, vol. 19, no. 5, pp. 924–934, May 2001.

[76] T. J. Richardson and R. L. Urbanke, "The capacity of low density parity check codes under message passing decoding," no. 47, pp. 599–618, Feb. 2001.

[77] T. J. Richardson, M. A. Shokrollahi, and R. L. Urbanke, "Design of capacity approaching irregular low-density parity check codes," *IEEE Trans. Inform. Theory*, no. 47, pp. 619–637, Feb. 2001.

[78] K. Fu and A. Anastasopoulos, "Performance analysis of LDPC codes for time selective complex fading channels," *IEEE Global Telecommunications Conference*, no. 2, pp. 1279–1283, Nov. 2002.

[79] M. Tanner, "A recursive approach to low complexity codes," *IEEE Trans. Inform. Theory*, no. 5, pp. 533–547, 1981.

[80] M. Luby, M. Mitzenmacher, A. Shokrollahi, D. Spielman, and V. Stemann, "Practical loss-resilient codes," no. 2, pp. 150–159, 1997.

[81] T. J. Richardson and R. L. Urbanke, "Efficient encoding of low density parity check codes," no. 47, pp. 638–656, Feb. 2001.

[82] L. R. Bahl, J. Cocke, F. Jelinek, and J. Raviv, "Optimal decoding of linear codes for minimizing symbol error rate," *IEEE Trans. Inform. Theory*, no. 2, pp. 284–287, Mar. 1974.

[83] J. Hagenauer, E. Offer, and L. Papke, "Iterative decoding of binary block and convolution codes," *IEEE Trans. Inform. Theory*, no. 2, pp. 429–445, Mar. 1996.

[84] P. Elias, "Error-free coding," *IRE Trans. Information Theory*, vol. IT-4, pp. 29–37, 1954.

[85] G. D. Forney, "Convolutional codes I: Algebaric structure," *IEEE Trans. Inform. Theory*, vol. IT-17, pp. 720–738, May 1970.

[86] S. Benedetto, D. Divsalar, G. Montorsi, and F. Pollara, "A soft-input soft-ouput APP module for iterative decoding of concatenated codes," *IEEE Commun. Lett.*, no. 1, pp. 22–24, Jan. 1997.

[87] A. J. Viterbi and J. K. Omura, *Principles of Digital Communication and Coding.* New York, NY: McGraw-Hill, 1979.

[88] J. Hagenauer, "Rate compatible punctured convolutional codes (RCPC codes) and their applications," *IEEE Trans. Commun.*, vol. 36, no. 4, pp. 389–400, April 1988.

[89] L. H. C. Lee, *Convolutional coding:Fundamentals and Applications.* Artech House, 1997.

[90] B. Vucetic and J. Yuan, *Turbo Codes:Principals and Applications.* Norwell, USA: Kluwer academic publishers, 2000.

[91] S. Benedetto and E. Biglieri, *Principles of Digital Transmission with wireless applications.* New York, NY: McGraw-Hill, 1979.

[92] M. P. C. Fossorier, F. Burkert, and S. L. J. Hagenauer, "On the equivalence between SOVA and max-log-MAP decodings," *IEEE Commun. Lett.*, vol. 2, pp. 137–139, May 1988.

[93] R. W. Chang and J. C. Hancock, "On receiver structures for channels having memory," *IEEE Trans. Inform. Theory*, vol. IT-12, pp. 463–468, Oct. 1966.

[94] K. Abend and B. D. Fritchman, "Statistical defection for communication channels with intersymbol interference," *Proc. IEEE*, vol. 58, pp. 779–785, May 1970.

[95] J. Raviv, "Decision making in Markov chains applied to the problem of pattern recognition," *IEEE Trans. Inform. Theory*, vol. IT-13, pp. 536–551, Oct. 1967.

[96] N. F. Kiyani and J. H. Weber, "Analysis of random regular LDPC codes on Rayleigh fading channels," *27th Symposium on Information Theory in the Benelux*, pp. 69–76, June 2006.

[97] B. Lu, G. Yue, and X. Wang, "Performance analysis and design optimization of LDPC-coded MIMO OFDM systems," *IEEE Trans. Signal Processing*, vol. 52, no. 2, pp. 348–361, Feb. 2004.

[98] A. Stefanov and T. M. Duman, "Turbo coded modulation for systems with transmit and receive antenna diversity over block fading channels:system model, decoding approaches and practical considerations," *IEEE J. Select. Areas Commun.*, vol. 19, no. 5, pp. 958–968, May 2001.

[99] X. Li, A. Chindapol, and J. A. Ritcey, "Bit-interleaved coded modulation with iterative decoding and 8PSK signaling," *IEEE Trans. Commun.*, vol. 50, no. 8, pp. 1250–1257, Aug. 2002.

[100] A. Chindapol and J. A. Ritcey, "Design, analysis, and performance evaluation for BICM-ID with square QAM constellations in Rayleigh fading channels," *IEEE J. Select. Areas Commun.*, vol. 19, no. 5, pp. 944–957, May 2001.

[101] Z. A. Khan and B. S. Rajan, "Bit and co-ordinate interleaved coded modulation," *Proc. IEEE Global Telecomm. Conf.*, vol. 3, pp. 1595–1599, Nov.-Dec. 2000.

[102] A. Chindapol and J. A. Ritcey, "Bit-interleaved coded modulation with signal space diversity in Rayleigh fading," *Proc. 33rd Asilomar Conf. Signals, Systems, Computers.*, vol. 2, pp. 1003–1007, Oct. 1999.

[103] T. Cover and J. Thomas, *Elements of Information Theory.* New York, NY: Wiley, 1991.

[104] G. Caire, G.Taricco, and E. Biglieri, "Bit-interleaved coded modulation," *IEEE Trans. Inform. Theory*, vol. 44, no. 3, pp. 927–945, May. 1998.

[105] S. ten Brink, "Convergence behavior of iteratively decoded parallel concatenated codes," *IEEE Trans. Commun.*, vol. 49, no. 10, pp. 1727–1737, Oct. 2001.

[106] ——, "Designing iterative decoding schemes with the extrinsic information transfer chart," *AEÜ Int. J. Electron. Comm.*, vol. 54, no. 6, pp. 389–398, Nov. 2000.

[107] M. Tüchler, "Design of serially concatenated systems depending on the block length," *IEEE Trans. Commun.*, vol. 52, no. 2, pp. 209–218, Feb. 2004.

[108] F. Schreckenbach and G. Bauch, "Irregular signal constellations, mappings and precoder," *Proc. International Symp. on Information Theory and its Applications*, Oct. 2004.

[109] ——, "Adaptive bit-interleaved coded irregular modulation," *Proc. 14th IST Mobile and Wireless Comm. Summit*, pp. 1332–1336, June 2005.

[110] J. Bingham, "Multicarrier modulation for data transmission: an idea whose time has come," *IEEE Commun. Mag.*, vol. 28, pp. 5–14, May 1990.

[111] H. Sari, G. Karam, and I. Jeanclaude, "Transmission techniques for digital terrestrial tv broadcasting," *IEEE Commun. Mag.*, vol. 33, pp. 100–109, Feb. 1995.

[112] J. Chow, J. Tu, and J. Cioffi, "A discrete multitone transceiver system for HDSL applications," *IEEE J. Select. Areas Commun.*, vol. 9, pp. 895–908, Aug. 1991.

[113] R. van Nee, G. Awater, M. Morikura, H. Takanashi, M. Webster, and K. W. Halford, "New high rate wireless LAN standards," *IEEE Commun. Mag.*, pp. 82–88, Dec. 1999.

[114] C. Eklund, R. B. Marks, K. L. Stanwood, and S. Wang, "IEEE standard 802.16: A technical overview of the WirelessMAN 326 air interface for broadband wireless access," *IEEE Commun. Mag.*, pp. 98–107, June 2002.

[115] W. Lu, "4G mobile research in asia," *IEEE Commun. Mag.*, pp. 104–106, Mar. 2003.

[116] T. S. Rappaport, A. Annamalai, R. M. Buehrer, and W. H. Tranter, "Wireless communications: Past events and a future perspective," *IEEE Commun. Mag.*, pp. 148–161, May 2002.

[117] Z.Wang, X. Ma, and G. Giannakis, "OFDM or single-carrier block transmissions?" *IEEE Trans. Commun.*, vol. 52, no. 3, pp. 380–394, Mar. 2004.

[118] Z. Liu, Y. Xin, and G. B. Giannakis, "Space-time-frequency coded OFDM over frequency-selective fading channels," *IEEE Trans. Signal Processing*, vol. 50, no. 10, pp. 2465–2476, Oct. 2002.

[119] S. M. Ross, *A First Course in Probability.* Upper Saddle River, NJ: Prentice Hall, 2002.

Publications by the Author

[J1] N. F. Kiyani and J. H. Weber, "Exit chart analysis of iterative demodulation and decoding of MPSK constellations with signal space diversity," Journal of Communications, vol. 3, pp. 43–50, July 2008.

[J2] N. F. Kiyani and J. H. Weber, "Performance analysis of partially coherent SSD systems," {accepted} Electronics Letter.

[J3] N. F. Kiyani, J. H. Weber, A. G. Zajić, and G. L. Stüber, "Performance analysis of a system using coordinate interleaving and constellation rotation," {submitted} IEEE Communications Letter.

[J4] N. F. Kiyani, G. L. Stüber and J. H. Weber, "Performance of MRC with coordinate interleaving and constellation rotation in correlated Nakagami fading channels," {to be submitted} IEEE Transactions on Communications.

[C1] N. F. Kiyani and J. H. Weber, "Performance analysis of a partially coherent system using constellation rotation and coordinate interleaving," IEEE Global Commun. Conf., Dec. 2008.

[C2] N. F. Kiyani and J. H. Weber, "Iterative demodulation and decoding of rotated MPSK constellations with BICM, signal space diversity and OFDM," IEEE Symposium on Commun. and Veh. Technol., Nov. 2008.

[C3] N. F. Kiyani and J. H. Weber, " EXIT chart analysis of rotated MPSK constellations with BICM-ID, signal space diversity and OFDM," IEEE Symposium on Commun. and Veh. Technol., Nov. 2008.

[C4] A. Nawaz, N. F. Kiyani and J. H. Weber, " PAPR reduction technique for an OFDM system with rotated MPSK constellations and signal space diversity," IEEE Symposium on Commun. and Veh. Technol., Nov. 2008.

[C5] N. F. Kiyani and J. H. Weber, "Performance Analysis of a System using Coordinate Interleaving and Constellation Rotation in Frequency-Selective Fading Channels." IEEE Asian-Pacific Conf. on Comm., Oct. 2008. **(Winner of Best Paper Award)**

[**C6**] N. F. Kiyani, J. H. Weber, A. G. Zajić, and G. L. Stüber, "Performance analysis of a system using coordinate interleaving and constellation rotation in Rayleigh fading channels." IEEE Veh. Technol. Conf., pp. 1-5, Sept. 2008.

[**C7**] N. F. Kiyani and J. H. Weber, "Performance analysis of coordinate interleaved systems over Rayleigh fading channels," 29th Symposium on Information Theory in the Benelux, pp. 69-76, May 2008.

[**C8**] N. F. Kiyani and J. H. Weber, " OFDM with BICM-ID and rotated MPSK constellations and signal space diversity," IEEE Symposium on Commun. and Veh. Technol., pp. 1-4, Nov. 2007.

[**C9**] N. F. Kiyani and J. H. Weber, "Iterative demodulation and decoding for rotated MPSK constellations with convolutional coding and signal space diversity," IEEE Veh. Technol. Conf., pp. 1712-1716, Oct. 2007.

[**C10**] N. F. Kiyani and M. Hajian,"Design, analysis and measurements of Reflectarray using variable length microstrip patch antennas at Ka-band," IEEE Personal, Indoor and Mobile Radio Comm. Conf., pp. 1-5, Sept. 2007.

[**C11**] N. F. Kiyani and J. H. Weber, "A novel iterative demodulation and decoding scheme with convolutional coding and co-ordinate interleaving," 28th Symposium on Information Theory in the Benelux, pp. 11-17, May 2007.

[**C12**] N. F. Kiyani, U. H. Rizvi, J. H. Weber, and G. J. M. Janssen, "Optimized rotations for LDPC-coded MPSK constellations with signal space diversity," IEEE Wireless Comm. and Networking Conf., pp. 677-681, Mar. 2007.

[**C13**] N. F. Kiyani, U. H. Rizvi, J. H. Weber, and G. J. M. Janssen, "Rotation optimization for MPSK/MQAM signal constellations with LDPC coding over Rayleigh fading channels," IEEE Symposium on Commun. and Veh. Technol., pp. 77-80, Nov. 2006.

[**C14**] N. F. Kiyani and J. H. Weber, "Analysis of random regular LDPC codes on Rayleigh fading channels," 27th Symposium on Information Theory in the Benelux, pp. 69-76, June 2006.

The table on the next page depicts the relation between the publications and the chapters of the dissertation; "•" is used to show this relation.

Publications	**Chap. 2**	**Chap. 3**	**Chap. 4**	**Chap. 5**	**Chap. 6**
J1				•	
J2	•				
J3	•				
J4		•			
C1	•				
C2					•
C3					•
C4					•
C5		•			
C6	•				
C7	•				
C8					•
C9				•	
C10*					
C11				•	
C12			•		
C13			•		
C14			•		

"*" denotes that the paper has no relation with the dissertation.

Samenvatting

Wireless Communication Systems using Signal Space Diversity

De volgende generatie communicatie-apparaten zullen naar verwachting niet alleen een grote verscheidenheid aan toepassingen ondersteunen, zoals spraak, audio en video, maar ook in staat zijn verbindingen te onderhouden met vele andere apparaten (in plaats van met alleen een enkel basisstation) in verschillende veranderende omgevingen. Het doel van de dissertatie is digitale modulatie- en codeertechnieken voor draadloze communicatiesystemen in realistische transmissiescenario's te analyseren. Een belangrijk oogmerk van de dissertatie is bovendien vrijheidsgraden te onderzoeken die kunnen worden benut om draadloze communicatiesystemen in hun geheel adaptiever te maken, hetgeen leidt tot systemen die ofwel minder vermogen voor een bepaalde prestatie verbruiken ofwel voor een bepaalde hoeveelheid gemiddelde energie een betere prestatatie bieden dan een conventioneel systeem. De technieken/algoritmen die in de dissertatie worden geanalyseerd zijn veelzijdig en geschikt voor zowel smalbandige als breedbandige draadloze communicatiesystemen voor binnen- en buitenscenario's (met geringe mobiliteit).

Signaalruimtediversiteit, ook wel modulatiediversiteit genoemd, wordt gebruikt om de totaal ontvangen signaal-ruisverhouding te verhogen en de detectiefout te verminderen. Een grondige prestatie-analyse van modulatiediversiteitssystemen wordt in de dissertatie gepresenteerd om de verschillen met conventionele systemen in smalbandige en breedbandige kanalen te begrijpen en ook de maximaal mogelijke prestaties te bereiken. Algemene methodes om de systeemparameters te optimaliseren en de beschikbare vrijheidsgraden te benutten worden gepresenteerd. Syste-

men voor kanaalcodering, samenwerkende demodulatie en decodering en Orthogonal Frequency Division Multiplexing (OFDM) worden gekoppeld aan modulatiediversiteit om het algehele vermogensverbruik te verminderen en systeemprestaties te verbeteren.

Nauman F. Kiyani

List of Symbols

α	Random channel amplitude
$\bar{\gamma}$	Average signal-to-noise ratio per bit
η	I interleaver
γ	Signal-to-noise ratio per bit
$\Gamma(\cdot)$	Gamma Function
γ_l	Conditional signal-to-noise ratio per bit per path
γ_t	Conditional signal-to-noise ratio per bit
γ_{th}	Threshold γ
Λ	Intrinsic information
μ	Q interleaver
Ω	mean square value of α
$\tau_{\max}$	Maximum delay spread of the channel
θ	Rotation angle
$\wp$	Mapping function
$\{\alpha\}_{l=1}^{L}$	Random channel amplitudes

$\{\tau\}_{l=1}^{L}$	Random channel delays
$\{\theta\}_{l=1}^{L}$	Random channel phases
$cov(\cdot)$	Covariance
$E[\cdot]$	Statistical average
f_d	Doppler spread
f_{ch}	Channel coherence bandwidth
I	Inphase channel
$I_0(\cdot)$	Modified Bessel function of the first kind
$J_0(\cdot)$	Zero-order Bessel function of the first kind
K	The Rician factor
N	Number of symbols
N_0	One-sided power spectral density
P_b	Average probability of bit error
P_s	Average probability of symbol error
P_{out}	Outage probability
Q	quadrature phase channel
T_c	Coherence time of the channel
T_s	Symbol duration
$var(\cdot)$	Variance
$\mathcal{S}_M^{\theta}$	Rotated MPSK signal constellation
$\mathcal{S}_M$	MPSK signal constellation
${}_1F_1(\cdot;\cdot;\cdot)$	Kummer confluent hypergeometric function
$\mathbf{x}$	Bold face lowercase letters denote row vectors

List of Abbreviations

AF	Amount of fading
AWGN	Additive white Gaussian noise
BEP	Bit error probability
BICM	Bit interleaved coded modulation
BICM-ID	Bit interleaved coded modulation with iterative demodulation and decoding
BPSK	Binary phase shift keying
CCI	Co-channel interferes
CDF	Cumulative distribution
CSI	Channel state information
DFT	Discrete Fourier transform
DSL	Digital subscriber line
EGC	Equal gain combining
EXIT	Extrinsic information transfer
HF	High frequency
HIPERLAN	High performance radio local area network
ICI	Inter carrier interference
ISI	Inter symbol interference

LAN	Local area network
LDPC	Low density parity check
LLR	Log likelihood ratio
Log-MAP	Logarithm maximum *a posteriori*
LoS	Line of Sight
MAP	Maximum *a posteriori*
MIMO	Multiple input multiple output
ML	Maximum likelihood
MMAC	Multimedia mobile access communication
MMSE	Minimum mean square error
MPSK	M-ary phase shift keying
MQAM	M-ary quadrature shift keying
MRC	Maximum ratio combining
OFDM	Orthogonal frequency division multiplexing
PAPR	Peak to average power ratio
PDF	Probability density function
PEP	Pair wise error probability
PLL	Phase Locked Loop
PSAM	Pilot symbol assisted modulation
PSK	Phase shift keying
QoS	Quality of Service
QPSK	Quadrature phase shift keying
RMS	Root mean square
RSC	Repeat systematic convolutional
RV	Random variable
SISO	Soft input soft output
SNR	Signal to noise ratio
SOVA	Soft output Viterbi algorithm
SSD	Signal space diversity
TCM	Trellis coded modulation
WLAN	Wireless local area network

Acknowledgements

Over the years during my affiliation with different cultures I have had the good fortune to meet many gifted human beings who have given me their time, professional and personal help and above all: companionship and patience, than perhaps was ever warranted by me and this melange of experiences is my most dearest and precious asset. I thank you all for this generosity.

This dissertation is a result of four-years of work done in the Wireless and Mobile Communications (WMC) Group , on the 19^{th} floor of the EWI building. I thank the chair, Prof. Ignas Niemegeers, for giving me the opportunity to pursue my doctoral studies. This work would not have been possible without the guidance, help and support of my mentor and teacher Dr. Jos Weber. I, sincerely thank him for his continual support and encouragement. His unquenchable curiosity, opulence of patience, generous smile and his meticulous concentration on the mot juste has been a sheer inspiration. I would also like to thank the members of the McAT project which I have been a part of and to all the members of my examination committee.

WMC and NAS groups have provided me with a home away from home on this sojourn of mine. I thank each member of these groups for their friendship and love. I would also like to thank all my office mates for having the patience to bear me, Przemek, Chang, Prasad, Zoubir, Jing, Zulkuf and Weidong. I would specially like to thank Umar and Santpal for those wonderful dinners and those pageantry discussions ranging from regional politics to the anatomy of black holes. I also wish to extend a special thanks to the wonderful ladies of the secretariat Laura, Wendy, Marjon and Rowena and from the 18^{th} floor Marion and Lynn for showing such

tremendous patience in listening to all my requests.

This dissertation is dedicated to my parents, Abujee and Mamajee, for their unconditional love, unflinching support and untiring patience. I am, and would always be, deeply grateful to them. Last but not the least, I wish to thank my sisters, brother and my special friend Tayyaba.

Delft, *Nauman Farooq Kiyani*

January 2009

Curriculum Vitae

Nauman Kiyani was born in Kohat, Pakistan, on March 23, 1980. He graduated with a bachelors degree in electrical engineering from National University of Sciences and Technology (NUST), Pakistan, in December 2001. From Januray 2002 to August 2003, he worked as an assistant manager in Advanced Engineering and Research Organization (AERO), Pakistan. He graduated with Masters of Science degree from University of Gävle, Sweden in telecommunication/electronics in December 2004. In February 2005, he started his research work towards a doctorate of philosophy (PhD.) degree in electrical engineering from Wireless and Mobile Communications group, Faculty of Electrical Engineering, Mathematics and Computer Science (EEMCS), Delft University of Technology, Netherlands. The research conducted by him in Delft University of Technology is presented here in this dissertation.